LA-4494-MS

c.3

LOS ALAMOS SCIENTIFIC LABORATORY
of the
University of California

LOS ALAMOS • NEW MEXICO

Quarterly Status Report on the

Advanced Plutonium Fuels Program

April 1-June 30, 1970

and Fourth Annual Report, FY 1970

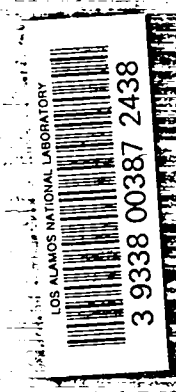

UNITED STATES
ATOMIC ENERGY COMMISSION
CONTRACT W-7405-ENG. 36

This LA. . .MS report presents the status of the LASL Advanced Plutonium Fuels Program. Previous Quarterly Status Reports in this series, all unclassified, are:

LA-3607-MS	LA-3820-MS	LA-4193-MS
LA-3650-MS	LA-3880-MS	LA-4284-MS
LA-3686-MS	LA-3933-MS	LA-4307-MS
LA-3708-MS*	LA-3993-MS	LA-4376-MS
LA-3745-MS	LA-4073-MS	LA-4437-MS
LA-3760-MS*	LA-4114-MS	

This report, like other special-purpose documents in the LA. . .MS series, has not been reviewed or verified for accuracy in the interest of prompt distribution.

Distributed: August 1970

LA-4494-MS
SPECIAL DISTRIBUTION

LOS ALAMOS SCIENTIFIC LABORATORY
of the
University of California
LOS ALAMOS • NEW MEXICO

Quarterly Status Report on the

Advanced Plutonium Fuels Program

April 1-June 30, 1970

and Fourth Annual Report, FY 1970

FOREWORD

This is the fourth annual report on the Advanced Plutonium Fuels Program conducted at the Los Alamos Scientific Laboratory. Results of the current quarter's work has been in most cases incorporated into the summary of the year's work, and is therefore specifically identified.

Most of the investigations discussed are of the continuing type. Results and conclusions described may therefore be changed or augmented as the work continues. Published reference to results cited in the report should not be made without obtaining explicit permission to do so from the persons in charge of the work.

TABLE OF CONTENTS

TABLE OF CONTENTS
(continued)

PROJECT 401

EXAMINATION OF FAST REACTOR FUELS

Person in Charge: R. D. Baker
Principal Investigators: J. W. Schulte
C. F. Metz

I. INTRODUCTION

This project is directed toward the examination and comparison of the effects of neutron irradiation on LMFBR Program fuel materials. Unirradiated and irradiated materials will be examined as requested by the Fuels and Materials Branch of DRDT. Capabilities are established for providing conventional pre-irradiation and post-irradiation examinations. Additional capabilities include less conventional properties measurements which are needed to provide a sound basis for steady-state operation of fast reactor fuel elements, and for safety analysis under transient conditions.

Analytical chemistry methods that have been modified and mechanized for hot cell manipulators will continue to be applied to the characterization of irradiated fuels. The shielded electron microprobe and emission spectrographic facilities will be used in macro and micro examinations of various fuels and clads. In addition, new capabilities will be developed with emphasis on gamma scanning and analyses to assess spatial distribution of fuel and fission products.

High temperature properties of unirradiated LMFBR fuel materials are now being determined by Contractor in an associated project (ident No. 07463). Equipment designs and interpretive experience gained in this project are being extended to provide unique capabilities such as differential thermal analysis, melting point determination, high temperature dilatometry, and high temperature heat content and heat of fusion for use on irradiated materials.

II. EQUIPMENT DEVELOPMENT

A. Inert Atmosphere Systems

(C. E. Frantz, P. A. Mason, R. F. Velkinburg)

1. Metallography Cells. A United States Dynamics recirculating Ar purifier was installed and equipped to provide inert atmosphere for the two metallography cells and the metallograph blister. Modifications to the piping were made to provide a once-through Ar purge system to remove air prior to start-up and to supply Ar to the manipulator boots. The purge system also serves as a back-up during those periods when the recirculating system is not functioning properly or when it is suspected that fumes from the chemical etchants or solvents might be deleterious to the chemical absorbents.

During initial testing of the purifier, failure in several defective valves occurred and an absorbent bed for the O_2 was poisoned. This difficulty was attributed to corrosion from HF and HCl which are decomposition products of Freon TF, a solvent used in the ultrasonic cleaners and as a vehicle for grinding metallographic specimens. Monel components have been installed to replace the corroded parts of the system, and a new charge of absorbent has been ordered. Controls and interlocks have been installed to obviate a recurrence of this difficulty.

Because of these difficulties encountered with the Ar repurifier, a once-through purge has been used most of the time for maintaining the inert atmosphere. A study showed that the O_2 concentration in the Ar atmosphere of the containment boxes is quite sensitive to the differential pressure between the box and atmospheric

pressure. Consequently a sentitive Photohelic pressure controller was installed which holds the differential pressure reliably at several hundredths of an inch of water negative when the purifier is operating.

The two metallography cells were extensively leak-checked on the interior using a special probe on a flexible extension to the cell sampling line. A continuous gas sample was drawn through the sample line into a sensitive oxygen analyzer. Air leaks were thus easily detected, with major leaks being found in the manipulator boots and the transfer systems. Air leaks through the manipulator boots could be adequately reduced by purging the boots with Ar, but the Ar usage was excessive. Therefore, manipulator through-tube seals and tape seals were designed. Initial tests on the seals are very promising since less than 5 cfh of Ar is required to purge a manipulator boot with much better results than the higher purge rate previously used. The transfer systems are now being studied to determine sources of leaks and means to eliminate them.

Performance tests of the Ar purifier were conducted to determine its capacities, capabilities, and characteristics. At 0.5 cfh air leakage into the cells, the O_2 content of the Ar atmosphere can be held below 60 ppm.

Typical impurities in the Ar atmosphere have been about 2500 ppm O_2 and 50 ppm H_2O. With new manipulator seals, improved transfer systems, and precise differential pressure control along with use of the Ar purifier, the oxygen level in the Ar atmosphere will probably be reduced below 100 ppm within the next 6 months.

2. Disassembly Cell. An investigation revealed that the absorbents in the recirculating Ar purifier were poisoned by oil from a pressure relief device. The poisoned absorbents were replaced, and the pressure relief device redesigned and repositioned so oil could not enter the purifier. The cell was internally leak-checked using the oxygen analyzer. Substantial leaks were found in the manipulator boots and the 7-in. transfer system.

Performance tests on the purifier showed that it could not continuously operate in a satisfactory manner if the containment box contained more than 30 ppm O_2, and consequently, the Ar purifier has not been used. However, with improvements in the manipulator seals and 7-in. transfer system, the purifier will be used in the near future.

The Photohelic pressure controller also was installed in this cell to improve control of the containment box differential pressure. During recent weeks and using a once-through Ar purge, the inert atmosphere has typically contained 10 ppm O_2 and 5 ppm H_2O.

3. Argon Supply. The large quantities of Ar used by the inert systems required a high pressure tank trailer as a primary Ar supply with a manifold (32 H-size cylinder capacity) as a back-up system.

4. Miscellaneous. A pair of CRL model L, sealed-type manipulators were ordered for use in a containment box where it is desired to maintain inert atmospheres having extremely high purities. The adaptors for providing the seal between the manipulators and the containment boxes have already been designed. Effectiveness of this first pair of sealed-type manipulators in an inert atmosphere box will determine whether their routine use is advisable.

Inlet and exhaust piping to the two cells in which the DTA equipment and the heat content apparatus are located have been modified to provide an inert atmosphere (single-pass Ar) on an intermittent basis. In testing this new capability, atmospheres containing less than 200 ppm O_2 were obtained. The same modifications are being made to the two alpha containment boxes in which chemical operations are carried out in order to provide inert atmospheres for special experiments. At the conclusion of this work the Hot Cell Facility will have three inert atmosphere boxes which are connected to recirculating purification systems and four containment boxes for which inert atmospheres can be provided on an intermittent basis using a once-through Ar purge system.

A residual gas analyzer has been procured for monitoring the inert atmospheres of the various containment boxes.

The existing station for filling various containers with inert atmosphere prior to connecting to the containment boxes has been improved for better operation.

B. In-Cell Equipment

(J. H. Bender, G. R. Brewer, D. B. Court, E. L. Ekberg, F. J. Fitzgibbon, C. E. Frantz, D. D. Jeffries, K. A. Johnson, L. E. Jones, M. E. Lazarus, J. M. Ledbetter, C. D. Montgomery, G. H. Mottaz, P. P. Osvath, J. R. Phillips, T. Romanik, T. J. Romero, A. E. Tafoya, J. R. Trujillo, R. F. Velkinburg, and L. A. Waldschmidt)

1. Metallography. The two alpha containment boxes for metallography were installed, equipped and "hot" operations were initiated on September 25, 1969. Most of the equipment functioned well and provided for increased throughput. Improvements have subsequently been accomplished on some items of equipment as a result of operating experience. The specimen loading-unloading fixture, the specimen storage facility and the electrolytic etcher are items which have undergone design changes for improved operation.

Some of the specialized equipment which has been installed in the new boxes is listed below.

a. Material Transfer Systems. In addition to the transfer systems employing the 7-in. and 18-in. diameter ports, other systems were devised and installed which also do not violate the "alpha seal" principle. Improvements were made in the transfer methods between the metallographic cells and blister.

Sphincter Pass-Throughs: These pass-throughs permit the transfer of cold material into the box from the operating area, and the discharge of empty containers and other materials with low beta-gamma contamination levels into a plastic bag located in the basement. The sealing mechanisms rely on 12 tapered neoprene washers in series and spaced 1/4 in. apart (Fig. 401-1). Plastic containers, which are 10 in. long and slightly larger in diameter than the inside diameter of the neoprene washers, are used to introduce supplies to the box. These containers serve as not only the carrier but also as the seal plug within the washers. An inerting station has been provided in the operating gallery for filling the containers with Ar prior to being passed into the box, thus minimizing the introduction of O_2 and H_2O impurities.

Bag-Out Port: The blister, housing the metallograph, was provided with a conventional bag-out port system and removable shield. This device permits the rapid removal of alpha and beta-gamma autoradiographs, replicas, and other samples having a low radiation level. The radiation from the samples is first surveyed through the port-hole before removing the samples.

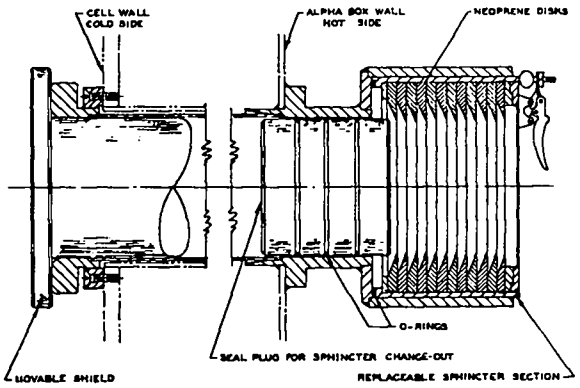

SPHINCTER SYSTEM

Fig. 401-1. Sphincter Pass-Through.

Intercell Transfer Systems: For transfers between the two metallographic cells and between these cells and the blister, a newly designed system was installed. This system employs large vacuum-tight valves for isolating the three boxes for inert atmosphere control. Motorized conveyors are used for movement of material between boxes. The system, which is also equipped with controls and safety interlocks, has proven very reliable.

b. Grinding-Polishing Equipment. A modified Unipol grinder-polisher is the basic component of this system. Custom designed hold-down clamps, with adjustable loading force, are incorporated along with special fluid delivery lines and an effluent collector system. There are three of these units in each of the two metallographic preparation boxes (Fig. 401-2). Two Syntron vibratory polishers are installed in the polishing box. This equipment can be removed remotely from the alpha box for maintenance or modification utilizing the master-

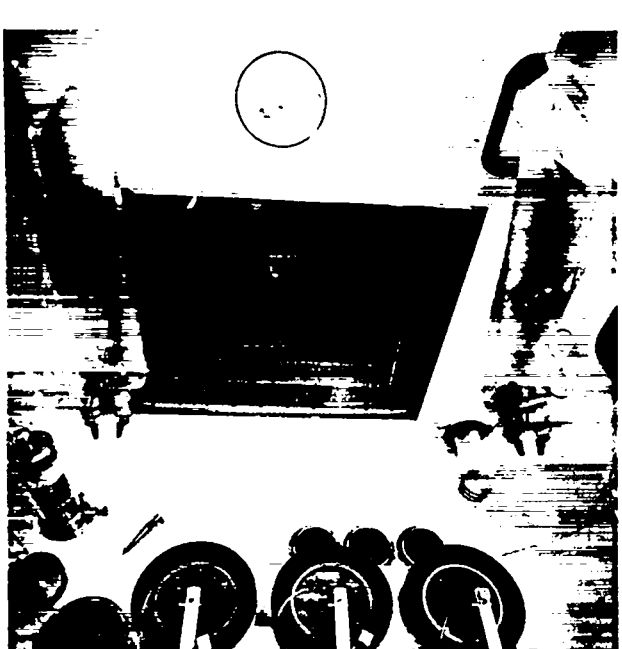

Fig. 401-2. View of Unipol Polishers in Metallographic Preparation Box.

slave manipulators, a small overhead monorail hoist within the alpha box, and the 18-in. transfer system and container.

c. Specimen Loading-Unloading Fixtures. Tools have been designed, fabricated, tested and are in use for loading and unloading the metallography specimens from the three multiple-hole (4, 5, and 6) specimen holders used in grinding and polishing. These fixtures are readily operable using the manipulators and can either be set aside in the alpha box when not in use or removed from the box for maintenance using the 18-in. transfer system. Special components to accommodate the hole configurations of the holders are filed on wall racks within the box.

d. Camera System for Macrophotography. A special camera system was designed and built incorporating a through-the-shield-wall camera, Pb shield, viewing port, reflector, specimen positioner, strobe light, and an optical data block method for identification of negatives. This system is in use to provide high resolution macrophotographs of metallographic specimens still in the multiple-specimen holders.

e. Waste Compactor. A waste compactor has been designed and built for use in the Pu metallography cells. It has been so successful in decreasing the number of waste transfers out of these cells that a second unit has been constructed for the disassembly cell. The unit compacts waste materials such as cleaning, grinding and polishing papers into one-gallon cans and presses the lids into place.

f. Metallograph Blister. A new Leitz metallograph is expected for use in the blister. A new and larger containment box with shielding is being designed to accommodate this equipment along with the present metallograph, a new ion etcher and a Quantimet analyzer.

A pair of Tru-motion mini-manipulators is on order from Programmed and Remote System Corporation to serve the new blister box.

2. Other Special Equipment

a. Shipping Casks

Fuel Element Cask: This shipping cask, shown in Fig. 401-3 and referenced in the preceding Anual Report (LA-4284-MS), was completed, approved, and put into service 9 months ago. The cask has been used

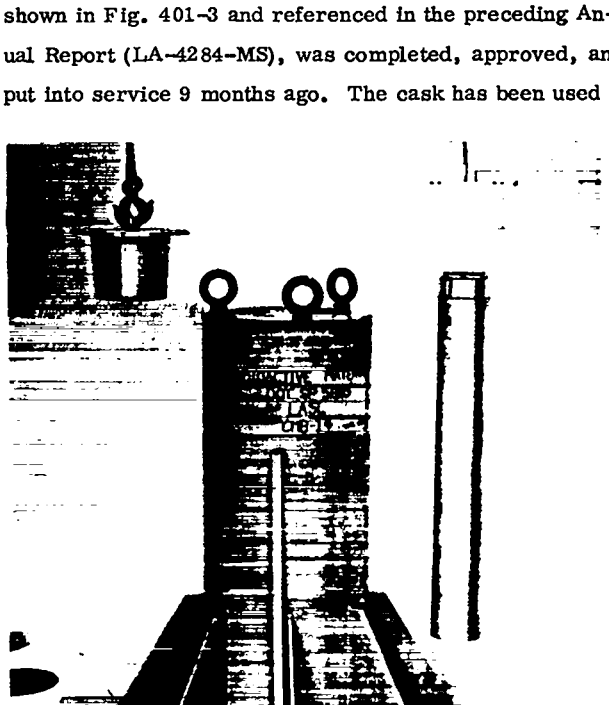

Fig. 401-3. Fuel Element Shipping Cask

in transferring material to and/or from EBR-II, BNWL, ANL-Illinois, DUN at Hanford, TAN Facility at Idaho Nuclear, and G.E.-Vallecitos.

The cask has 6-1/2 in. of depleted U for shielding, a cavity of 6 in. i.d. by 45 in. high, and weighs 12,200 lbs. There are now three types of inserts available for the shipping of irradiated capsules. The diameters and numbers of 40-in. long capsules which can be handled are tabulated below.

Table 401-I

Inserts for Shipping Cask

Insert No.	No. of Capsules	Diameter of Capsules, in.
1	19	0.37
2	6	1.13
3	7	0.75

Capsules of larger diameter can be placed in baskets, or other inserts can be fabricated as required.

Cask for Shipping Sections of Elements: A new cask for shipping sections of irradiated fuel elements is being designed for the following reasons: to provide increased capability, to conserve the larger cask for whole fuel elements, and to reduce freight costs. This cask will weigh approximately 1500 lb, will be constructed of depleted U encased in stainless steel, and will have a cavity approximately 1-1/2 in. diam by 11 in. high. The design is in accord with DOT requirements for shipment of radioactive materials.

b. Disposable Plastic Container for Wastes. Plastic containers consisting of a molded polycarbonate lid and a polypropylene bottom section (Fig. 401-4) were put into service in the 7-in. transfer systems for disposing of radioactive wastes. The containers worked well for their intended purpose. It was determined that 200 lb of force was required to remove a lid from the can. Since a cemented joint in the polycarbonate lids could separate during lid removal if poorly joined, a test fixture was designed and constructed to test each of the lids for strength. Each lid was tested to 350 lb tensile strength before acceptance. A chamber was constructed for purging the air with Ar prior to attaching the container to the alpha box. The plastic system is a significant

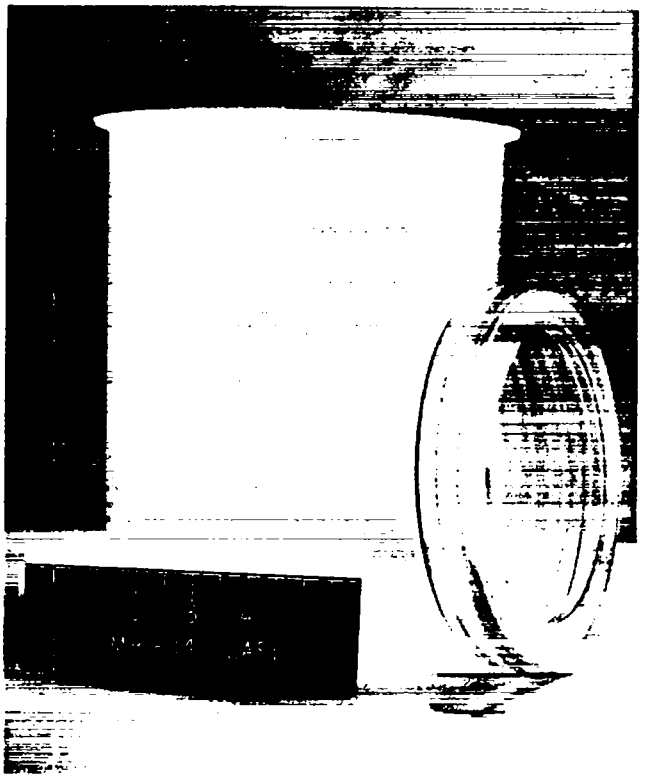

Fig. 401-4. Disposable Plastic Container for Radioactive Wastes.

advance in the technology of remote transfer techniques. A paper describing this development was submitted for publication.

c. Remote Encapsulator. A device for the remote encapsulation in an inert atmosphere of fuel segments (or other material) which are intended for shipment or long term storage has been installed and successfully used. The device, as shown in Fig. 401-5, relies on mechanically crimping a pre-formed and "tinned" stainless steel tube around a "tinned" cap. A resistance heating element is then used to melt the Aladdin 450 soft silver solder to effect a vacuum-tight seal. This equipment has been used thus far in preparing 66 closures for storing sections of mixed oxide and carbide fuel elements.

d. Element Sectioning Saw. Design drawings were completed and fabrication was started on a new element sectioning saw for use in the disassembly cell. This design utilizes components from a commercial "Econo-Saw" and will facilitate accurate cutting of various sizes of fuel elements with much less dust than was produced with the high speed abrasive saw. Final

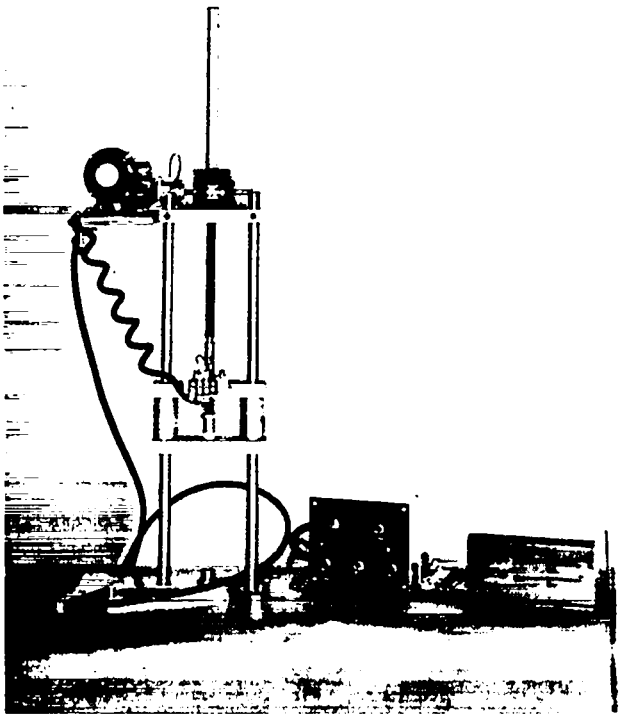

Fig. 401-5. Remote Encapsulator

assembly is held up pending arrival of a commercial, non-commutating feed motor.

e. Remotely Operated Porosimeter. An Aminco Model 5-7107 porosimeter was remotized and installed in the same containment box in which the heat content apparatus is located. This porosimeter is to be used in determining "connected porosities" on irradiated fuels for comparison with results obtained on unirradiated material.

f. Density by Immersion. Several precision bearings, whose dimensions can be traced to the National Bureau of Standards, have been obtained for use as reference standards in determining density of irradiated fuel pellet sections. Approximately 25 samples of irradiated carbide or oxide have been measured using bromobenzene as the immersion medium in an air atmosphere cell. Although the accuracy of the measurements is uncertain because of fuel porosity and the heat effects from the thermally hot pellets, the data obtained compare favorably with density changes expected with high burnups.

g. Remote Equipment for O and C Determinations:

The remotized equipment which had been tested in a mockup alpha box was moved to the shielded containment box where the irradiated material will be examined. An 18-in. diam transfer can will be provided to store the larger pieces of equipment at those times when the facility is being used for other tests.

h. Radioactive Standards for Dimensional Measurements.

Length and diameter standards are being prepared for dimensional calibration of the mechanical system. The standards consist of two ^{60}Co cylinders of precise dimensions separated by a Dural rod of known length. The entire assembly is about 12 in. long; the dimension of both the ^{60}Co cylinders and the Dural separator can be traced to NBS standards. With existing techniques the height of irradiated fuel columns can be determined with an accuracy of ± 0.010 in.

i. Microsampling Apparatus. Preliminary design was started on the conversion of a commercial ultrasonic impact grinder to a remotely operated micro-sampling apparatus for taking small cores from irradiated fuel.

j. Gages for Betatron Radiography. Three different sets of Ta gages were machined (the accuracy of the measurements are traceable to dimension standards of NBS) in a continuing program to provide suitable images on the Betatron radiograph for length and diameter comparisons. It is possible to place the standard gage on the fixture near the fuel pin during radiography in such a manner that each negative taken (~ 11/ pin) would contain an image of the gage.

C. Heat Content Measurement

(G. R. Brewer, C. E. Frantz)

The electrical and mechanical functions of the drop calorimeter have been tested at 2300°C. No problems which would limit the intended use of the calorimeter were observed.

The heat content of an alumina standard was determined, and the results are tabulated below. The accuracy of the data is not know at this time.

Consistency and reproducibility of electrical

Table 401-II

Heat Content of Alumina

Temperature (^{o}C)	ΔH_t -25^{o}C (Kcal/mole)
1298	35.90
1431	40.74
1522	42.84
1598	45.15
1656	47.38
1781	51.90
1866	55.03
1973	58.95

calibrations of the drop calorimeter could not be obtained after October. Recently a coat of GE Glyptal was applied to the resistance thermometer winding on the calorimeter, binding the winding to the calorimeter block. Apparently this has restored the consistency and reproducibility of the measurements.

Difficulties are being encountered in determining an adequate method for reducing the raw calorimetry data to obtain heat content. (Reliable calculations are required to obtain accuracy and also to obtain correlation with the calorimeter used in measuring heat contents on unirradiated fuels.) The method of Jessup[1,2,3] is under investigation. No tentative conclusion regarding the applicability of the method can yet be made.

Sufficient experience has been gained with the welding fixture to weld capsules satisfactorily for both heat content and DTA measurements.

Equipment (shown in Fig. 401-6) for obtaining heat content and porosimetry measurements on irradiated fuels was ready for operation on July 1. However, recent developments concerning the design of the calorimeter have postponed the immediate use of the equipment on irradiated fuels

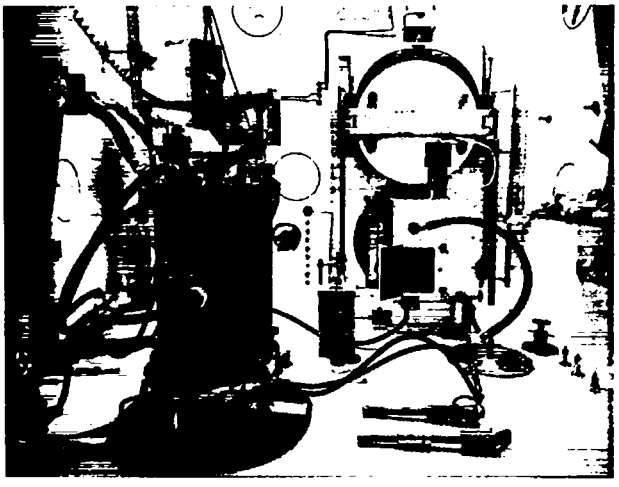

Fig. 401-6. Heat Content and Porosimetry Equipment.

III. DP WEST FACILITY

(D. B. Court, F. J. Fitzgibbon, M. E. Lazarus, C. D. Montgomery, G. H. Mottaz, J. R. Phillips, T. Romanik, J. R. Trujillo)

This area which houses four hot cells is being altered to provide space and equipment for the examination of fast reactor fuel elements. Engineering was completed on the structural changes, AEC approval was obtained, then the construction work on the modifications to Building 401 was held up until the latter part of June awaiting settlement of a statewide construction fitters' strike. Work has now been initiated and is proceeding on a schedule which calls for completion of this phase by August 8, 1970.

The cart for moving casks between the hot cell corridor and the 25-ton hoist outside is nearing completion. The 25-ton hoist and 1/2-ton crane bridge (for manipulator removal) have arrived from the vendor. The 3-ton bridge crane for the hot cell corridor has been shipped from PaR in St. Paul.

After completion of the construction phase, additional work will be required of the maintenance crafts. Concurrent with the latter work phase, installation and check-out of the specialized equipment will be made by the technical operating groups.

Major systems and equipment for operations at DP West and their status are detailed as follows:

A. Fission Gas Sampling

A capsule gas sampling system has been built and is ready for installation at DP. This system uses a drill to penetrate the cladding and is similar to the system presently being employed in the Wing 9 Facility. (Fission gas sampling of the pin, however, will continue to be made in the inert atmosphere disassembly cell at Wing 9.).

B. Profilometry

The present status of the profilometry system is as follows:

1) Light Source -- Commercial components on hand; system not yet assembled.

2) Pin Transport System -- All commercial components available except main drive screw. Construction of unit almost complete.

3) Periscope System -- On hand.

4) Electro-Optical Sensor -- Expected at LASL and in operating condition by July 17, 1970.

5) Sensor Positioning Stand -- All commercial components available, design not completed.

6) Data Storage System -- Commercial components on order. It is expected that the system will be operational by early September 1970 except for the electronic data storage system. This will probably be operational by January 1971. Therefore, profilometry data will be recorded on a strip chart until this time.

C. Gamma Scanning System

A system for high resolution gamma scanning of irradiated fuel pins and sections has been designed and is being fabricated. Status of the individual items of the system are itemized as follows.

1. The gamma scanning shield has been fabricated using lead of low Sb and low activity content. The in-cell vertical transport and handling mechanism to accommodate fuel pins up to 61 in. long has been designed and fabricated.

2. Final assembly of the in-cell portion of the Gamma Scanning System has been held up pending receipt of delayed shipment of the Saginaw ball screws.

3. During check-out and acceptance testing of the electronic portion of the vendor-supplied system it was discovered that the control and response of the Slo-Syn motor and encoder system furnished was unsatisfactory. The vendor is now exploring possibilities of furnishing an electronics package which will provide the require compatibility.

4. Designs for five new collimators and the adjusting mechanism for installation in the shielding wall of the gamma scanning cell have been completed. These designs are in review and fabrication will be initiated soon.

D. Macro-Photography

Various means have been investigated to obtain photographs of the exterior surfaces of pins at 0°, 120°, and 240° orientations. Experiments were carried out with a two mirror system to obtain three views of a fuel element on one photograph, and a design has been completed and construction started on a positioning system. The light will be provided by twenty fluorescent lamps and a 300-watt quartz-iodine lamp. Frontal illumination will be obtained by reflecting the light from the quartz-iodine lamp with a beam-splitting mirror.

IV. METHODS OF ANALYSIS

A. Measurement of U and Pu

(J. W. Dahlby, G. R. Waterbury)

Controlled-potential coulometric equipment for titrating U and Pu in the chemical characterization of irradiated mixed oxide or carbide fuels was modified for remote operation and tested in-cell by repeated analyses of solutions containing known amounts of each metal. Equipment modification included magnetic stirring of samples and minor changes in cell design especially in the electrical contact to the Hg pool electrode. In these in-cell tests of the equipment, the relative precision (1 σ) was 0.07 to 0.08% for a single determination of U or Pu in the unirradiated samples. For the measurement of U, the titration current was integrated as U(VI) was coulometrically reduced at a Hg electrode to U(IV) following a preliminary reduction of more-easily reduced impurities. The current for the coulometric oxidation of Pu(III) to Pu(IV) at a Pt electrode was integrated in determining Pu. A slight bias that occurred in the titrations of U in the presence of Pu was eliminated by changing the location of the working electrode.

The method was tested further by successfully analyzing an irradiated oxide pellet (less than 0.1% burnup) having low beta and gamma activity levels. The relative precision (1 σ) of the method was 0.07 to 0.08% for a single determination of either U or Pu in this sample, which was equal to the precision found in the analyses of unirradiated samples.

The method gave high and erratic results in initial titrations on mixed oxide fuels having approximately 1% burnup. The difficulties were assumed to be caused, at least in part, by the hydrogen peroxide generated by the

intense radioactivity of the sample solution. Removal of the peroxide from solution by reaction with peroxidase and catalase enzymes or by addition of sulfamic acid did not eliminate the bias. Use of a glassy carbon working electrode instead of a Hg pool in the U titration also was not an improvement. Reduction of the sample size to 1 mg, fuming the sample with H_2SO_4 immediately before the titration, and redox cycling reduced the bias to 0.1% absolute. The redox cycling technique involved repeated titrations of the Pu between the (III) and (IV) oxidation states until consecutive values for Pu obtained during either the coulometric reduction or oxidation agreed within 2 μg. Usually three or four cycles were necessary. By using these techniques, the average obtained for 14 measurements of Pu in the mixed oxide fuel having undergone 1% burnup was 22.1% which was equal to the Pu content found in fuel from the same batch before irradiation. The precision (1 σ) was 0.12% (absolute) or 0.5% (relative).

A method for determining a reliable correction factor was developed to reduce the bias in the titration of U. A 1-mg sample was titrated in the usual way. Then the sample was left in the titration cell for a short waiting period and retitrated. The waiting period was adjusted to make the total time involved in this second titration equal to the time required for the first titration. Subtraction of the blank obtained by this second titration reduced the bias to 0.2%. An average of 66.0% was obtained for U in the mixed oxide fuel with 1% burnup as compared to 66.2% measured in the same batch of fuel before irradiation. The precision (1 σ) was 0.3% (absolute) or approximately 0.5% (relative).

The effectiveness of these minor modifications in the method and equipment in reducing bias and improving precision is being determined now using samples having undergone higher (5 to 10%) burnups.

B. Gamma Scanning
(J. Phillips, J. Deal)

Locating anomalies and areas of interest for further analyses in irradiated fuel elements is an important use of gross gamma scanning provided the results are obtained quickly to avoid delays in destructive sampling of the fuel capsule. To ensure the required speed, a simple gross gamma scanning system was assembled to complement the complex system for detailed gamma scanning. This simple system uses the scanning mechanism, slit, and Ge (Li) detector of the detailed gamma scanner for accurate resolution of scan position and reliable measurements. An amplifier, single channel analyzer set to accept all gamma energies above a preset background, a scaler timer, and a printer complete the system. Measurements of fuel lengths with this system were accurate within 0.01 in. The gross gamma scanner was satisfactory in all tests and in the analyses of irradiated fuel elements for which only a rapid gross gamma scan was required.

Components for the new high resolution gamma scanning system (Nuclear Data 50/50) were assembled following several minor modifications, and tests were started to ensure proper functioning. The detector system, which consists of an anticoincidence shield with a sodium iodide annulus and a high efficiency (12.1%) Ge(Li) detector, also was being tested prior to installation in the DP West hot cell facility.

Computer codes for data reduction are being developed to be compatible with the special magnetic tape drives on the CDC 6600 computer. These codes will be used for the spectral unfolding and plotting of data.

A study of the design and construction of collimators was completed and fabrication of a prototype collimator was started. The new collimators will be constructed of W because its high density (19.3 g/cc) will provide a significant improvement in the spatial resolution over the Pb collimators presently being used.

C. Shielded Electron Microprobe
(W. V. Cummings, D. B. Court, C. D. Montgomery, G. R. Waterbury)

Detailed examination of areas as small as 0.5 μ in diameter to determine the chemical compositions of various features in irradiated reactor fuels and cladding is a capability unique to the shielded electron microprobe. Information from these examinations is essential in determining the chemical behavior of the fuel element components. Following the recent installation and testing of a MAC shielded electron microprobe, a program of

examinations was started to aid in the evaluation of fuels. Goals of this program included investigations of (a) fission product distributions and migrations, (b) redistribution of fuel components, (c) fuel-cladding interactions, (d) fission product precipitates and inclusions, (e) reactions of fission product elements with the fuel and with the cladding, (f) unusual features found metallographically or by other techniques, such as gamma scanning, and (g) variations in burnup relative to position. Selection of samples to be examined was based upon metallography gamma scanning, or other test results showing features in the sample that should provide desired information about fuel element behavior.

Proper functioning of the electron microprobe and associated equipment was demonstrated in the analyses of several irradiated metal, mixed oxide, and mixed carbide reactor fuels. The examination program to aid the evaluation of fuels is being carried out concurrently with the examinations of specific fuel specimens as requested by other contractors.

D. Determination of O_2 and C in Irradiated Reactor Fuels (C. S. MacDougall, M. E. Smith, T. K. Marshall, G. R. Waterbury)

For the determination of O_2 in irradiated fuels, a portable analytical system was fabricated and tested for measuring the CO and CO_2 evolved by reacting the O_2 in various types of samples with C at 2000°C. Following installation of a fused-silica furnace tube and auxiliary equipment in the hot cell facility, the analytical system was connected to the furnace exhaust line at the face of the hot cell. Initial tests of the RF generator for heating the furnace tube and crucible showed that the power output was more than adequate. Analyses of trial samples were started. Testing of the resistance furnace, fused-silica furnace tube, and other equipment, that had been installed in the hot cell for measurement of C, was deferred until the capability to analyze samples for oxygen was developed.

V. REQUESTS FROM DRDT

A. Examination of Irradiated Material (D. M. Holm, K. A. Johnson, J. W. Schulte, G. R. Waterbury)

Argonne National Laboratory (Idaho). Examinations of two EBR-II driver fuel elements containing AGC fuel were completed with the test described below, and Weekly Reports giving the results were sent to DRDT.

1. Nondestructive tests on fuel elements: Element 2249 from batch 100 was radiographed, tested by the eddy current method to detect the Na level and voids, and measured to obtain its length and diameter.

2. Chemical analyses of fuel and sodium: Concentrations of U, Mo, Ru, and Pd were determined in samples from the top, middle, and bottom of irradiated fuel pin 1682, and impurities were measured spectrographically in samples from the top and bottom halves of this fuel pin. Three metallographically polished sections from the pins were examined with the shielded electron microprobe. Metallic impurities in the Na taken from fuel element 1682 were determined by a semiquantitative emission spectrographic method.

Atomics International. Seven of the 120 UC pellets doped with W from NRX-9-101 Irradiation Experiment were examined metallographically, and replicas from six specimens from these pellets were prepared and sent to AI for evaluation. Gamma scans were completed on the 4 flux monitor wires, and seven 0.25-in. sections from each of the two Al-Co wires were analyzed radiochemically to measure the absolute specific activity of each section. Three samples were sent to Idaho Nuclear for burnup analyses. Reports of the results of all examinations were sent to AI. Proper disposal is being made of the irradiated materials from the experimental test.

Battelle Northwest Laboratory. The following types of samples were removed in an inert (Ar) atmosphere from each of the seven pins, designated PNL-X-1, 3, 4, 6, and 7 and PNL-1-16 and -18, and most of the items listed were shipped to BNLW: tube burst test samples -- 5; metallography sample -- 4; burnup sample-- 1; depleted UO_2 -- 2; Ni reflectors -- 1; miscellaneous hardware.

In addition, two tube burst test samples from each of five pins (BNW-1-9 and -11, and PNL-1-15, -17, and -19) and two fuel samples from PNL-1-19 were shipped to BNWL. Each of the tube burst test samples was packaged in an inert atmosphere in Swagelok fittings.

Metallographic examinations including macrophotography, alpha and beta-gamma autoradiography, optical metallography, and preparation of replicas were completed on one transverse section from each of the pins numbered PNL-1-15, -16, -17, -18, and -19, and PNL-X-1, -3, -4, -6, and -7, and BNW-1-9 and -11. Samples were prepared and examined in an inert (Ar) atmosphere.

Electron microprobe examinations were completed on a cross section from each of two pins, PNL-1-17 and BNW-1-11. Data reports were forwarded to the Sponsor as different phases of the work were completed.

Los Alamos Scientific Laboratory. Experimental capsules OWREX 12, 13, and 14, irradiated in the Omega West Reactor at LASL, were dissassembled in an inert atmosphere and visually examined. One fuel clad sample from OWREX 12 and four from OWREX 13 were examined metallographically to include macrophotography, alpha and beta-gamma autoradiography and optical metallography.

The following operations were performed on experiment OWREX 14: gamma scan, radiography, capsule sectioning, and Na removal from pellets by heat and dissolution. Because the fuel pellets were cracked it was not possible to remove a 1/16-in. diam core by drilling as planned. The core was to have been examined radiochemically to evaluate the "skin effects" produced in thermally irradiated (U, Pu)C pellets.

Experiment OWREX 15 was received in June; nondestructive tests will start in July 1970.

Nuclear Materials and Equipment Corporation. The following operations, examinations, and measurements were completed on NUMEC B-1, -9, and -11 capsules and pins: (1) visual inspections, (2) contamination, radiation, and temperature measurements, (3) radiography, (4) diameter measurements, (5) cover and fission gas analyses, (6) macrophotography, (7) profilometry, (8) gamma scanning, and (9) density measurements. Metallographic examination, including alpha and beta-gamma autoradiography are in progress. Removal of the capsule cladding and Na, sectioning of the pins, and several of the examinations were carried out in an Ar atmosphere. A section of capsule cladding in the vicinity of a breach in the pin cladding was slit longitudinally, the Na removed, and detailed macrophotography was done on the interior surface of the cladding. At the request of the experimenter, diameter measurements of the spiral wrap wire from NUMEC B-1 pin were made remotely with a micrometer.

Data reports were forwarded to NUMEC and DRDT as various phases of the work were completed.

United Nuclear Corporation. Examinations of ten fuel pins or sections received from UNC were completed by performing the tests, measurements, or operations listed briefly below. Partial examinations of UNC-87, -89, and -90, including operations 1 through 7 below, had been completed and reported earlier. Examinations of these three pins were finished and complete examinations were made on UNC-81, -82, -83, -84, -85, -86, and -101.

1. Visual inspection and photography
2. Measurements of contamination and radiation
3. Measurements of temperature
4. Radiography
5. Micrometer measurements
6. Gamma Scanning
7. Profilometry
8. Analyses of cover gas in capsules and fission gas in pins
9. Sectioning in an inert (Ar) atmosphere
10. Measurements of density by immersion method
11. Metallographic examinations including macrophotography, alpha and beta-gamma autoradiography, and optical metallography on the samples listed below and also on one plenum cladding specimen from UNC-87.

Element No.	Number of Samples of Nb Disks	Number of Samples of Fuel Cladding Specimens
UNC-81	1	4
UNC-82	-	5
UNC-83	-	6
UNC-84	-	2
UNC-85	-	2
UNC-86	-	3
UNC-87	2	4
UNC-89	4	4
UNC-90	4	4
UNC-101	-	4

12. Electron microprobe examinations on cross sections from UNC-87, -89, and -90.

13. Radiochemical measurement of absolute specific activities of 18 Fe flux monitor wires.

14. Preparation of a replica of the surface of one fuel-cladding specimen from each pin.

15. Shipment of samples for burnup measurement to Idaho Nuclear Corporation.

Examinations of four additional pins (UNC-125, -126, -127, and -128) are in progress. Operations 1 through 5 are completed on each pin at this time. Data report have been sent to UNC and DRDT as the various phases of the examinations were completed.

Westinghouse Atomic Reactor Division. Gamma scanning of three irradiated fuel capsules (W-1-G, W-2-G, and W-3-G) was completed and the final reports of the data were sent to WARD and DRDT. The three capsules and a sample of unirradiated Al-Co wire identical to that used as a flux monitor on the capsules were shipped to ANL (Illinois) in accordance with the decision of DRDT to have these Na-bonded fuel pins examined at that Site.

VI. EXAMINATION OF UNIRRADIATED FUELS
(J. A. Leary, G. R. Waterbury, E. A. Hakkila, R. T. Phelps, K. A. Johnson)

Battelle Northwest Laboratory

The following tests and analyses were performed on pellets from BNWL mixed-oxide fuel batches ME-20 and ME-21 (representing fuel elements PNL-X-1, -3, -4); metallography, alpha-autoradiography, spectrochemical, U, Pu, and O analyses, electron microprobe, weights, measurements, mechanical and immersion densities and powder x-ray diffraction.

These results have been reported in document CMB-11-9602. Copies were sent to AEC/RDT and BNWL.

United Nuclear Corporation Oxides

The following tests and analyses were performed on pellets from UNC mixed-oxide fuel batches, UN-OX-14, -18, and -19; metallography, alpha-autoradiography, spectrochemical, U, Pu, and O analyses, electron microprobe, weights, dimensions, mechanical and immersion densities, and powder x-ray diffraction.

These results have been reported in CMB-11-9511. Copies were sent to AEC/RDT and UNC.

United Nuclear Corporation Carbides

$(U_{0.8}Pu_{0.2})C$ pellets from UNC batches 13-4, G, and I were examined. Chemical analyses, metallography, and electron microprobe examinations were performed. Results were reported in document CMB-11-9603, June 18, 1970. Copies were sent to AEC/RDT and UNC.

Westinghouse ARD Carbides

Seven unirradiated pellets of $U_{0.8}Pu_{0.2}C_{1+x}$ were examined for WARD. These specimens were typical samples from WARD Batches 535, 536, 539, 548, and 549. Pellet densities were determined, followed by metallography, microhardness, and electron microprobe examination. Results have been summarized in document CMB-11-9604. Copies were sent to AEC/RDT and to WARD.

VII. REFERENCES

1. Jessup, R. S., J. Appl. Phys, 13, 128 (1942).

2. West, E. D. and Churney, K. L., J. Appl. Phys., 39, 4206 (1968).

3. Oetting, F. L., Paper in Publication

VIII. PUBLICATIONS AND PAPERS PRESENTED

"Containment Boxes for Plutonium Fuels Examination," C. D. Montgomery, 17th Conference on Remote Systems Technology (American Nuclear Society) December 1-4, 1969, San Francisco, California.

"X-ray Fluorescence Spectrometric Determination of Plutonium and Zirconium in Uranium Base Alloys," R. G. Hurley, E. A. Hakkila and G. R. Waterbury, 13th Conference on Analytical Chemistry in Nuclear Technology, September 30 to October 2, 1969, Gatlinburg, Tennessee.

"X-ray Spectrometric Determination of Rhodium and Palladium in Uranium Base 'Fissium' Alloys," E. A. Hakkila, R. G. Hurley and G. R. Waterbury, 13th Conference on Analytical Chemistry in Nuclear Technology, September 30 to October 2, 1969, Gatlinburg, Tennessee

"X-ray Spectrometric Determination of Rhodium and Palladium in Uranium-Base 'Fissium' Alloys," E. A. Hakkila, R. G. Hurley, and G. R. Waterbury, LA-4438, 1970.

PROJECT 462

SODIUM TECHNOLOGY

Person in Charge: D. B. Hall
Principal Investigator: J. C. Biery

I. INTRODUCTION

For the successful operation of high temperature sodium systems contemplated for use in fast, central station reactor concepts, impurities in the sodium must be monitored and controlled. Nonradioactive impurities such as oxygen must be maintained at low concentration levels to limit corrosion processes. To control the levels of these impurities, a knowledge of their behavior and interactions in sodium must be developed.

The sodium technology program at LASL included the control and monitoring of impurities with precipitation processes and design of equipment to sample sodium cover gas at operating temperatures.

The LASL sodium program is being terminated as of the end of this fiscal year. This report summarizes the results of the program during the past year. The active projects during the period were:

A. Study and Design of Precipitation Devices
   1. Study of Plugging Meter Kinetics

B. Sampling and Analysis
   1. Development of a High Temperature Quadrupole Mass Spectrometer for Cover Gas Analysis
   2. Total Carbon Analysis Development

The following projects were being phased out about midyear because of funding reductions and were reported on as the final data were generated and analyzed.

C. Phaseout Programs
   1. Study of Carbon Transport in Thermal Convection Loops
   2. Study of Gas Diffusion Through Metals
   3. Study of Soluble Getters in Sodium
   4. Study of Sodium Leaks
   5. Development of Remotely Operated Distillation Sampler for EBR-II
   6. Analysis of Dynamic Cold Trap Performance

II. STUDY AND DESIGN OF PRECIPITATION DEVICES

A. Study of Plugging Indicator Kinetics

(J. C. Biery, D. N. Rodgers, W. W. Schertz, J. L. Bacastow)

1. General

Plugging meters have been used on sodium systems for many years. They are relatively simple to design, install, and operate; however, the meaning of the data obtained from these instruments has not always been clear, and, as a result, the value of the instrument has sometimes been questioned in the past. Previously reported LASL work[1] indicates, however, that the plugging meter is a valuable instrument and that it can be used with confidence. The three areas of investigation indicated below should be continued in order to better understand and use the meter.

(a) Characterization of the plugging indicator's dynamic behavior with type of impurity.

(b) Studies of orifice configurations and materials to improve nucleation and dynamic characteristics at low concentrations (~1 ppm or less range).

(c) Development of a prototype plugging indicator system incorporating the research results of (a) and (b).

2. Results During FY 1970

The plugging meter research program at LASL was conducted in two loops; Plugging Indicator Loop No. 1 (PIL-1), formerly named Analytical Loop No. 2, and Plugging Indicator Loop No. 2 (PIL-2), formerly named Cold Trap Loop. The characteristics of the two loops are summarized in a previous quarterly report.[2]

(a) Research in Plugging Indicator Loop No. 1 - (PIL-1)

During the year PIL-1 was filled with sodium and put into operation. For approximately six months

the characteristics of the loop were studied with vacuum distillation analysis, gas chromotography and the plugging indicator. The characteristics of this startup procedure are summarized in an earlier LASL quarterly report.[3]

The main research effort with the loop occurred in the last quarter of FY 1970. A series of runs were made in which the characteristics of the plugging indicator were studied as increasing amounts of oxygen were added to the system. Before oxygen was added, the system was cold trapped at 99°C for approximately two weeks. A vacuum distillation measurement after the cold trapping indicated residual impurities equivalent to 0.85 ppm of oxygen.

Oxygen was added by introducing metered amounts of gaseous oxygen to the side loop servicing the vacuum distillation sampler. The oxygen stream was cold trapped in a dry ice-acetone bath before being introduced to the space above the flowing sodium in the sampler. The flow in the sampler was reduced to a low level to produce the maximum amount of sodium-wetted surfaces for reaction with the oxygen. Solid dendrites were observed to grow outward from the sodium-wet walls as the oxygen-sodium reaction proceeded. The color of the dendrites varied from grey or black to a light green. The dendritic solids were then dissolved into the system by increasing the liquid flow in the sampler and raising the sodium level well above the normal cup overflow level. The dissolution of all solids into the sodium required up to four hours.

In total, 37.1 ppm of oxygen were added to the 45.7 gal of sodium. The first additions were made successively in 0.7 ppm increments. The final addition was 12.6 ppm. In all cases, the amount of oxygen found in the sodium (by analysis) was less than that added. In the initial additions no changes in oxygen concentration could be detected on the plugging meter or by vacuum distillation. In the middle additions, approximately one-third of the oxygen appeared in solution and of the final 12.6 ppm added, a 9.2 ppm increase in concentration was noted by the plugging indicator. (The linear Rutkauskas curve was used with the plugging indicator saturation temperature.)[4] The oxygen that disappeared was probably adsorbed on the walls of the stainless steel tank and tubing.

The plugging meter was highly sensitive to the onset of precipitate growth in the orifices for two reasons: 1) The EM meter used to monitor the flow produced an easily read signal of 8.3 mV/gpm, about four times the sensitivity of meters utilized earlier. 2) The flow through the plugging meter circuit was adjusted by a separate d.c. pump, instead of the usual method of an upstream throttling valve. This latter feature enabled flow to be adjusted for proper heat transfer in the orifices without complications caused by division of available ΔP across two throttling devices. With this increased sensitivity of the plugging meter to changes within the orifice, new phenomena were observed as oxygen was added to the system. For discussion, these observations can be divided into three categories: 1) Detection of impurities with saturation temperatures below 105°C. 2) Detection of multiple impurities. 3) Determination of precipitation and dissolution rates as a function of concentration driving force.

(1) Detection of impurities with saturation temperatures below 105°C

After cold trapping at 99°C, the effective saturation temperature of the system appeared to be near 100°C. This temperature was determined by running long-term (8-15 h) constant temperature runs at 99-100°C. A precipitate would grow slowly on the orifice. If the runs were made above 100°C, no precipitate would grow in this period of time.

However, when this precipitate was slowly dissolved off, it did not completely dissolve at 105°C but required temperatures as high as 175°C to remove all of the precipitate. The explanation of this observation appeared to be that impurities (other than oxygen) with low concentrations (1 ppm or less) but relatively high saturation temperatures (up to 175°C) existed in the sodium. The concentration of these impurities was low enough to prevent nucleation and growth of the individual impurity on the orifice at temperatures above 105°C. Below this temperature, other impurities with low saturation temperatures but with significant concentration (above 1 ppm) did precipitate and co-precipitate the high temperature impurities with them. However, on dissolution the high temperature impurities would not dissolve until its individual saturation temperature was exceeded. This high temperature dissolution was the first indication that the system contained many low concentration impurities other than oxygen.

(2) Detection of multiple impurities with the Plugging indicator

As oxygen was added to the system a plug was more readily formed and the pseudo-saturation temperature steadily increased. However, as the temperature was oscillated about the pseudo-saturation temperature the maximum and minimum in the flow curve for each oscillation did not indicate the same saturation temperature as they should if the system contained only one impurity. Also, the flow curve was very irregular and contained many secondary inflection points. Finally, after carefully investigating the stability of the flow system, this "noise" on the flow curve was determined to be associated with phenomena occurring in the orifice.

To check the characteristics of the noise, the temperatures associated with each small maximum and minimum on the curve were recorded for each temperature oscillation. Thus, the dissolution and precipitation characteristics of the plug were scanned periodically by varying the orifice temperature in slow oscillation about the pseudo-saturation temperature. These temperatures were recorded and a frequency function was formed by determining the frequency that a given temperature appeared in 20 or more half-cycle scans of the plug. The resulting frequency plot versus temperature was not random in nature but contained well defined peaks with very sharp resolution. (The peak heights with an 0.0-1.0 possible maximum range varied between 0.25 and 0.60; the valleys between peaks range between 0.0 and 0.11; and the peak bases varied between 2-4°C in width.) If no oxygen was added to the system between determinations, the frequency charts could be reproduced day after day with the same size peaks in the same positions.

Each peak is thought to be associated with an individual soluble specie in the sodium. The peak occurs at the saturation temperature of the specie. The temperature scans indicated that there were at least 30 such species. As oxygen was added to the system, some of the peaks shifted position while others remained fixed. The nature and numbers of the shifting peaks (oxygen-associated) has not as yet been determined. (The data are still being processed.) However, many of the peaks did not shift, and thus, these impurities are not oxygen-related or are at least not in equilibrium with the soluble oxygen in the sodium.

(3) Determination of precipitation and dissolution rates as a function of oxygen concentration

After a sufficient amount of oxygen was added to the system, the rate of formation and dissolution of the plug was dominated by the effects of oxygen. Near the saturation temperature, the effects of the other impurities became small as the oxygen concentration increased. In this state the rates of precipitation and dissolution were studied with constant temperature plugging indicator runs. In both cases these rates are a function of the concentration driving force. By using data obtained within a narrow band of plug fractions (0.50-0.70), the effects of velocity and plug characteristics were made small in comparison to the effects of concentration driving force. In this case, the log of observed rate, R, should be a linear function of reciprocal obsolute temperature if the solubility curve is also a similar function of absolute temperature. This relationship can be seen from Eqs. 1 through 4.

$$R = kaA(C-C_e) \tag{1}$$

where $$C_e = Ke^{-\Delta H/RT} \tag{2}$$

$$A = A_{BO}\sqrt{1-P_f}$$

let $$R' = kaA_{BO}C$$

then

$$ln\left(R' - \frac{R}{\sqrt{1-P_f}}\right) = ln\left(kaA_{BO}K\right) - \frac{\Delta H}{RT} \tag{4}$$

where R = precipitation or dissolution rate

ka = mass transfer coefficient

A = precipitation area in orifice

C = impurity concentration in sodium

C_e = impurity saturation concentrations at temperature of orifice

K = solubility constant

ΔH = heat of solution of impurity

T = absolute temperature

R = gas constant

A_{BO} = precipitation area of bare orifice

P_f = plug fraction of orifice cross sectional area covered by plug

Thus a plot of $R' - R/\sqrt{1-P_f}$ versus 1/T on semilog paper should produce a straight line with the proper choice of R'.

The rate data obtained with the oxygen concentration near 19 ppm was processed with the above procedure. The proper choice of R' was determined

by trial and error. The data did produce a straight line over the temperature range of 200-250°C. The slope of the curve gave a ΔH of solution equal to 19-20 kcal/mole. This number compares with 16 kcal/mole determined by Rutkauskas.[4] The slightly steeper slope should be expected since the sodium appears from this work to contain many other impurities which would bias vacuum distillation results to slightly high values in the low concentration range.

(b) Research in Plugging Indicator Loop 2 - (PIL-2)

Some work was completed in which five or more impurities were studied. However, the termination of the program forced the research in the loop to be stopped before definitive results could be obtained. Before the end of the fiscal year, the loop was dismantled and discarded.

The plugging indicator was sectioned after dismantling. No corrosion of the holes could be observed. However, a small crystalline deposit of copper was found in the orifices and on the orifice plate. Copper was probably in the system from broken UNC electrolytic cells which contain a Cu-CuO reference junction.

III. SAMPLING AND ANALYSIS

A. Development of a High Temperature Quadrupole Mass Spectrometer for Cover Gas Analysis
(J. P. Brainard, C. R. Winkelman)

1. General

The purpose of this research was to develop a method for continuous on-line analysis of high temperature (up to 650°C) cover gas in an LMFBR. The analyzer had to be capable of detecting impurities such as nitrogen, oxygen, hydrogen, carbon dioxide, methane, and fission products in the cover gas with a sensitivity varying from the part-per-million range to the percent range. A response time of about 1 min was necessary if the analytical data are to serve as an error signal for activating devices for continuous control of cover gas composition.

A quadrupole mass spectrometer was obtained in order to meet the above requirements. It is believed that reasonably representative sampling can be accomplished by transporting the sample gas in sodium loop containment materials and at sodium loop temperatures until it has passed through the spectrometer for analysis.

2. Results During FY 1970

The analyzer design was completed and assembly was almost complete before the project was terminated. The unit was expected to have very high sensitivity and a high signal to noise rate because of two characteristics of the analyzer: 1) The high-temperature gas was to be charged into the analyzer as a molecular beam. Thus, the problems of elution of gases on the walls of the unit would be greatly reduced. 2) The beam was to be chopped to produce an intermittent signal. By locking onto the frequency of the chopped beam, additional noise in the output signal could be eliminated. The project was terminated before the unit could be completed, and, as a result, no data were obtained.

A report of the molecular beam work was published.[5]

B. Analytical Methods Development
(K. S. Bergstresser)

1. General

Refinements in the low-temperature combustion method of Kallman and Liu[6] were investigated with the objective of developing a practical method for measurement of carbon at the 1-10 ppm concentration range in metallic sodium used as a nuclear reactor coolant. This method avoids some problems of high temperature (1100°C) ignitions, but quantitative determination of low ppm concentrations of carbon following low temperature combustion requires development of reliable techniques for the formation of an aqueous solution of the oxidized carbon and sodium, separation of the trace amount of CO_2 from the acidified aqueous solution, and a very sensitive measurement of the CO_2 using a high-sensitivity gas chromatograph or other instrument.

2. Results During FY 1970

Two major efforts were made to solve the problem of separating and drying trace amounts of CO_2 from the large volumes of acidified solutions obtainec after oxidation of the sodium samples in a specially designed nickel vessel heated to 300-500°C. In one case, a bubbler tube, using a stream of helium in the form of fine bubbles, was used to remove the CO_2. Then the helium gas was dried partially with anhydrous $Mg(ClO_4)_2$ and more completely with an auxiliary chromatographic column. Quantitative removal of the moisture was necessary because it interfered serious-

ly with measurement of the CO_2 by the high sensitivity gas chromatograph selected for this purpose. In the other case, the entire solution of the oxidized sodium was acidified within the nickel combustion chamber, and measured portions of the gas phase were dried and analyzed for CO_2. In both cases, lack of control of the apparatus blank value made quantitative measurements impossible. This difficulty was the result of exposure of the inner surface of the combustion vessel to laboratory atmosphere at the beginning of each sample determination. The exposure, which occurred as the vessel was cleaned between analyses, produced a large, variable background in the carbon determinations. Further experimentation with the low temperature combustion method, therefore, was discontinued.

A brief investigation of a high-temperature ignition method was made to test a combination of equipment and operating conditions not used previously by other investigators. Oxygen was used for the combustion and also as a carrier gas to transport the CO_2 formed to a trap cooled in liquid N_2. The quantity of gas collected in the trap was measured manometrically at room temperature using an accurate pressure meter (MKS Baratron, Type 77). Blank determinations were uniformly equivalent to approximately 0.5 μg of carbon, and the method seemed promising. The investigation was terminated at this time, however, as a result of changes in the Sodium Technology Program.

IV. OTHER PROJECTS PHASED OUT IN FY 1970

Status of other programs which were phased out because of funding cuts are discussed below.

A. Study of Carbon Transport in Thermal Convection Loops

(J. C. Biery, J. R. Phillips)

1. General

Studies have indicated that the use of carbon beds may be useful in the gettering of ^{137}Cs in sodium systems. Carbon, however, is slightly soluble in sodium and can carburize austenitic stainless steels and refractory metals. Therefore, the purpose of this study was to determine the conditions, if any, under which carbon mass transfer rates are sufficiently low to allow the use of carbon beds in a sodium system.

The carbon transfer rates from carbon rods were being studied in thermal convection loops. The Type 304 stainless steel loop itself is serving as the carbon sink.

2. Results During FY 1970

Before the run was terminated, 8244 h of time were accumulated on the loop. A summary of time and temperatures is presented in Table I.

Table I

Temperature - Time Summary - Thermal Convection Harp

Number of Hours	Temperature - °C	
	Hot Leg	Cold Leg
336	485	455
1608	520	480
5700	510	450
360	330	130

The loop was destructively examined after termination of the run. Metallographic examination of the stainless steel tubing in the loop showed that no observable carburization had occurred. Also, the 1/4 in. dia carbon rod was removed and cleaned. It contained a number of small longitudinal cracks, but remained in one piece after cleaning in alcohol. Sodium had diffused into the rod and a 15% weight increase was observed. This sodium could not be removed by the alcohol leaching.

B. Study of Gas Diffusion Through Metals

(J. P. Brainard)

1. General

Very little quantitative information is available on the diffusion of gases in reactor system containment materials, although the phenomenon has been observed in several high temperature, liquid-metal-cooled systems. Diffusion of nitrogen through stainless steel in such systems may be misinterpreted as evidence of an air leak in the plumbing. If quantitative information on diffusion were available, the expected rate of nitrogen influx could be estimated, and the existence of small hard-to-find leaks might be substantiated or dismissed by comparing the expected and observed rates of nitrogen accumulation in the system.

2. Results During FY 1970

Nitrogen permeation through stainless steel experiments have been run with the temperatures at 278, 433, 545, 620, 715 and 780°C for periods of about five days each. No significant nitrogen permeation has been observed; the effective sensitivity of the instrument is such that a flow of about 10^{-6} Torr-cm^3/sec-cm^2 could have been detected. Using the permeation value of nitrogen through iron at 780°C, a flow of 10^{-2} is calculated for the dif-

fusion cell; the time to reach equilibrium is a few minutes. Either nitrogen permeation through stainless steel is much less than through iron (by a factor >10,000) or the light oxide coating formed on the diffusion cell when it was inadvertently exposed to air while at temperature is a very good barrier to N_2 diffusion.

C. Study of Soluble Getters in Sodium
(D. N. Rodgers, J. C. Biery)

1. General

For large sodium-cooled reactor systems, it may be desirable to use soluble getters for control of oxygen and other dissolved impurities in lieu of the more conventional hot and cold trapping techniques. The soluble getters of interest occur in the sodium coolant either naturally, as an impurity (calcium), or are produced during reactor operation (as with magnesium). The techniques for the controlled additions of these getters, maintenance of fixed getter levels, and the selective removal of depleted getter metals and other impurities from dynamic sodium systems must be developed if their usefulness is to be evaluated. The significant chemical reactions occurring in a sodium system containing these soluble getters must be understood and controlled. This mode of purity control has the potential for effectively controlling not only oxygen, but also carbon, hydrogen, nitrogen, and possible metallic impurities.

2. Results During FY 1970

All experimental work has been terminated, and a final report is in preparation. A summary of the results obtained from the project were presented in a previous quarterly[2] and a topical report.[7]

D. Study of Sodium Leaks
(J. P. Brainard)

1. General

The correlation of sodium leak development with measured helium leak rates observed during acceptance testing provides information on the degree of component integrity which must be attained for safe, long-term sodium plant operation. No firm criteria now exist that establish acceptable levels of leak-tightness for various situations.

This study used fabricated stainless steel leak and leaks that occur naturally in stainless steel bar stock. Selected samples having a range of helium leak rates were incorporated into small sodium systems (cells) held at a predetermined temperature until sodium leakage occurred. From these observations it may be possible to establish, for mass spectrometer acceptance tests on sodium system components, the maximum tolerable helium rate which is consistent with adequate long-term containment of sodium by that component.

An interesting side effect from this work has been observation of the elusiveness of what are considered to be large leaks (10^{-5} to 10^{-6} atm cm^3/sec). Normal fabrication contaminants such as grease, water and some solvents can completely mask leaks of this size and invalidate a leak test, unless proper pretreatment of the component is performed; and in some cases this can involve firing of the component in a hydrogen atmosphere. If meaningful helium leak tests are to be performed on LMFBR components, procedures must be developed for treating and handling of the part prior to leak test.

2. Results During FY 1970

Cells 1, 2 and 3 remained leak tight after 14,750 h at 400°C. Cell 4 (400°C) had about the same leak rate (2×10^{-2} cm^3 of sodium per day) as reported for most of the year; the rate was increasing slightly. The leak rate of Cell 8 (650°C) decreased by nearly a factor of 100, and there was no loss of nitrogen gas in the reaction chamber as previously reported. It may be that a reaction between the steel and nitrogen has formed a plug in the leak.

E. Development of a Remotely Operated Distillation Sampler for EBR-II
(E. O. Swickard, J. R. Phillips)

1. General

The original objective of the project was to produce three remotely-operated distillation samplers: one as a prototype, one for installation on the EBR-II primary loop, and one for installation on the EBR-II secondary. Because of program funding reductions, the objective was subsequently curtailed to the production of the prototype unit only.

The sampler was an engineering loop version of a laboratory model in use on Sodium Analytical Loop No. 1 and Plugging Indicator Loop No. 2 at LASL. Samples were taken from a continuously flowing bypass stream. The sampler was fabricated from Type 304 stainless steel, and energy for sodium evaporation was supplied by induction heating.

2. Results During FY 1970

The prototype sampler was not completed because of midyear funding reductions.

F. Analysis of Dynamic Cold Trap Performance
(J. C. Biery, W. W. Schertz, D. N. Rodgers)

1. General

In sodium coolant systems for future LMFBR's it will be necessary to use cold traps for removal and control of oxygen and other contaminants. These cold traps should be designed to handle adequately the impurity loads and to maintain the impurity concentration level below some specified upper limit. For economic reasons, cold traps must be as small and simple as possible, while still satisfying the design requirements.

Knowledge of the mechanism of impurity deposition in cold traps is necessary to reach the optimum design for a given sodium coolant system. The rate of mass transfer of impurity species to cold trap surfaces must be measured and the effect of various flow patterns, surface conditions, and temperature on the mass transfer rates must be determined. The purpose of this study was to determine the effect of the above variables on the mass transfer coefficient for removal of oxygen from sodium systems. Knowledge of the mechanisms involved and the mass transfer coefficients will allow calculation of the rate of oxygen removal and the location of deposited oxides in the cold trap for any given system size and cold trap geometry. Proposed cold trap designs could be evaluated in terms of total oxide capacity and expected system cleanup rates.

Cold trap tests were conducted with a 60-gal sodium system which has analytical capabilities including a vacuum distillation sampler, a plugging indicator, and two UNC oxygen meters. The cold trap tests consisted of measurement of the rates of change of oxygen concentration in the system. Various cold trapping conditions of temperature and flow rates were tested to determine the effect of these variables on the oxygen removal rates. When the rate of change of oxygen concentration, the cold trap temperatures and the deposition surface area is known, an overall mass transfer coefficient can be calculated.

2. Results During FY 1970

Cold trap research in the Cold Trap Loop was terminated in October, 1969, after finishing a series of runs with the packed trap; the data have not been analyzed. An attempt was made to drain the trap and pull out its removable core. The attempt failed because of sodium leakage through an isolation valve. As a result, the impurity deposits on the trap were dissolved off and lost.

Flushing off deposited impurities on the walls of the gas space in the loop produced a large increase in impurity concentration in the loop. These deposits represented an impurity source that has not been taken into consideration in the cold trap calculations. Steady state runs at low cold trap temperatures have shown the influx of impurities from this source to be very small and probably not significant in the calculations of mass transfer coefficients. However, for similar type research where impurity balances are made, attempts should be made to remove deposits that accumulate above the gas-liquid interface.

The computer simulation results of the cold trap research program has been published.[8]

V. REFERENCES

1. C. C. McPheeters and J. C. Biery, "The Dynamic Characteristics of a Na_2O Plugging Indicator," Nuclear Applications, 6, pp 573-81, June, 1969.
2. "Quarterly Status Report on Advanced Plutonium Fuels Program," July 1 to September 30, 1969, Report LA-4307-MS, Los Alamos Scientific Laboratory.
3. "Quarterly Status Report on Advanced Plutonium Fuels Program," October 1 to December 31, 1969, Report LA-4376-MS, Los Alamos Scientific Laboratory.
4. V. J. Rutkauskas, "Determination of the Solubility of Oxygen in Sodium Using the Vacuum Distillation Analytical Technique," Report LA-3879, Los Alamos Scientific Laboratory.
5. J. P. Brainard, "Molecular Beams from Long Parallel Tubes," Report LA-4280-MS, Los Alamos Scientific Laboratory.
6. S. Kallmann and R. Liu, "The Determination of Total Carbon and Sodium Carbonate in Sodium Metal," Anal. Chem. 36, 590 (1964).
7. D. N. Rodgers, G. E. Meadows and J. C. Biery, "Calcium As a Soluble Getter for the Control of Oxygen in Sodium Systems," Report LA-4436, Los Alamos Scientific Laboratory.
8. B. C. Goplen, J. C. Biery and C. C. McPheeters, "Numerical Simulation of a Cold Trap for Sodium Purification," Report LA-4435, Los Alamos Scientific Laboratory.

PROJECT 463

CERAMIC PLUTONIUM FUEL MATERIALS

Person in Charge: R.D. Baker

Principal Investigator: J.A. Leary

I. INTRODUCTION

The principal goals of this project are to prepare pure, well characterized plutonium fuel materials, and to determine their high temperature properties. Properties of interest are: (1) thermal stability, (2) thermal expansion, (3) thermal conductivity, (4) phase relationships by differential thermal analysis, (5) structure and phase relationships by X-ray diffraction, high temperature X-ray diffraction, neutron diffraction and high-temperature neutron diffraction, (6) density, (7) hardness and its temperature dependence, (8) compatibility, including electron microprobe analysis, and (9) compressive creep (deformation).

II. SYNTHESIS AND FABRICATION

(R. Honnell, C. Baker, W. Hayes, G. Moore, and R. Walker)

A. Carbide Samples for Properties Measurements

A number of different uranium, plutonium, and mixed carbide compositions were synthesized, characterized, and fabricated into test specimens for physical property measurements. Figure 463-1 is a photograph of typical (U, Pu)C test specimens presently being used in the program. The two pellets at the top are specimens for EBR-II irradiations, on the right is a thermal conductivity sample, at the lower right is an EMF specimen, at the lower left is a DTA sample, on the left is a compressive creep specimen and the large disc is a hot hardness sample.

B. (U, Pu)C Pellets for EBR-II Irradiation

Well characterized (U, Pu)C fuel pellets for EBR-II irradiation experiments and compatibility testing were prepared using the following basic process steps:

1. Multiple arc melting of weighed charges of U, Pu, and C using a graphite electrode.
2. Solution treatment of the arc melted button for 24 h at 1600°C.
3. Comminution of the button in a WC vibratory mill to a particle size range ≤ 62 μ.

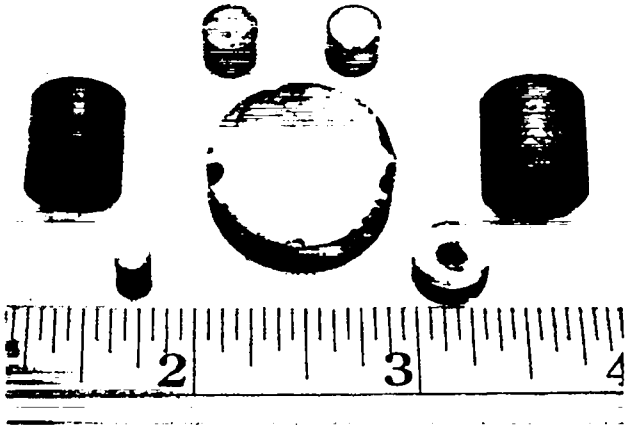

Figure 463-1. Typical (U, Pu)C test specimen

4. Elimination of higher carbides by reaction with H_2 at 850°C.
5. Cold compaction at 15 tsi into pellets without the use of binders or sintering aids.
6. Sintering the pellets in Ar at 1800°C for 8 h followed by 1400°C heat treatment for 2 h.
7. Characterization of the pellets by linear dimensioning, weighing, metallography, X-ray diffraction analysis, chemical analysis for U, Pu, C, N, O, and trace impurities, radiography for the determination of possible internal cracks and isotopic analysis of uranium and plutonium.

Eighty-three (^{233}U, ^{239}Pu)C pellets for irradiation testing in the EBR-II were prepared and characterized using the procedures described. Weighted averages were calculated from the analytical results obtained on the 8 lots from which the pellets were selected. These are tabulated in Table 464-I.

Table 464-I

COMPOSITION OF (^{233}U, ^{239}Pu)C PELLETS
(weighted averages)

U	75.3 w/o	^{233}U	97.15 w/o
Pu	19.46 w/o	^{234}U	1.19 w/o
C	4.73 w/o	^{235}U	0.46 w/o
Fe	53(a)	^{238}U	1.12 w/o
Si	78	^{239}Pu	94.22 w/o
Cu	10	^{240}Pu	5.42 w/o
Mo	47	^{241}Pu	0.31 w/o
W	32		
N	534		
O	404		

Immersion Density = 12.71 g/cm^3
Lattice Constant = 4.9634 Å

(a) All values reported in ppm by weight unless noted

Other trace impurities identified in some of the pellet lots were 30 ppm Ni, 20 ppm Al, 8 ppm Na, and 5 ppm Ca. All other elements were below the limit of detection. Metallographic examination showed that 6 of the pellet lots representing 57 pellets contained a small amount of grain boundary precipitate (0.1 v/o or less). The remaining 2 pellet lots were single phase MC. Also, it should be noted that the processing of ^{233}U into pellets did not introduce a serious radiation handling problem at the present level of operations. The gamma dose from a 60 gram alloyed button prepared from newly separated ^{233}U metal increased from 15 to 175 mr/h on contact over a 3 month interval.

Pellets with varying carbon contents were prepared and characterized for the purpose of determining the compatibility of hyperstoichiometric (U, Pu)C material composed only of monocarbide (MC) and sesquicarbide (M_2C_3) phases with potential fuel clad and metal coolant systems. Process procedures were the same as previously described, with the exception that the sintering temperatures were held between 1550 and 1525°C for intervals of 24 to 33 hrs. The pellets were sampled by lot and subjected to chemical and physical analyses. The results from these analyses are tabulated in Table 463-II and III. Metallographic examination of the sintered pellets indicates that they are quite porous and contain 3 phases. The two major phases appear to be MC and M_2C_3. This is corroborated by X-ray diffraction measurements. The third phase is very minor and acicular in shape. Because of particle size and the small quantity present, identification of the acicular phase is impossible by either X-ray powder diffraction or microprobe analysis.

Two hundred twenty-four (^{235}U, ^{239}Pu)C pellets for irradiation and compatibility testing were also prepared and characterized. Weighted averages calculated from pellet lot analytical results are given in Table 463-IV. Other trace impurities detected in some of the pellets but not listed in the table were 20 ppm Al, 35 ppm Ni, 20 ppm Cr, 5 ppm Ca, 10 ppm V, and 20 ppm Zn. All the pellets in this group had a density of 12.70 g/cm^3 or higher. Metallographic examination of randomly selected pellets from each pellet lot comprising the group showed the microstructures to be single phase monocarbide with or without a grain boundary precipitate of 0.1 v/o or less. The chemistry of similar precipitates

Table 463-II

CHARACTERISTICS OF MC_{1+x} PELLETS

Lot Number	Lattice Parameter, Å		Immersion Density, g/cc
	MC	M_2C_3	
HNL 8-36-1	4.9643	8.0986	11.86
HNL 8-36-2	4.9628	8.0970	12.03
HNL 8-38-1	4.9619	8.0967	10.61
HNL 8-38-2	4.9633	8.0953	10.35
HNL 8-40-1	4.9555	8.0941	10.23

Table 463-III

CHEMICAL COMPOSITION OF MC_{1+x} PELLETS

Element	Lot No. HNL 8-36-1	HNL 8-36-2	HNL 8-38-1	HNL 8-38-2	HNL 8-140-1
U	76.5 w/o	76.1 w/o	76.3 w/o	75.6 w/o	75.4 w/o
Pu	18.33 w/o	18.61 w/o	18.41 w/o	18.62 w/o	18.38 w/o
C	5.32 w/o	5.46 w/o	5.58 w/o	5.78 w/o	6.02 w/o
Al	--	10	--	--	--
Si	30[a]	12	40	25	10
V	(b)	5	5	5	5
Cr	5	12	12	--	10
Fe	--	35	100	65	75
Cs	50	--	25	5	5
Cu	--	--	--	--	25
Zn	--	20	20	20	20
Ga	20	(b)	(b)	(b)	(b)
Mo	25	(b)	10	10	--
W	--	40	300	100	120
O	430	360	850	610	390
N	87	320	650	102	2200

(a) ppm by weight, unless otherwise specified
(b) Not reported
-- Below detectable limits

Table 463-IV

CALCULATED WEIGHTED AVERAGES OF (^{235}U, ^{239}Pu)C PELLETS

U	75.8 w/o	^{234}U	0.853 w/o
Pu	19.03 w/o	^{235}U	92.280 w/o
C	4.68 w/o	^{236}U	0.299 w/o
Fe	83[a]	^{238}U	6.51 w/o
Si	27	^{239}Pu	94.30 w/o
Cu	8	^{240}Pu	5.35 w/o
Mo	19	^{241}Pu	0.300 w/o
W	22		
N	435		
O	554		

Immersion Density = 12.91 g/cm^3
Lattice Constant = 4.9632 Å

(a) ppm by weight unless otherwise specified.

in (U, Pu)C pellets was identified as a 60 Pu - 40 U alloy with silicon and iron as major impurities and lesser amounts of Ni, Cr, Cu, and occasionally W.

III. PROPERTIES

1. Differential Thermal Analysis

(J.G. Reavis, L. Reese)

Differential thermal analysis studies of transformations of mixed uranium-plutonium dicarbides and of melting behavior of single phase (U, Pu)C compositions containing 0-50 mole % PuC have been completed. Thermal arrest temperatures and liquidus temperatures have been determined in the Pu-C system over the composition range $PuC_{0.75}$ to PuC_2. Samples of irradiated UO_2-25% PuO_2 have been examined in the new hot cell DTA apparatus.

(U, Pu)C Melting Behavior: Data describing the melting of (U, Pu)C solid solutions have been augmented by additional DTA and quenching experiments. A plot of observed solidus and liquidus temperatures is shown on Figure 463-2. Solidus and liquidus temperatures for UC are 2520 and 2540°C, respectively. Solidus and liquidus temperatures for $U_{0.80}Pu_{0.20}C$ are 2275° and 2485°, respectively. Uncertainties in these temperatures are ± 20°. The curves shown on Figure 463-2 are the calculated solidus and liquidus curves assuming ideal solution formation between UC and PuC. The heats of fusion of UC and PuC were assumed to be 20 kcal/mole and 10 kcal/mole, respectively. Other choices were considered but the above values lead to calculated transformation temperatures most consistent with observation. Using these assumptions, the heat of fusion of $U_{0.80}Pu_{0.20}C$ is calculated to be 18 kcal/mole with an estimated uncertainty of ± 5 kcal/mole. The heats of fusion involved in

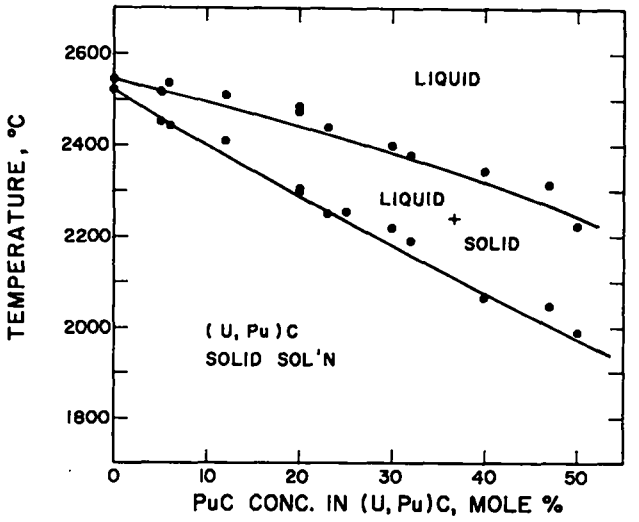

Figure 463-2. Melting behavior of U-Pu monocarbides

these calculations imply unexpectedly large values for the entropy of fusion of a diatomic compound.

Transformations of (U, Pu) Dicarbides: Additional DTA and X-ray powder diffraction analyses of quenched samples have allowed a more complete description of the (U, Pu)C_2 (excess C) phase fields to be made. The new plot is shown on Figure 463-3. Tentative identities have been assigned to the phase fields by use of X-ray powder diffraction results from quenched samples and by use of high temperature X-ray diffractometer results.[1] The PuC_2 to Pu_2C_3 + C transformation occurs at 1660 ± 10°C and the PuC_2(+C) solidus is 2230 ± 20°C. The heat of the PuC_2 to Pu_2C_3 + C transformation at 1660° was found to be 5 ± 1.5 kcal/mole of PuC_2 by comparison of DTA traces for PuC_2 with those for UC_2 which has a reported[2] α-β transformation heat of 2.9 kcal/mole.

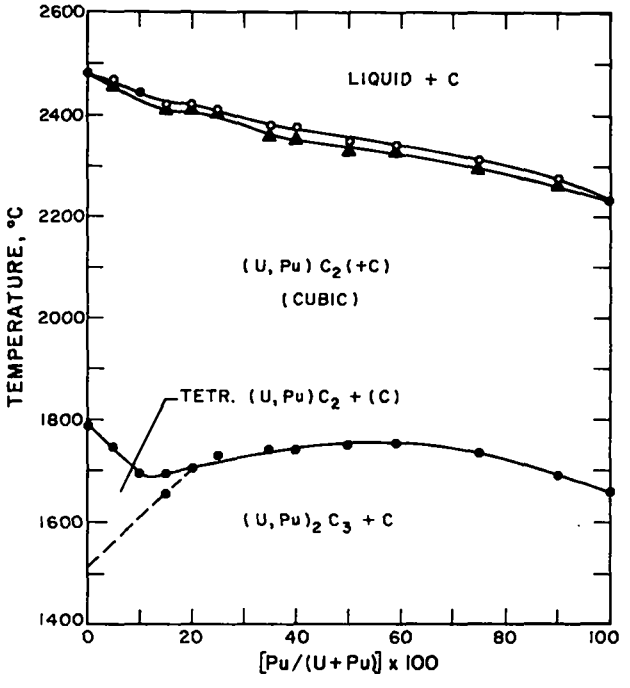

Figure 463-3. Transformation temperatures of U-Pu dicarbides

Transformation Temperatures in the Pu-C System: A large number of DTA observations and macro examinations of quenched samples have been made. A revised diagram of the Pu-C system is shown by Figure 463-4. Thermal arrests have consistently been seen at 1600 ± 10°C for compositions in the range $PuC_{0.85}$ to $PuC_{1.26}$. The transformation involved is believed to be the peritectic decomposition of the monocarbide to form liquid and sesquicarbide. Compositions between $PuC_{1.53}$ and PuC_8 showed thermal arrests at 1660 ± 10°C which are believed to be due to the PuC_2 to Pu_2C_3 + C transformation. Compositions in the range $PuC_{1.48}$ to $PuC_{1.94}$ exhibited arrests at 2010 ± 10°C which are believed to be due to peritectic decomposition of Pu_2C_3. Compositions in the range $PuC_{1.98}$ to PuC_8 showed arrests at 2230 ± 20°C which are attributed to peritectic decomposition of PuC_2.

Metallographic examination of samples quenched from the various phase fields revealed structures con-

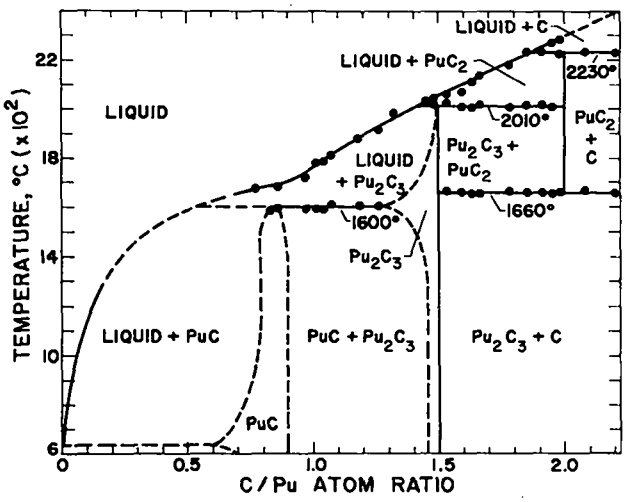

Figure 463-4. Transformations in the Pu-C system

sistent with the processes proposed in the preceeding paragraph and with the general form and phase field identities shown in Figure 463-4. No eutectics were seen, but quench rates were rather slow (~ 1000 deg/min above 1000°C, and slower at lower temperatures) and eutectoidal structures could have been lost during later stages of cooling. Due in part to the slow quenching rates, vertical phase boundaries of the three Pu-C compounds existing at temperatures above 1000° could not be located well.

Liquidus temperatures were determined for compositions in the range $PuC_{0.75}$ to $PuC_{1.98}$ by macro observations of specimens heated at rates of the order of 50 deg/min and quenched from selected temperatures. Carburized Ta crucibles were used as containers. The liquidus temperature was taken as the center of the range (~ 20° range) between the temperature at which a mound of material was found on the bottom of the crucible, and the temperature at which a smooth meniscus was found. Accuracy of temperature measurement was sacrificed by the rapid cycling procedure, but reaction between specimen and container was minimized. Ta concentration in samples after melting was generally 0.1 to 1%. This level of contamination probably did not significantly affect liquidus temperatures.

DTA of Irradiated Samples: The DTA apparatus in the hot cell has been used to examine irradiated fuel samples. Base-line data were obtained using unirradiated UO_2, UO_2-25% PuO_2 and $U_{0.80}Pu_{0.20}C$. This was considered necessary for two reasons. First, the thermal effects produced by small concentrations of fission products may be small enough to require an accurate base-line for comparison. Secondly, the window correction for optical pyrometry is so large (~ 500°C at an observed 2300°C) that a small fractional change with time can lead to a large error in temperature. The unirradiated samples, therefore, serve as secondary calibration standards. Oxide samples were contained in W crucibles and carbide samples were contained in carburized Ta crucibles. Both types of crucibles were covered by loose-fitting lids and the furnace was filled with Ar at ~ 0.5 atm pressure.

Serious experimental difficulties were experienced in DTA of irradiated samples. As the samples were heated, a film formed on the cooler parts of the furnace, including the window through which the light beam to the pyrometer and the DTA sensors emerged. This necessitated frequent interruption of thermal cycling to allow the window to be changed. At times, fouling of the window led to uncertainties in temperatures of the order of 100°C. During DTA of an irradiated $U_{0.8}Pu_{0.20}C$ sample, the furnace window was changed five times. A partial qualitative analysis of the deposits was made by counting with a gamma spectrometer. Cs activity dominated in samples vaporized up to 1800°C. Cs, Ba and Ce were equally prominent in the range 1800-2100°C, while Ce activity dominated in the range 2100-2430°C. Fission products which could not be detected by gamma counting were probably also present in the deposits.

Arcing of the induction-heated furnace was also a serious problem. It is believed that the presence of the volatile material aggravated this problem. Arcing results in variation in power input to the furnace, making thermal cycles nonlinear. This makes detection of valid arrests in T and ΔT curves difficult. It is estimated that a transformation must involve release or absorption of the order of 10 cal/g over a temperature range of 10°C or less to be detected under these conditions.

Samples were studied from 1300° to the solidus temperatures. No transformations were detected below the solidus temperatures. A summary of observed solidus and liquidus temperatures is given in Table 463-V. Although minor differences were noted between temperatures observed for irradiated and unirradiated samples of the same composition, these differences are less than the

Table 463-V

SOLIDUS AND LIQUIDUS TEMPERATURES OF FUEL MATERIALS

Composition	Irradiation Level, MWD/T[a]	Solidus, °C	Liquidus, °C
UO_2-25% PuO_2	0	2675 ± 25	2775 ± 25
UO_2-25% PuO_2	~ 9000	2750 ± 50	2825 ± 50
UO_2-25% PuO_2	~ 9000	2680 ± 25	——
$U_{0.8}Pu_{0.2}C$	0	2335 ± 25	——
$U_{0.8}Pu_{0.2}C$	60,000	2325 ± 50	>2430 ± 25

(a) EBR-II irradiation.

uncertainties. The error limits shown in Table 463-V should be taken as a measure of precision in this series of measurements and not as a measure of absolute accuracy. The number of observations in the hot cell has not been sufficient to allow evaluation of absolute accuracy.

2. Room Temperature X-ray Diffraction
(C.W. Bjorklund)

The results of the characterization of plutonium fuel materials by X-ray powder diffraction techniques have been incorporated in other sections of this report.

A precision linear comparator is now being used for many of the powder diffraction film measurements. This comparator was designed specifically for X-ray diffraction film measurements and is capable of direct readings to the nearest 0.001 mm. This may be compared to a maximum precision of ± 0.05 mm obtained with typical desk top film readers. Several modifications have been made to improve its usefulness for routine measurements. It is possible to add a photoelectric scanning device with automatic readout of line position and density similar to the equipment currently being used for measuring spectrographic plates. An evaluation of the potential usefulness of this capability is currently under way.

Additional measurements of self-irradiation damage induced lattice expansion have been made on the samples of plutonium compounds which have been stored in X-ray capillaries over a period of years. Very little deviation from the results reported previously has been observed. The lattice dimensions of plutonium compounds slightly enriched with ^{238}Pu remain constant within experimental error, and the dimensions of compounds of normal isotopic composition continue to increase slowly toward the predicted saturation values. No change in the quality of the X-ray patterns of any of the compounds has been observed over the past year.

3. High Temperature X-ray Diffraction
(J.L. Green and K.L. Walters)

Investigation of the high temperature crystallographic properties of materials associated with the carbon-rich fields of the U-Pu-C phase diagram is continuing.

The results of phase identification studies on the carbon-rich portion of the Pu-C binary and preliminary measurements of the thermal expansion of bcc Pu_2C_3 and fcc PuC_2 have been reported previously. The thermal expansion of these compounds has been redetermined and the final results are now available. Using material having a nominal composition of $PuC_{2.2}$, the lattice dimensions of Pu_2C_3 were determined as a function of temperature from room temperature to 1600°C. A plot of the results is shown in Figure 463-5. A least squares fit of these data yielded

$$\Delta a/a_o = (1.29 \pm 0.02 \times 10^{-5})\,(T-25) + (2.07 \pm 0.14 \times 10^{-9})\,(T-25)^2$$

where a is the lattice dimension in angstrom units and T is the temperature in °C. It may be seen from this figure that the high temperature lattice dimensions for carbon saturated Pu_2C_3 reported by Dalton[3] agree reasonably well with those from the present study. It should be noted, however, that the value reported in that study for 1700°C was necessarily determined under non-equilibrium conditions. The lattice dimension reported by Harper,[4] is substantially larger than the corresponding value from the present study. The lattice expansion for carbon deficient Pu_2C_3 has been reported for low temperatures by Rand[5] and Pallmer.[6] Although not strictly comparable, the results of these studies are

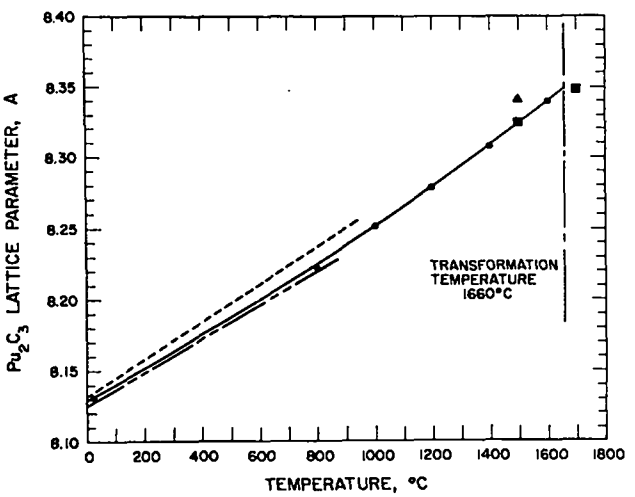

Figure 463-5. Lattice dimensions of Pu_2C_3 as a function of temperature. ———•———, this study; ■, Ref. 1; ▲, Ref. 2; — — — —, Ref. 3; ——— — — ———, Ref. 4.

included in Figure 463-5.

The results of lattice dimension measurements for fcc PuC_2 are shown in Figure 463-6. A least squares fit of these data yielded

$$\Delta a/a_o = (17.9 \pm 1.6 \times 10^{-6})\ (T-1660)$$

As may be seen from this figure, the lattice dimensions reported by Harper agree with those from the present study; however, that reported by Dalton is considerably larger. No expansion data for fcc PuC_2 are available for comparison, but Bowman[7] reported an average expansion coefficient of $25.2 \times 10^{-6}/^{\circ}C$ for fcc UC_2 over the temperature range from 1765°C to 2300°C.

The temperature at which the Pu_2C_3 to fcc PuC_2 transition occurs was determined to be 1660°C. This is the same as the value reported by Reavis[8] from DTA studies.

Studies of the mixed uranium-plutonium carbides have been begun with the composition $(U_{0.65}Pu_{0.35})C_{2.1}$. Using samples prepared from this material, thermal expansion data for carbon rich $(U_{0.65}Pu_{0.35})_2C_3$ have been obtained in the temperature interval from room temperature to 1700°C. The fractional expansion of this phase as a function of temperature may be represented by

$$\Delta a/a_o = (9.54 \pm 0.21 \times 10^{-6})\ (T-25) + (1.65 \pm 0.12 \times 10^{-9})\ (T-25)^2.$$

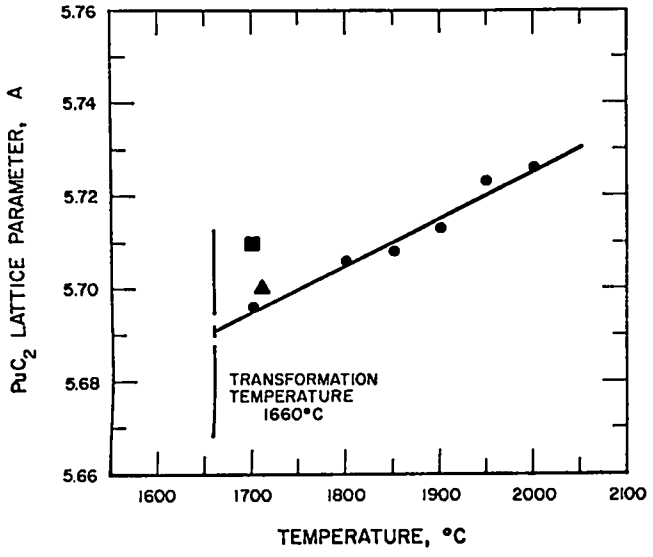

Figure 463-6. Lattice dimensions of PuC_2 as a function of temperature. ——•——, this study; ■, Ref. 1; ▲, Ref. 2.

This corresponds to an average thermal expansion coefficient over the temperature range from 25°C to 1700°C of $12.3 \times 10^{-6}/^{\circ}C$. This is somewhat smaller than the corresponding value of $16.4 \times 10^{-6}/^{\circ}C$ for Pu_2C_3. No single set of data has been published for U_2C_3 that covers this particular temperature interval. The average expansion coefficient for U_2C_3 over this temperature interval was estimated to be $10.3 \times 10^{-6}/^{\circ}C$ by using high temperature data reported by Bowman[7] and a lattice dimension of 8.088 Å for U_2C_3 at 25°C. These expansion coefficients appear to be a linear function of the Pu/U + Pu ratio. A small amount of high temperature data for $(U_{0.65}Pu_{0.35})_2C_3$ has been reported by Dalton.[3] Thermal expansion coefficients were not presented, but a value of $12.0 \times 10^{-6}/^{\circ}C$ for the temperature interval of interest can be estimated from the data that were presented. This is in good agreement with the results of the present study. Possibly, this correspondence should be considered somewhat fortuitous. The lattice dimensions reported by Dalton for higher temperatures agreed well with those from the present study. However, those reported for lower temperatures were considerably smaller than those from the present study. Agreement between expansion coefficients computed for lower temperatures would, therefore, be poorer than indicated above.

An independent determination of the sesquicarbide to cubic dicarbide transformation has been completed for $(U_{0.65}Pu_{0.35})C_{2.1}$. The transformation was observed to occur at $1735^{\circ}C < T < 1750^{\circ}C$. Differential thermal analysis data were not available for this particular composition; therefore, a sample was prepared and the transformation temperature was measured using that technique. The result was 1740 ± 5°C, which is in excellent agreement with the value reported above. Dalton[3] has reported that two face centered cubic $(U_{0.65}Pu_{0.35})C_2$ structures exist at high temperatures as stable species. Below 1900°C, no evidence of these phase changes was found in this study. Various asymmetric features were noted on dicarbide diffraction peaks during heating cycles, but if the sample were homogenized at high temperature, e.g., 1900°C, the

asymmetric components disappeared and did not reappear on slow cooling. These effects appear to be associated with transient composition changes occurring during the sesquicarbide to dicarbide transformation and subsequent homogenization.

Lattice dimensions for fcc $(U_{0.65}Pu_{0.35})C_2$ were determined between 1775°C and 1900°C. Data were gathered during cooling cycles after high temperature homogenization. The temperature interval is limited, but the estimated expansion coefficient is 20×10^{-6}/°C. This is intermediate to the values for PuC_2 and UC_2.

Several low intensity reflections not belonging to the sesquicarbide pattern have been repeatedly observed throughout the temperature range of stability of $(U_{0.65}Pu_{0.35})_2C_3$. Further, these lines have been found to be stable toward annealing. The two and occasionally three lines observed at lower temperatures were identified as belonging to bct dicarbide by comparison to patterns from quenched samples that contained positively identifiable amounts of the tetragonal modification. At 1550°C, these lines disappear and are replaced by two lines belonging to the fcc dicarbide. This identification is based on the fact that on further heating, the interplanar spacings for these reflections join smoothly with high temperature data for the fcc dicarbide. Study of the bct to fcc dicarbide transformation at 1550°C indicates that the phase change is reasonably rapid and reversible. Comparisons of peak heights for the fcc phase immediately above and below 1740°C indicate that approximately 8% of the dicarbide remains stable below that temperature. DTA techniques were used in an attempt to obtain a corroborative observation of the transformation at 1550°C. It is estimated that an energy release corresponding to approximately 5% of that associated with the dicarbide to sesquicarbide transformation would have been detectable. The transformation energy for the bct to fcc dicarbide transformation is estimated to be approximately 50% of that for the decomposition reaction; therefore, 10% of the sample would have to be involved before the transformation would be positively detectable. Since only approximately 8% of the sample was expected to be involved, the experiment was clearly marginal. On about half of the DTA cycles, irregularities were noted in the 1530-1545°C region; however, these were so faint that they could not be regarded as positive thermal arrests. This result can be interpreted as indicative but it does not constitute an independent observation of the transition. It does not appear that positive identification will be possible using DTA.

Annealing studies on a quenched sample of bct dicarbide showed that at approximately 500°C the dicarbide decomposed rapidly until an amount equal to that observed in slowly cooled samples was reached. Heating for an additional 5 hours at 500°C resulted in minor decreases in the dicarbide reflections. However, this observation was complicated by what appeared to be sample oxidation. It is not possible to conclude that the residual amount of dicarbide is stable at 500°C, but clearly, amounts in excess of that are unstable.

At present, the most reasonable interpretation of these observations appears to be that two three-phase fields exist at this composition which have not been previously reported. Between 1740°C and 1550°C the phases observed are the body centered cubic sesquicarbide, graphite and a small amount of the face centered cubic dicarbide. The field beginning at 1550°C and having an undefined lower boundary contains the sesquicarbide, graphite and a small amount of the body centered tetragonal modification of the dicarbide.

B_4C Structural Study

The summary of a recent attempt to characterize the powder diffraction patterns of various samples of B_4C reported[9] analytical difficulties in that experimental X-ray diffraction data could not be satisfactorily indexed in terms of the published structure[10, 11] for B_4C. The precise nature of the problem was not indicated. However, it was clear that the structure description of B_4C was considered to be in question. Similar difficulties have been reported by other investigators.[12] In other instances, no apparent attempt was made to index the back-reflection pattern even though the position of particular lines as functions of composition were reported.[13] No indexed, high angle line lists for experimentally observed powder patterns have been reported

in the literature. This apparent indexing difficulty may account, in part, for the fact that no high precision lattice parameters have been reported. Uncertainties regarding the basic structure must be eliminated before crystallographic data may be effectively used for properties studies or in routine materials characterizations.

In order to demonstrate that observed powder patterns are consistent with a particular structure, it is necessary to show first that observed line positions are proper and second that observed reflection intensities are those defined by the structural model. The first requirement shows that the reported size and shape of the crystal lattice is correct while the second shows that the atomic positions defined by the structure description are consistent with observations.

Neutron diffraction techniques have never been applied to the study of B_4C. It is possible that neutron data would be useful in certain areas of the problem. Neutron diffraction patterns characteristically have low resolution; therefore, studies of precise line positions are best carried out using X-ray techniques. The area in which neutron data would be most useful, is the study of reflection intensities. The accurate measurement of X-ray reflection intensities is a difficult problem; however, neutron intensities can be measured with good accuracy under appropriate experimental conditions.

The published structure description for B_4C is based on a rhombohedral unit cell containing 3 molecules and having symmetry corresponding to the space group $R\bar{3}m$. The 12 B atoms contained in the unit cell are located in two nonequivalent sets of 6 h special positions. The position parameters for these sets are such that the B sites are arranged in nearly regular icosahedral groups centered at each corner of the unit cell. The three remaining atoms are identified as C atoms which are arranged in a linear chain laying on the long [111] body diagonal of the rhombohedral unit cell. The two terminal members of the chain occupy 2c positions while the center atom is in the 1b position at the center of the diagonal. It should be noted that the published atomic position parameters for B_4C are refered to the 1935 edition of the International Tables. The hexagonal general position set given for the space group $R\bar{3}m$ is not the same as that given in the 1952 edition. The coordinate system used in the earlier tables are based on the reverse setting of the rhombohedral cell whereas the obverse setting is standard in the modern tables. For this reason, the published hexagonal parameters must be transformed before use with the modern position set or with computer programs utilizing symmetry generators based on the modern set.

Several samples of commercial grade, carbon-rich B_4C were obtained for use in the study. Debye-Scherrer powder diffraction patterns were obtained and analyzed. The patterns from the various samples appeared to be essentially identical. Therefore, numerical data will be reported only for the sample having the highest purity. The analytical data for this material is shown in Table 463-VI.

The powder patterns were taken using a 114.6 mm diameter Norelco Debye-Scherrer camera. Copper radiation was used; however, a 6×10^{-4} inch thick

Table 463-VI

B_4C ANALYTICAL DATA[a]

Pycnometric Density	2.52 gm/cm^3
Bulk Density	0.57 gm/cm^3
Tap Density	0.92 gm/cm^3

Element	Conc.[b]	Element	Conc.
B	75.9%		
C	21.8%		
O_2	0.76%		
N_2	320		
Li	< 10	Ni	< 30
Be	< 3	Cu	30
Na	< 100	Zn	< 100
Mg	< 3	Sr	< 30
Al	30	Zr	< 100
Si	300	Nb	< 300
K	< 300	Ag	< 3
Ca	< 30	Cd	< 30
Ti	< 300	Sn	< 30
V	< 100	Ba	< 30
Cr	< 30	W	< 300
Mn	10	Pb	20
Fe	500	Bi	< 10
Co	< 30		

(a) Supplied by Kawecki Chemical Co. (Lot No. 292-83).
(b) Chemical analyses reported as ppm by weight unless otherwise indicated.

internal Ni filter was used to eliminate the Kβ component. In order to enhance weak lines a large capillary (0.5 mm diameter) and relatively long exposures were used. This allowed most of the lines in the pattern to be recorded. It resulted in severe overexposure of several of the low angle lines, however, observed interplanar spacings and relative intensities are listed in Table 463-VII. The observed intensities were assigned by visual estimate relative to a 10 unit scale. These data are numerically meaningful only in the sense that they represent local relative intensities. No attempt has been made to make the scale linear; in fact, it can be seen from Table 463-VII that 6 of the 10 steps in the visual scale correspond to calculated intensities of less than 15% of the strongest line in the pattern. This is a result of the fact that 90% of the lines in the pattern are within this intensity range. Using relative intensities and line positions calculated from the published structural description and estimated lattice parameters, these data were indexed as indicated. The unambiguous back-reflection lines were used to compute least squares fitted lattice parameters. The fit appears to be good, with all deviations reasonably accounted for by random errors in measurement. The fit was made using a Nelson-Reiley extrapolation function; however, no adsorption corrections are incorporated into the calculated data in Table 463-VII. The program used in the fitting was not directly applicable to a rhombohedral lattice; therefore, the fit was done in terms of the alternate hexagonal unit cell. The results of the fit are

$a_o = 5.6016 \pm 0.0010$Å

$c_o = 12.072 \pm 0.003$Å

where the error limits are 95% confidence intervals with respect to internal consistency. These correspond to a rhombohedral unit cell with

$a_o = 5.1625$Å

$\alpha = 65.65$ deg.

The only lattice parameters available in the literature for comparable material are those reported by Allen[14] for $B_{4.0}C$. He reported a_o to be 5.61Å and c_o to be 12.07Å for the hexagonal unit cell as calculated from low angle data. Agreement is satisfactory. Elliot[13] presented the results of diffraction measurements on B_4C as a function of composition by reporting the angular position of what he termed "the strong back-reflection of B_4C". The strongest high angle line in the B_4C pattern is the $\overline{5}\overline{1}\overline{1}-33\overline{3}\alpha_1$ which was observed in the present study at 152.77° 2θ. Elliot reported the line at 152.84° 2θ for carbon saturated B_4C. The two line positions are identical to within errors in measurement.

The graphite lines observed are listed in Table 463-VII. The graphite lattice parameters estimated from these data are

$a_o = 2.51$Å

$c_o = 6.66$Å.

Although these parameters are very approximate, they imply rather large boron solution in the graphite.[15]

Two minor anomolies were observed in the pattern. The first has to do with the line occurring at 48.08° 2θ. This reflection was indexed as the B_4C 220; however, the observed intensity appears somewhat larger than would be expected from calculated intensities. The reason for this discrepancy is not known; however, it could be due to minor inaccuracies in the positional parameters used in the calculations. The second problem is in regard to the weak line observed at 151.03° 2θ. It has not been possible to identify this reflection. It does not appear to belong to the B_4C pattern. It may be due to the graphite phase but sufficient data are not available to allow an assignment to be made. Except for these items, the observed pattern appears to be satisfactorily consistent with the published structure with respect to both line position and estimated intensity. It is concluded, therefore, that X-ray powder data for carbon saturated B_4C present no basis for challenging the published structure. It should be noted, however, that the intensity considerations presented above are not sufficiently sensitive to constitute a thorough test of all the details of the structure description to which powder data can be applied, e.g., positional parameters, etc.

Neutron diffraction studies have been undertaken to investigate the B_4C structural details that must be evaluated by reflection intensity analysis. The primary experimental difficulties are associated with absorption

Table 463-VII

POWDER DIFFRACTION PATTERN OF CARBON SATURATED B_4C

HKL (Rhomb.)	Intensity Obs.	Intensity Calc.(b)	d (A) Obs.	d (A) Calc.(a)	HKL (Rhomb.)	Intensity Obs.	Intensity Calc.(b)	d (A) Obs.	d (A) Calc.(a)
100	6	5	4.5063	4.5013	$\bar{3}03\,\alpha_1$	4	4.7	0.9336	0.9336
111	7	17	4.0329	4.0240	$54\bar{4}\,\alpha_1$	2	1.8	0.9116	0.9121
110	9	81	3.7871	3.7812	$41\bar{2}\,\alpha_1$	3	4.3	0.9093	0.9094
Graphite 002	6	--	3.3337	--	$402\,\alpha_1$	2	1.8	0.9064	0.9064
					$500\,\alpha_1$		2.7		0.9003
$10\bar{1}$	6	15	2.8027	2.8008	$541\,\alpha_1$	(c)	1.9	(c)	0.8985
$21\bar{1}$	9	49	2.5650	2.5626	$500\,\alpha_2$		1.4		0.9003
$11\bar{1}$	10	100	2.3841	2.3780	$541\,\alpha_2$	5	1.0	0.8959	0.8985
210	3	8	2.3020	2.2988	$530\,\alpha_1$		11.4		0.8957
Graphite 100	2	--	2.1694	--	$\bar{5}30\,\alpha_2$	2	5.7	0.8955	0.8957
					$\bar{4}22\,\alpha_1$	3	2.4	0.8771	0.8772
$22\bar{0}$	2	0.1	1.8923	1.8906	$412\,\alpha_1$	3	4.4	0.8690	0.8690
201	5	7	1.8149	1.8127	$\bar{5}53\,\alpha_1$	3	5.8	0.8670	0.8672
311	6	12	1.7136	1.7112	$412\,\alpha_2$		2.2		0.8690
Graphite 004	1	--	1.6634	--	$\bar{5}53\,\alpha_2$	1	2.9	0.8672	0.8672
					$\bar{3}23\,\alpha_1$	3	6.7	0.8622	0.8623
$\bar{3}22$	4	3	1.6282	1.6249	$\bar{3}23\,\alpha_2$	2	3.9	0.8623	0.8623
221, 300	6	10	1.4985	1.5004	$511\,\alpha_1$	4	14.5	0.8570	0.8571
320	7	17	1.4613	1.4602	$\bar{6}22\,\alpha_1$		8.6		0.8556
$33\bar{2}$	7	17	1.4431	1.4409	$51\bar{1}\,\alpha_2$	4	7.3	0.8549	0.8571
$20\bar{2}$	7	17	1.4019	1.4004	552, 633 α_1		4.8		0.8542
$21\bar{2}$	5	12	1.3380	1.3372	$\bar{6}32\,\alpha_1$	2	3.8	0.8507	0.8504
$31\bar{1}$	5	11	1.3249	1.3226	$52\bar{1}\,\alpha_1$	(c)	2.7	(c)	0.8469
301	5	13	1.3137	1.3132	$441\,\alpha_1$		3.0		0.8456
422	3	4	1.2830	1.2813	621, 540 α_1	3	6.9	0.8310	0.8310
411, 330	7	6	1.2597	1.2604	621, $\bar{5}40\,\alpha_2$	2	3.5	0.8310	0.8310
421		11		1.2562	$432\,\alpha_1$		1.8		0.8196
$\bar{4}32$	3	3	1.2086	1.2098	$631\,\alpha_1$	(c)	2.7	(c)	0.8183
$31\bar{1}$		3		1.2067	$642\,\alpha_1$		1.9		0.8170
222	4	6	1.1899	1.1890	$611\,\alpha_1$		2.5		0.8161
410	3	2	1.1767	1.1753	$551\,\alpha_1$	3	11.8	0.8138	0.8137
431	4	5	1.1656	1.1651	$\bar{5}51\,\alpha_2$	1	5.9	0.8138	0.8137
420	4	3	1.1497	1.1494	$22\bar{4}, \bar{4}22\,\alpha_1$	2	6.7	0.8086	0.8085
$40\bar{0}$	2	1	1.1265	1.1253	224, 422 α_2	1	3.4	0.8084	0.8085
312	2	1	1.0954	1.0945	$555\,\alpha_1$	1	3.2	0.8049	0.8048
$44\bar{2}\,\alpha_1$	3	2.6	1.0813	1.0807	?	1	-	0.7955	--
$411\,\alpha_1$	4	2.4	1.0447	1.0442	$\bar{5}11, \bar{3}33\,\alpha_1$	6	28.3	0.7925	0.7927
$44\bar{1}, 52\bar{2}\,\alpha_1$	5	7.7	1.0324	1.0324	511, $\bar{3}33\,\alpha_2$	6	14.2	0.7906	0.7927
401, $32\bar{2}\,\alpha_1$	1	1.0	1.0241	1.0238	$41\bar{3}\,\alpha_1$		4.7		0.7906
$444\,\alpha_1$	2	1.3	1.0062	1.0060	$413\,\alpha_2$	1	2.4	0.7906	0.7906
$511\,\alpha_1$	1	0.5	0.9929	0.9920	$653\,\alpha_1$	2	6.2	0.7803	0.7803
$531\,\alpha_1$	2	2.1	0.9680	0.9687	$65\bar{3}\,\alpha_2$	1	3.1	0.7804	0.7803
$440\,\alpha_1$	1	0.7	0.9447	0.9453	$31\bar{4}\,\alpha_1$	1	3.5	0.7768	0.7768

(a) Interplanar spacings computed for $a_o = 5.1625$ Å and $\alpha = 65.65^o$.
For $2\theta < 90^o$ $\lambda = 1.54178$ Å.
For $2\theta > 90^o$ $\lambda\,(\alpha_1) = 1.54051$ Å and $\lambda\,(\alpha_2) = 1.54433$ Å.

(b) Calculated relative intensities based on reference (2).

(c) Broad unresolved band - not measurable.

(d) Interplanar spacings for conglomerate lines calculated using $\lambda\,(\alpha_1)$.

effects. Due to the fortuitous near equality of the coherent scattering amplitudes of ^{12}C and ^{11}B, it is necessary to use material containing a substantial amount of ^{10}B to make it possible to differentiate between C and B positions in the structure. This addition of ^{10}B increases the difference in scattering amplitudes, but it also results in very large increases in thermal absorption which severely depresses reflection intensities. Natural boron was chosen as a satisfactory balance between these factors. Since the absorption is larger, very thin targets are required. Targets prepared from uncompacted B_4C powder 0.020 in. thick have transmissions of only approximately 30%. A major problem was the development of techniques for the preparation of targets that are sufficiently thin and uniform but that still contain enough material to produce a satisfactory pattern. It has been found that very uniform powder cakes can be prepared by applying a B_4C powder - vythene slurry to the surface of a thin Ti-Zr null matrix support plate. The dried cake is sufficiently strong to allow planing to the desired thickness using a flat blade and a jig assembly to control thickness and to maintain accurately flat surfaces. Targets prepared in this way were found to be uniform with respect to thermal neutron absorption to the limits of sensitivity of neutron radiographic examinations.

Preliminary diffraction data have been obtained using a target prepared from the same material used in the X-ray study. The powder cake was 0.0222 ± 0.0002 in. thick and had a transmission of 33.3%. Intensities for 13 reflections were obtained from the counting data using a gaussion least squares fitting program. These observed intensities were then least squares fitted to a structural model having atomic positions approximately the same as those defined by the published structure. Refinement of the position parameters was carried out. The results are not significantly different than those originally published. A comparison of these data is given in Table 463-VIII. In addition, the scattering amplitudes of the species at the various sites were fitted. This essentially tests the identity of the atoms located in each position. The results of these calculations

Table 463-VIII

RHOMBOHEDRAL ATOMIC POSITION PARAMETERS FOR B_4C

Space Group:	$R\bar{3}m$
6 BI and 6 BII in 6(h):	Icosahedral positions ±(x, x, z; x, z, x; z, x, x)
2 CI in 2(c):	Terminal positions of central chain ± (x, x, x)
1 atom in 1(b):	Central position of central chain 1/2, 1/2, 1/2

	Clark and Hoard[10]		This Study	
	x	z	x	z
BI	0.193	0.693	0.198	0.692
BII	0.007	0.325	0.005	0.330
CI	0.385	—	0.383	—

are shown in Table 463-IX in addition to the published values for the scattering amplitudes of natural boron and carbon. Due to the limited number of reflections for which intensity data are presently available, the uncertainty in these fitted scattering amplitudes is substantial. Even so, the implications of these results are clear. The positions in the icosahedral groups located at the corners of the unit cell are occupied by B atoms. The terminal positions of the 3 atom chain located on the 3 hold axis are C atoms. The central position in this chain is assigned as a C position in the published structure. This is clearly not consistent with the fitted scattering amplitude for this position. Instead, the result is very near to that of pure B. Due to the uncertainty in the fitted results, the possibility of a random substitutional occupation of the site by both B and C cannot be eliminated. If this is the case, however, the site appears to be predominantly occupied by B. The r

The recognition of this discrepancy in the published

Table 463-IX

SCATTERING AMPLITUDES

		Central Chain	
	Icosahedral Positions	Terminal Position	Central Position
$b \times 10^{12}$ (cm)	0.522	0.665	0.535

Natural C 0.661×10^{-12} cm
Natural B 0.54×10^{-12} cm

structure is not entirely new. Zhdanof[16] first suggested the possibility as a mechanism for accomodating excess B in the structure. Silver and Bray[17] concluded from NMR studies on single crystals of B_4C that greater than 60% of these control positions were occupied by B atoms.

This result could be of considerable importance in the analysis of the structural effects of neutron irradiation. Tucker and Lenio[18] have for instance reported that one of the atoms in the central chain is particularly prone to displacement during irradiation. They reported that after complete burn-up of ^{10}B from B_4C prepared from natural B that 48% of the central chains contained only two atoms. It should be noted, however, that if the central member of the chain is entirely occupied by B, the burn-up of all the ^{10}B would only account for approximately 40% of the missing atoms. It would appear that large amounts of damage in this specific area still must be attributed to recoiling ^4He and ^7Li.

4. High Temperature Electrochemical Studies of the Thermodynamics of Plutonium Compounds (G. M. Campbell)

Studies of the Pu-C system have continued. After the results of conventional type emf cells were found not to be easily reconcilable with growing evidence of higher temperature vapor pressure measurements[19,20,21] it seemed imperative that improved electrochemical techniques be used to examine individual electrode reactions. Since the conventional $Pu(\ell)/Pu^{+3}$ electrode is stable only for a limited period in the LiCl-KCl eutectic, a galvanostatic transient method was developed so that this potential could be measured unambiguously without requiring continuous presence of the corrosive $Pu(\ell)$. The success of this technique was demonstrated by measuring the emf of the PuN electrode over a wide temperature range[22,23] in LiCl-KCl. When the method was applied to the $PuC_{1.5}$ + C system, the results, although in agreement with other studies using a solid electrolyte,[24] still could not be reconciled with the vapor pressure data. To be certain this was not characteristic of the Pu-C system alone, studies were also made in the Pu-Fe system. The results indicated that the secondary reaction was again present and influencing the $PuFe_2/Pu^{3+}$ rest potential. These studies also indicated that the reaction was related to the Pu^{3+} activity and was most probably Pu^{4+}. The results of all the experiments could be explained by a mechanism such as

Anode: $Pu(\ell) = Pu^{3+} + 3\ e^-$ (1a)

Cathode: (a) $Pu^{3+} + 3\ e^- + 1.5\ C = PuC_{1.5}$ (1b)

(b) $Pu^{4+} + e^- = Pu^{3+}$ (1c)

If these equilibria are present, the potential of (1a) vs (1b) can be calculated from the rest potential provided the standard potential of (1c) is known. Subsequent studies using $PuN(s)/Pu^{3+}$ as a reference indicated that the standard potential of (1a) vs (1c) in the temperature range 910 to 1048°K is

$$E = 1.233 - 0.000496\ T,\ ^oK,\ V. \quad (2)$$

In these calculations, it was necessary to assume that the Pu^{3+}/Pu^{4+} ratio was a function of Pu activity in the Pu compound (PuN). The rest potential of $PuC_{1.5}$ vs Pu in the fused salt system was

$$E = 0.534 - 0.000196\ T,\ ^oK,\ V. \quad (3)$$

Combining equation (2) and equation (3) and using the assumption concerning the Pu^{3+}/Pu^{4+} ratio results in

$$E = 0.3034 - 0.0000867\ T,\ ^oK,\ V \quad (4)$$

for the potential of (1a) vs (1b) and

$$\Delta G_f = -21,000 + 6.0\ T,\ ^oK\ (cal/mole) \quad (5)$$

for the free energy of formation of $PuC_{1.5}$. Although the temperature dependence of these functions is questionable, these results are more consistent with the vapor pressure studies.

To check the model further, the system $PuC_{1.5}$ + $PuC_{0.9}$ was studied. The Pu activity in this system was expected to be larger than in those discussed above. Although the initial emf was compatible with the proposed model, sharp drifts to positive potentials coupled with the results of analyses of the electrode residues indicated that Pu was consistently dissolved from the electrode. This demonstrated that the assumption that the Pu^{3+}/Pu^{4+} ratio was a function of the Pu activity in the electrode was not applicable for this system.

The most probable alternative explanation for the presence of Pu^{4+} in the system, would be that it was the result of a reaction with oxygen such as

$$4\ PuCl_3 + O_2 = 3\ PuCl_4 + PuO_2. \quad (6)$$

The Pu-O phase diagram is sufficiently complex that no

single mechanism can be chosen a priori. Experience with the $PuCl_3$, LiCl-KCl mixtures indicates that at the temperatures of interest, however, Pu oxides have low solubilities. The complete exclusion of oxides from the system over the periods required for the studies can not as yet be guaranteed. The possibility that the results stem from an adsorbed surface layer of oxide impurity seems most plausible. Galvanostatic and voltammetric rapid potential cycling of the W microelectrode, where measurable current from the secondary reaction was initially present, supported the surface impurity postulate. These studies indicate that the secondary reaction is slow or irreversible and can be driven to completion at potentials more negative than 0.18 V vs the Pu/Pu^{3+} potential.

The best method for examining the secondary electrochemical reaction of adsorbed surface material in competition with the primary electrode reaction has been discussed by Bockris and Srinivasan.[25] The technique involves a potentiostatic pre-electrolysis step. The electrode is held at a potential where current from the secondary reaction is at a maximum while that from the primary reaction is minimized. After the reaction of surface material is driven to completion, as determined by monitoring the current, the electrode is allowed to regain its open-circuit equilibrium. Studies using this procedure were made on the $PuC_{1.5}$+ C and $PuC_{1.5}$ + $PuC_{0.9}$ electrodes. Two electrodes of this type were used in each cell, one as a reference and the other as an auxiliary electrode. A temporary reference electrode was created by plating Pu onto the W microelectrode. The primary reference electrode could then be maintained at the desired potential by using a potentiostat (M-T Electronics Co., San Leandro, Calif., 94579). Potentiostating of the $PuC_{1.5}$ + C electrode at 0.15 V until the current stabilized followed by open circuit equilibration resulted in stable equilibria in about 5 min. Potentiostating this electrode at 0.05 V until the current was stable resulted in the same potential at equilibrium, after a brief arrest at ca. 0.08 V, with an equilibration period greater than 15 min. Currents at the potentiostated electrodes became stable at 2.5 to 6 mA in less than 1 min. When the process was repeated at any one temperature the equilibrium potential was reproduced to ± 2 mV. Mixed $PuC_{1.5}$ + $PuC_{0.9}$ electrodes were potentiostated at ca. 0.05 V to avoid high anodic currents from the primary electrode reaction.

In this way the emf for the cell $Pu(\ell)/PuCl_{3(x=0.00454)}$, LiCl-KCl/$PuC_{1.5}$ + C(s) in the temperature range 922-1060°K was found to be

$$E = 0.2407 - 5.094 \times 10^{-6} T,\ ^{\circ}K,\ V. \qquad (7)$$

This gives for the standard free energy of formation of $PuC_{1.5}$(s)

$$\Delta G_{f_{986}} = -16,650 + 0.352\,T,\ ^{\circ}K\ (cal/mole). \qquad (8)$$

For the cell $Pu(\ell)/PuCl_{3(x=0.00723)}$, LiCl-KCl/$PuC_{1.5}$ + $PuC_{0.9}$(s) in the temperature range 915-1057°K the emf was

$$E = 0.1469 - 5.00 \times 10^{-5} T,\ ^{\circ}K,\ V. \qquad (9)$$

This gives

$$\Delta G_{986} = -10,161 + 3.46\ T,\ ^{\circ}K\ (cal/mole) \qquad (10)$$

for the reaction

$$1.5\ Pu_{1.5}(s) + Pu(\ell) = 2.5\ PuC_{0.9}(s). \qquad (11)$$

When the free energies of equations (8) and (10) are combined, the free energy of formation of $PuC_{0.9}$ is found to be

$$\Delta G_{f_{986}} = -14,059 + 1.6\,T,\ ^{\circ}K\ (cal/mole). \qquad (12)$$

These results have been compared with those of other studies in a recent report.[26] The emf of these two cells are shown in Figure 463-7.

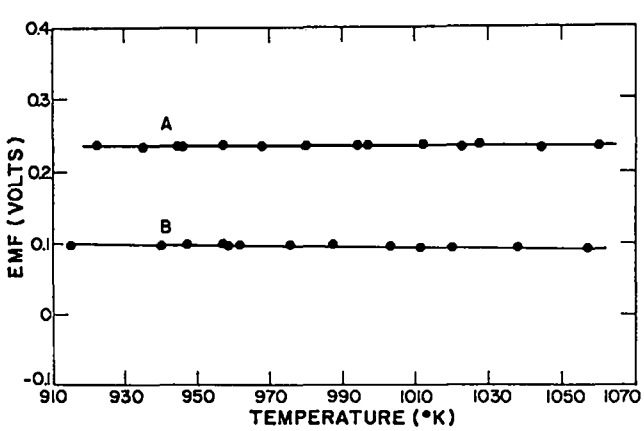

Figure 463-7. Emf of the Cells (A), $Pu(\ell)/PuCl_{3(x=0.00454)}$, LiCl-KCl/$PuC_{1.5}$ + C(s) and (B), $Pu(\ell)/PuCl_{3(x=0.00723)}$, LiCl-KCl/$PuC_{1.5}$+ $PuC_{0.9}$(s)

5. Mass Spectrometric Studies of the Vaporization of Pu Compounds

(R. A. Kent)

A. The Plutonium-Carbon System

As a first step in the investigation of the vaporization behavior of the U-Pu-C ternary system, a comprehensive study of the vaporization behavior of the Pu-C binary system as a function of composition has been made. This investigation, some aspects of which have been reported previously,[27-31] has been completed and all of the data were combined to yield the vapor pressure and thermodynamic values listed below.

The mass spectrometer-Knudsen cell assembly which was employed in this work has been described in detail previously.[32] The vacuum system is such that background pressures of 10^{-8} to 10^{-7} torr were routinely achieved with the Knudsen cell at 1600°C.

A large number of samples having stoichiometries ranging from Pu to $PuC_{2.13}$ were studied over the temperature range 1450-2170°K. Chemical, X-ray diffraction, and metallographic analyses were obtained for all starting materials and residues. The results of these studies indicate that there are four regions of the Pu-C phase diagram which give rise to invarient, but not congruent vaporization:

(1) $PuC + Pu_2C_3$

(2) $Pu_2C_3 + C$

(3) $Pu_2C_3 + PuC_2$

(4) $PuC_2 + C$

The only vapor species observed above the first three of these composition regions was gaseous Pu. The Pu^+ ion current (AP = 5.8 ± 0.5 eV) was monitored as a function of temperature in the usual manner. The same apparatus was previously employed to measure the vapor pressure of Pu metal.[33] Thus, in order to convert the ion current data to absolute pressure values, one has only to compare the Pu^+ signal above the carbides with that above Pu(ℓ) at the same temperature and to correct for changes in the gain of the electron multiplier. Above the fourth composition region, $PuC_2 + C$, the predominate vapor species was gaseous Pu although at temperatures greater than 2100°K, small amounts (< 0.1%) of $PuC_2(g)$ were observed. These trace amounts of $PuC_2(g)$ were insignificant in the thermodynamic calculations below.

The vaporization behavior of the Pu-C system may be described as follows. As one adds C to Pu(ℓ), the pressure of Pu(g) at a given temperature decreases as the Pu activity is lowered. When the low carbon boundary of the monocarbide is reached, the Pu(g) pressure decreases more rapidly. As one continues to heat the sample and to add C, the monocarbide reacts to form Pu(g) and the sesquicarbide. The Pu(g) pressure is invarient so long as both the monocarbide and sesquicarbide are present as solid phases. When the low carbon boundary of the sesquicarbide is reached the Pu(g) pressure again falls sharply. The sesquicarbide on heating gives off Pu(g) with free C appearing in the condensate. Again the pressure of gaseous Pu is invarient so long as both sesquicarbide and free C are present. The low carbon phase boundary of the sesquicarbide curves toward lower C/Pu ratios at high temperatures, passing near $PuC_{1.46}$ at 1320 ± 50°C, $PuC_{1.41}$ at 1530 ± 50°C and $PuC_{1.31}$ at 1595 ± 10°C.

Above 1660°C, the sesquicarbide decomposes to gaseous Pu and the dicarbide with a resultant change in the Pu(g) pressure, which is again invarient so long as the condensate consists of both sesqui- and dicarbide. At temperatures above 1660°C and at C/Pu ratios equal to greater than $PuC_{1.98\pm 0.02}$, the condensate consists of the dicarbide plus free C, and again the Pu(g) pressure is invarient.

Values of the vapor pressure of gaseous Pu above various condensate compositions are listed in Table 463-X.

Table 463-X

PLUTONIUM PRESSURES ABOVE VARIOUS Pu-C COMPOSITIONS

Condensate	Temp., °K	Pu Pressure (atm)
Pu(ℓ)	1700	4.75×10^{-6}
$PuC_{0.70}(s)$	1700	4.53×10^{-6}
$PuC_{0.76}(s)$	1700	4.05×10^{-6}
['PuC' + 'Pu_2C_3'](s)	1700	9.75×10^{-7}
$PuC_{1.46}(s)$	1700	5.30×10^{-7}
['Pu_2C_3' + C](s)	1700	2.25×10^{-8}
['Pu_2C_3' + 'PuC_2'](s)	2100	6.82×10^{-6}
['PuC_2' + C](s)	2100	4.00×10^{-6}

The vapor pressure data obtained above the various condensate compositions were used to calculate expressions for the free energies of formation for $PuC_{0.9}(s)$, $PuC_{1.5}(s)$, and $PuC_2(s)$. These free energy expressions were reduced to 298°K employing published functions for Pu(ℓ),[33,34] Pu(g),[35] C(s),[36] and $PuC_{0.9}$.[37] No heat capacity data exist for $PuC_{1.5}(s)$ or for $PuC_2(s)$. Functions for $PuC_{1.5}(s)$ were estimated from a combination of known functions for C(s) and $PuC_{0.9}(s)$ and are listed in Table 463-XI. The functions employed for $PuC_2(s)$ were those estimated by Oetting,[38] with the value of S^o_{298} adjusted to fit the data.

In order to study the vaporization behavior of the sesqui- and dicarbide a number of samples were prepared and effused from W Knudsen cells and/or from graphite cups contained in W Knudsen cells over the range 1668-2170°K. The initial stoichiometries of these samples were: $PuC_{1.5}$, $PuC_{1.54}$, $PuC_{1.59}$, $PuC_{1.78}$, $PuC_{1.98}$, and $PuC_{2.13}$.

Plutonium Sesquicarbide plus Carbon

Plutonium sesquicarbide in the range 1668-1927°K decomposes according to the reaction

$$PuC_{1.5}(s) = Pu(g) + 1.5\ C(s) \qquad (1)$$

with the Pu(g) pressure given by

$$\log_{10} P_{Pu}(atm) = -20,598 \pm 106/T, {}^{\circ}K + (4.468 \pm 0.057). \qquad (2)$$

In eq (2), and all such subsequent equations, the quoted uncertainties are the standard deviations generated by the least-squares program.

When the free energy expression for the decomposition of $PuC_{1.5}(s)$, obtained from eq (2), is combined with that for the vaporization of Pu metal at the same temperature,[33] we have for the formation of $PuC_{1.5}(s)$

Table 463-XI

ESTIMATED THERMODYNAMIC FUNCTIONS FOR $PuC_{1.5}(s)$

Temp., °K	C_p, cal/mole/°K eu	$H^o_T - H^o_{298}$, cal/mole	$S^o_T - S^o_{298}$, eu	$-(F^o_T - H^o_{298}/T)$, eu
298	11.59	0	0	20.70
1000	16.62	9,994	16.63	27.34
1400	18.78	17,092	22.58	31.07
1600	19.67	20,939	25.15	32.76
1800	20.43	24,951	27.51	34.35
2000	21.06	29,104	29.70	35.85
2200	21.57	33,369	31.73	37.26

$$Pu(g) + 1.5\ C(s) = PuC_{1.5}(s);$$
$$\Delta G_{1842} = -94,252 + 20.44\ T, \text{ (cal/mole)} \qquad (3)$$
$$Pu(\ell) = Pu(g);$$
$$\Delta G_{1842} = 80,154 - 22.64\ T, \text{ (cal/mole)} \qquad (4)$$
$$Pu(\ell) + 1.5\ C(s) = PuC_{1.5}(s);$$
$$\Delta G_{f\,1842} = -14,098 - 2.20\ T, \text{ (cal/mole)} \qquad (5)$$

Equation (5) when reduced to 298°K, yields for $PuC_{1.5}(s)$ the second law values $\Delta H^o_{f298} = -13.3 \pm 0.7$ kcal/mole and $\Delta S^o_{f298} = +5.4 \pm 0.6$ eu. The third law heat of formation is $\Delta H^o_{f298} = -13.2 \pm 0.2$ kcal/mole and S^o_{298} is taken to be 20.7 eu.

These values at 298°K are, of course, based on estimated functions for $PuC_{1.5}(s)$, and a final value for the heat of formation will depend on the results of a bomb calorimetry experiment which will be available shortly.*

Equation (5), when extrapolated to 1000°K, yields $\Delta G_f = -16.3$ kcal/mole, the same value as that obtained at that temperature from the emf measurements performed in this laboratory (previous section).

Plutonium Sesquicarbide plus Dicarbide

Above 1660°C, and in the composition range $PuC_{1.50 \pm 0.02}$ to $PuC_{1.98 \pm 0.02}$, the sesquicarbide decomposes according to the reaction

$$4\ PuC_{1.5}(s) = Pu(g) + 3\ PuC_2(g). \qquad (6)$$

The Pu(g) pressure in the range 1933-2170°K is given by

$$\log_{10} P_{Pu}(atm) = -24,569 \pm 223/T, {}^{\circ}K + (6.533 \pm 0.109). \qquad (7)$$

When the free energy expression for eq (6) is combined with equations (4) and (5) corrected to the same temperature we have

$$4\ PuC_{1.5}(s) = Pu(g) + 3\ PuC_2(s);$$
$$\Delta G_{2053} = 112,423 - 29.89\ T, \text{ (cal/mole)} \qquad (8)$$
$$Pu(g) = Pu(\ell);$$
$$\Delta G_{2053} = -80,768 + 22.95\ T, \text{ (cal/mole)} \qquad (9)$$
$$4\ Pu(\ell) + 6\ C(s) = 4\ PuC_{1.5}(s);$$
$$\Delta G_{2053} = -53,006 - 10.58\ T, \text{ (cal/mole)} \qquad (10)$$
$$Pu(\ell) + 2\ C(s) = PuC_2(s);$$
$$\Delta G_{f\,2053} = -7,177 - 5.84\ T, \text{ (cal/mole)} \qquad (11)$$

Equation (11) when reduced to 298°K yields for $PuC_2(s)$ the second law values $\Delta H^o_{f298} = -6.4 \pm 12$ kcal/mole and $\Delta S^o_{f298} = +8.4 \pm 0.8$ eu. The third law heat of formation is $\Delta H^o_{f298} = -6.8 \pm 0.1$ kcal/mole where $S^o_{298} = 24.1$ eu.

*A sample of pure $PuC_{1.5}$ has been supplied to ANL for combustion calorimetry.

Plutonium Dicarbide plus Carbon

Above 1660°C and at C/Pu ratios equal to or greater than 1.98 ± 0.02, the dicarbide decomposes according to the reaction

$$PuC_2(s) = Pu(g) + 2\ C(s). \quad (12)$$

The Pu(g) pressure in the range 1934-2140°K is given by

$$\log_{10} P_{Pu}(atm) = -19,288 \pm 171/T, {}^{\circ}K + (3.787 \pm 0.084). \quad (13)$$

When the free energy expression for the decomposition reaction is combined with eq (4) corrected to the same temperature we have

$$Pu(g) + 2\ C(s) = PuC_2(s);$$
$$\Delta G_{2026} = -88,258 + 17.33\ T, \text{ (cal/mole)} \quad (14)$$
$$Pu(\ell) = Pu(g);$$
$$\Delta G_{2026} = 80,684 - 22.91\ T, \text{ (cal/mole)} \quad (15)$$
$$Pu(\ell) + 2\ C(s) = PuC_2(s);$$
$$\Delta G_{f2026} = -7,574 - 5.58\ T, \text{ (cal/mole)} \quad (16)$$

When reduced to 298°K, eq (16) yields for $PuC_2(s)$ the second law values $\Delta H^{\circ}_{f298} = -6.8 \pm 0.9$ kcal/mole and $\Delta S^{\circ}_{f298} = +8.2 \pm 0.6$ eu. The third law heat of formation is $\Delta H^{\circ}_{f298} = -6.8 \pm 0.2$ kcal/mole where S°_{298} for $PuC_2(s)$ is 24.1 eu.

From a combination of equations (5) and (6) we obtain for the transition from sesqui- to dicarbide, the expression

$$PuC_{1.5}(s) + 0.5\ C(s) = PuC_2(s);$$
$$\Delta G_T = 6,524 - 3.38\ T, \text{ (cal/mole)} \quad (17)$$

Equation (17) yields for the transition temperature 1930°K (1657°C), in agreement with the value (1660 ± 10°C) obtained by Reavis from DTA studies performed in this Laboratory.

Plutonium Sesquicarbide plus Oxygen

In an effort to determine the effect of oxygen on the vaporization of the sesquicarbide, a pellet was deliberately oxidized until the sample contained 0.1 wt % oxygen. The pellet was placed in a graphite cup in a W Knudsen cell and heated to 1914°K. Although no Pu-O gaseous species were observed, the initial Pu (g) pressure was only 77 percent of that observed above the usual oxygen-free samples. After 45 minutes at 1914°K the Pu(g) pressure had risen to that observed above the oxygen-free samples. The sample was then quenched and analyzed and found to contain 80 ppm oxygen. From this, we conclude that heating the sesquicarbide in the presence of excess carbon will remove oxygen from the sample. However, so long as the sample contains oxygen, the observed Pu(g) pressure will be low.

Plutonium Monocarbide plus Sesquicarbide

In order to study the vaporization behavior of the monocarbide and of monocarbide-sesquicarbide mixtures, a number of samples were prepared and heated in W Knudsen cells over the range 1450-1979°K. The initial stoichiometries of these samples were: $PuC_{0.70}$, $PuC_{0.84}$, $PuC_{0.99}$, $PuC_{1.01}$, $PuC_{1.24}$, $PuC_{1.26}$, $PuC_{1.37}$, and $PuC_{1.46}$. The results indicate that in the temperature range of the experiments the low carbon phase boundary for single phase monocarbide is $PuC_{0.84 \pm 0.02}$ and the high carbon limit for the two phase mixture, mono-plus sesquicarbide, is near $PuC_{1.4}$. There is some uncertainty as to the upper C composition limit for single phase monocarbide, the value being somewhere between $PuC_{0.86}$ and $PuC_{0.96}$. For the purposes of the thermodynamic calculations below, the monocarbide is taken to be $PuC_{0.9}$.

Thus, we may write that plutonium monocarbide in the range 1450-1848°K decomposes according to the reaction

$$2.5\ PuC_{0.9}(s) = Pu(g) + 1.5\ PuC_{1.5}(s). \quad (18)$$

The Pu(g) pressure is given by

$$\log_{10} P_{Pu}(atm) = -18,919 \pm 72/T, {}^{\circ}K + (5.118 \pm 0.027). \quad (19)$$

When the free energy expression for the decomposition reaction is combined with equations (4) and (5) corrected to the same temperature, we have

$$Pu(g) + 1.5\ PuC_{1.5}(s) = 2.5\ PuC_{0.9};$$
$$\Delta G_{1662} = -86,570 + 23.42\ T, \text{ (cal/mole)} \quad (20)$$
$$Pu(\ell) = Pu(g);$$
$$\Delta G_{1662} = 79,713 - 22.38\ T, \text{ (cal/mole)} \quad (21)$$
$$1.5\ Pu(\ell) + 2.25\ C(s) = 1.5\ PuC_{1.5}(s);$$
$$\Delta G_{1662} = -21,860 - 2.89\ T, \text{ (cal/mole)} \quad (22)$$
$$Pu(\ell) + 0.9\ Pu(s) = PuC_{0.9}(s);$$
$$\Delta G_{f1662} = -11,487 - 0.74\ T, \text{ (cal/mole)} \quad (23)$$

When eq (23) is reduced to 298°K, we obtain for $PuC_{0.9}(s)$ the second law values $\Delta H^{\circ}_{f298} = -10.8 \pm 0.9$ kcal/mole and $\Delta S^{\circ}_{298} = +2.9 \pm 0.7$ eu from which we calculate S°_{298} to be 17.3 eu. The third law heat of formation is $\Delta H^{\circ}_{f298} =$

-10.9 ± 0.1 kcal/mole. This value is in good agreement with the value, obtained in a recent oxygen-bomb calorimetry study,[39] $\Delta H^{o}_{f298} = -11.4 \pm 0.6$ kcal/mole for $PuC_{0.88}(s)$. Equation (23) extrapolates to yield $\Delta G_f = -12.2$ kcal/mole at $1000^{o}K$. The recent emf work performed in this laboratory yields $\Delta G_f = -12.5$ kcal/mole at the same temperature.

Until such time as there are heat capacity data and combustion calorimetry data available, we recommend for the plutonium carbides, the values listed in Table 463-XII.

Table 463-XII

RECOMMENDED THERMODYNAMIC VALUES FOR THE PLUTONIUM CARBIDES

Carbide	ΔH^{o}_{f298} (kcal/mole)	ΔS^{o}_{f298} (eu)	S^{o}_{298} (eu)
$PuC_{0.9}$	-10.9 ± 1.0	$+2.9 \pm 0.8$	$+17.3 \pm 0.5$
$PuC_{1.5}$	-13.2 ± 2.5	$+5.5 \pm 2.0$	$+20.7 \pm 1.5$
$PuC_{2.0}$	-6.8 ± 3.0	$+8.2 \pm 2.5$	$+24.1 \pm 2.0$

Some of the vapor pressure data are shown in Figures 463-8 and 463-9.

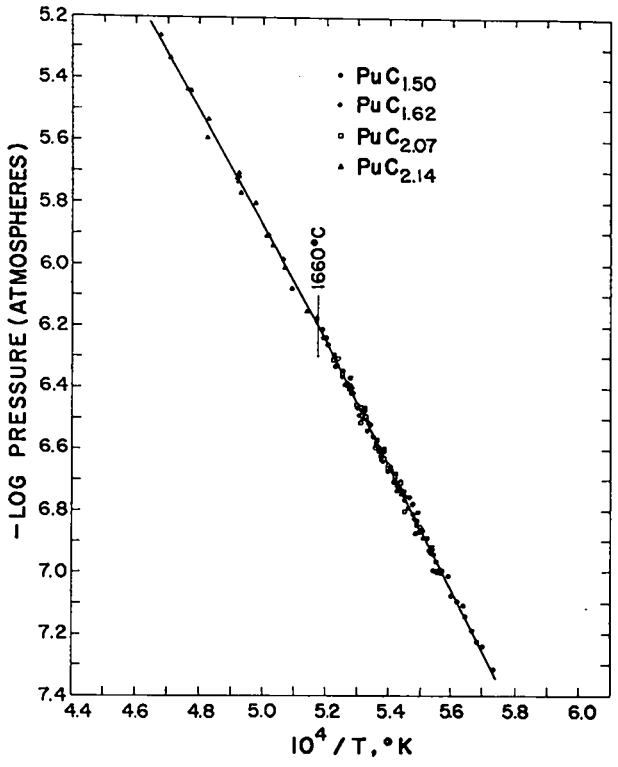

Figure 463-8. Plutonium gas pressure above plutonium sesquicarbide and plutonium dicarbide.

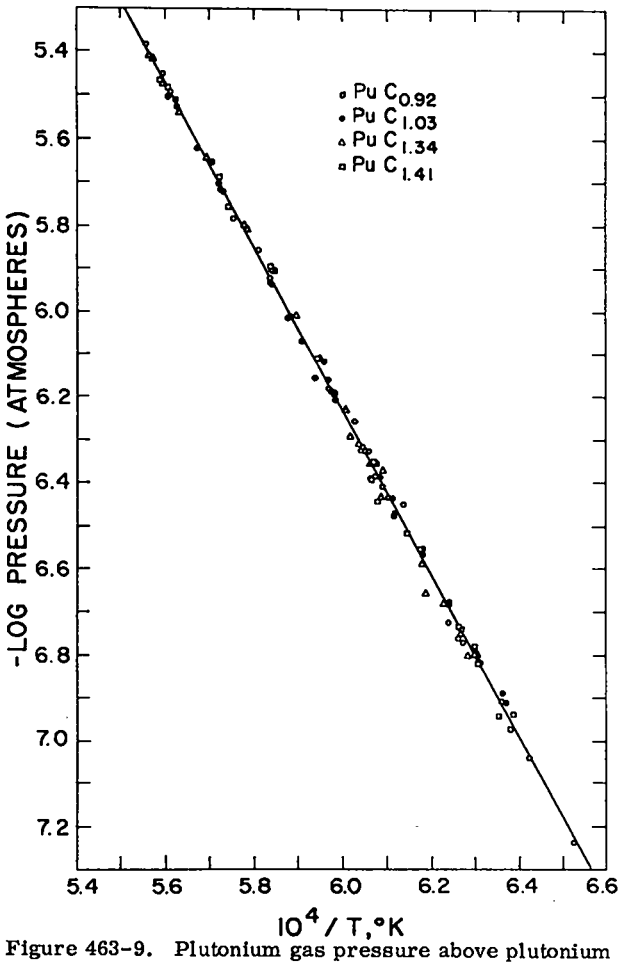

Figure 463-9. Plutonium gas pressure above plutonium monocarbide plus plutonium sesquicarbide.

B. Magnetic Mass Spectrometer

Installation and Calibration

The installation of the new Hitachi RM6-K mass spectrometer by factory personnel has been completed. This unit employs an 8 in., 90^{o} magnetic sector and has a theoretical resolution of $(M/M + \Delta M) = 6,000$ with a 50% valley between peaks. In tests conducted to date, the unit, in an "off the shelf condition", has proved capable of resolving to baseline the mass 29 peak consisting of $^{14}N^{15}N^{+}$ and $C_2H_5^{+}$. The Knudsen cell has been heated to $2100^{o}C$ using less than half the rated power of the heater supply. The optical windows have been calibrated for use with an optical pyrometer. The glovebox enclosure for work with Pu-containing materials has been designed and ordered.

In order to become familiar with the operation of the unit and to calibrate it for vaporization studies, a

series of experiments were performed with a gold standard sample.

A sample consisting of 0.5 g Au wire (99.999 percent pure) obtained from the NBS was contained in a graphite cup in a Mo Knudsen cell and effused over the range 1329-1698°K. The ion current of the $^{197}Au^{+}$ signal was monitored as a function of temperature in the usual manner. The resultant-least squares equation is

$$\log_{10}(IT) = -18,041 \pm 177/T,\ ^{o}K + (21.317 \pm 0.116) \quad (24)$$

At 1553°K, $\log_{10} P_{Au}(atm) = -5.876$.[40] The value obtained for $\log_{10}(IT)$ at the same temperature is 9.719. Thus, from the relationship P = K(IT), one obtains $K = 3.75 \times 10^{-16}$ atm/amp deg K and eq (24) becomes

$$\log_{10} P_{Au}(atm) = -18,041/T,\ ^{o}K + (5.981). \quad (25)$$

Equation (25) yields for the heat and entropy of vaporization at 1533°K the values 82.55 ± 0.81 kcal/mole and 26.96 ± 0.53 eu, respectively. Published thermodynamic functions for Au(ℓ)[41] and Au(g)[42] were employed to reduce these values to 298°K. The second law values obtained are $\Delta H^{o}_{V\,298} = 87.9 \pm 0.8$ kcal/mole and $\Delta S_{V\,298} = 31.9 \pm 0.5$ eu. The third law heat of vaporization is calculated to be $\Delta H^{o}_{V\,298} = 87.7 \pm 0.3$ kcal/mole. The values listed for the NBS standard gold reference material are $\Delta H^{o}_{V\,298} = 87.7$ kcal/mole and $\Delta S^{o}_{V\,298} = 31.8$ eu. The vapor pressure data for the reactions Au(ℓ) = Au(g), together with the third law heat values are listed in Table 463-XIII.

Table 463-XIII

VAPOR PRESSURE DATA FOR GOLD

Pt*	Temp., °K	P_{Au} (atm) (x 10^{6})	$\Delta H^{o}_{V\,298}$ kcal/mole
A 1	1567	2.29	87.87
A 2	1623	6.11	87.65
A 3	1592	3.94	87.47
A 4	1588	3.40	87.73
A 5	1350	0.0357	87.57
A 6	1376	0.0661	87.48
A 7	1504	0.652	88.30
A 8	1526	1.00	88.22
A 9	1553	1.72	88.02
A 10	1533	1.28	87.86
A 11	1520	0.918	88.15
A 12	1520	0.918	88.15
A 13	1513	0.809	88.15
A 14	1513	0.832	88.07
A 15	1507	0.738	88.10
A 16	1507	0.738	88.10
A 17	1506	0.667	88.35
A 18	1378	0.0698	87.45
B 1	1468	0.420	87.60
B 2	1514	0.805	88.22
B 3	1583	3.24	87.62
B 4	1611	5.06	87.65
B 5	1592	3.75	87.62
B 6	1561	2.19	87.83
B 7	1557	2.14	87.55
B 8	1530	1.20	87.89
B 9	1608	4.99	87.54
B 10	1616	5.28	87.76
B 11	1638	7.53	87.73
B 12	1638	7.50	87.75
B 13	1638	9.14	87.10
B 14	1575	3.33	87.11
B 15	1641	9.53	87.12
B 16	1645	10.2	87.11
B 17	1665	11.3	87.75
B 18	1698	17.3	87.94
B 19	1692	14.4	88.27
B 20	1626	5.89	87.92
B 21	1582	3.35	87.46
B 22	1583	3.22	87.64
B 23	1526	1.21	87.65
C 1	1515	1.03	87.54
C 2	1541	1.46	87.88
C 3	1529	1.18	87.88
C 4	1504	0.840	87.55
C 5	1472	0.509	87.26
C 6	1472	0.496	87.34
C 7	1501	0.820	87.45
C 8	1457	0.342	87.58
C 9	1421	0.137	88.12
C 10	1421	0.129	88.28
C 11	1389	0.0791	87.76
C 12	1329	0.0244	87.27
			Av = 87.74 ± 0.34

*Data for runs B and C were normalized for changes in multiplier gain from that for run A.

Modifications

The results of the experiments with the gold standard sample indicate that the instrument will adequately perform the tasks planned when the unit was purchased. However, as a result of these experiments, certain modifications designed to extend the range and increase the sensitivity of the measurements have been planned. Other modifications have been planned to increase the ease of operation of the unit and to simplify the installation of the glove box enclosure.

The following modifications have been or are being made:

(1) Replacement of the 10-stage electron multiplier with a 16-stage unit.

(2) Installation of a new shutter slit to provide sharper peak profiles.

(3) Enlargement of ion source exit slit to increase sensitivity.

(4) Replacement of Hitachi ion gauges with standard U.S. Bayard-Alpert gauges.

(5) Replacement of Geissler discharge tubes with thermocouple gauges.

(6) Modification of ion source for RPD measurements.

6. High Temperature Calorimetry

(A.E. Ogard)

A knowledge of the high-temperature heat content of PuO_2 is desirable both for theoretical reasons and for practical reactor safety considerations. Heat content data determined on PuO_2 can be combined with the heat content and heat of fusion data of UO_2 for calculations of some of the safety parameters of fast breeder oxide reactor fuels. The heat content of PuO_2 has been measured up to 1400°K.[43] The present study extends the measurements up to the melting point.

The drop calorimeter previously described[44] for measurements of UO_2 and $U_{0.8}Pu_{0.2}O_2$ was modified for these experiments. A tungsten-mesh vacuum furnace was used rather than the graphite furnace, and a new burnable-tungsten-wire dropping mechanism was used.

The calorimeter was calibrated electrically. The energy equivalent of the calorimeter is defined as $E = Q/\Delta T$ where Q is the electrical heat input and ΔT is the corrected temperature rise of the calorimeter block. The corrected ΔT is obtained from

$$\Delta T = T_1 - T_0 + A \int_{t_0}^{t_1} (T_1 - T_0)\, dt \qquad (1)$$

where T_0 and T_1 are the initial and maximum temperatures of the calorimeter. The integral term in equation (1) is the heat lost by the calorimeter to the isothermal surroundings during the experiment. The calorimeter cooling factor A and the energy equivalent E were obtained experimentally using several rates and total amounts of heating. The energy equivalent E was defined as being constant for all conditions including the extreme conditions of rapid heating and large ΔT (up to 10°C) experienced in high temperature heat content measurements.

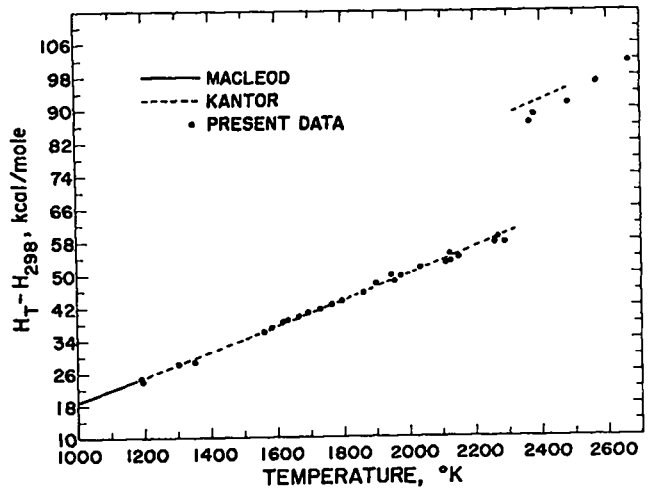

Figure 463-10. Heat content of synthetic sapphire, Al_2O_3

The heat content of synthetic sapphire, Al_2O_3, was measured as a check on the calibration procedure. The results are shown in Figure 463-10 along with the results of Macleod[45] and Kantor.[46] Other investigations are not shown in order to simplify the graph. The present results tend to be lower at the higher temperatures than the results of Kantor. However, up to the melting point of Al_2O_3, agreement is certainly within the limits of error of high temperature calorimetry.

Heat content data of PuO_2 was obtained on high-purity sintered pellets enclosed in a welded tungsten capsule. Analytical details of the PuO_2 are shown in Table 463-XIV.

Table 463-XIV

ANALYSIS OF PuO_2 PELLETS

Weight PuO_2: 55.7450 g
Weight tungsten capsule: 102.8692
Lattice parameter: $a_o = 5.3958 \pm 0.0003$ Å - single phase
Metallographic analysis: single phase
Chemical analysis: $PuO_{2.001}$ (pretest)

Pu	87.93%		
O	11.78%		
C	< 10 ppm	Ti	3 ppm
N	4	Cu	3
Mg	12	Zr	< 10
Al	32	Cr	12
Mo	5	Fe	100
Si	35	Ni	10
K	9	Zr	20
Ca	28		

Li, Be, B, Na, V, Mn, Co, Rb, Sr, Y, Cd, Sn, Cs, Ba, La, Hf, Pb, Bi -- All < 1 ppm.

Table 463-XV

HIGH-TEMPERATURE HEAT CONTENT OF PuO_2

Temp., °K	H_T-H_{298}, kcal mole^{-1} Observed	Calculated	% Difference
1500	25.35	25.19	- .63
1640	29.25	28.55	- 2.38
1700	29.39	30.02	2.14
1795	32.35	32.37	.37
1895	34.36	34.88	1.52
1920	35.68	35.52	- .46
1985	37.74	37.18	- 1.49
2055	38.66	38.98	.84
2160	41.16	41.73	1.39
2195	42.65	42.66	.02
2260	45.18	44.39	- 1.75
2370	47.19	47.36	.36
2470	53.22		
2570	57.88	Av.	± 1.1%
2610	61.06		
2640	67.38		
2715	75.30		

The heat content data obtained for PuO_2 were all corrected for the self-heating of the plutonium. New time-temperature curves of the calorimeter block were generated by correcting each minute for self-heating before ΔT was calculated by equation (1). The magnitude of this correction varies from 1.5% at 1500°K to 0.5% at 2715°K. The rate of self-heating for the PuO_2 was experimentally determined in the calorimeter as 2.20 watts/g plutonium.

The results of the high-temperature heat content of PuO_2 are shown in Table 463-XV. Calculated values of H_T-H_{298} were obtained from the equation

$$H_T-H_{298} = -6.36 + 0.0180\,T + 1.95 \times 10^{-6} T^2 + 2.46 \times 10^{2}\, T^{-1} \text{ kcal mole}^{-1} \qquad (2)$$

This equation resulted from a computor least-squares analysis of the data with the fixed parameters $\Delta H_{298} = 0$ and $C_{p\,298} = 16.4$ cal deg^{-1} mole^{-1}.

The results from 2470 to 2715°K were not used in the least-squares analysis since a very prominent positive deviation of the results was present.

The $H_T - H_{298}$ results and derived equation (2) are shown in Figure 463-11 along with a portion of the equation of Kruger and Savage.[43] The two sets of results agree within the limits of accuracy. A reasonable limit of accuracy placed on the present results is ± 1% at best.

Above 2370°K $H_T - H_{298}$ increases rapidly with

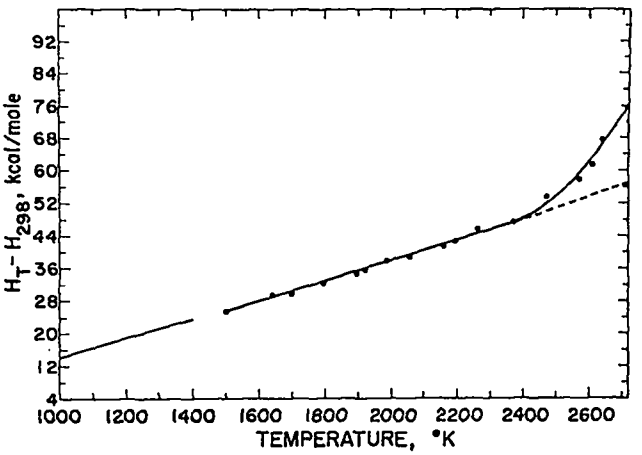

Figure 463-11. High temperature heat content of PuO_2.

increase in temperature to the melting point. The production of point defects in the PuO_2 lattice at these temperatures near the melting point may be related to this excess heat content.

The highest possible temperature in the furnace with the present tungsten-mesh heating element is 2715°K. An X-ray radiograph of the sample after the drop from this temperature showed that the PuO_2 had been molten. However, additional measurements should be made on molten PuO_2 to make certain the sample did not partially freeze during the drop into the calorimeter block. Until additional measurements are made, $H_T - H_{298}$ at 2715°K should be considered as a minimum value for that temperature. The heat of fusion of PuO_2 estimated from the difference of the 2715°K data and an extrapolation of the 1500 to 2370°K curve to the melting point is 18 kcal mole^{-1}.

Additional measurements have been made on the heat content of UO_2. The results calculated from the data in a similar manner to that reported above for PuO_2 are shown in Table 463-XVI.

Table 463-XVI

HIGH-TEMPERATURE HEAT CONTENT OF UO_2

Temp., °K	H_T-H_{298}, kcal/mole	Temp., °K	H_T-H_{298}, kcal/mole
1415	22.07	2460	47.72
1770	29.70	2575	49.96
2165	40.07	2660	53.88
2275	41.08	2720	56.54
2290	42.27	2745	56.66
2370	43.49		

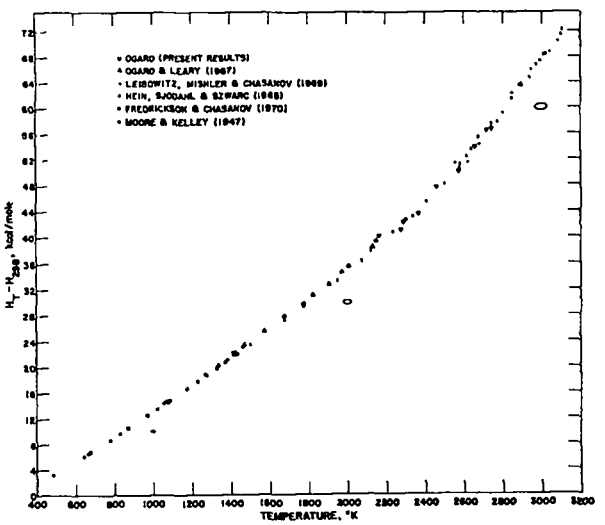

Figure 463-12. High temperature heat content of UO_2.

These results are shown in Figure 463-12 along with the actual results of Moore and Kelley,[47] Ogard and Leary,[44] Hein, Sjodahl and Szwarc,[48] Leibowitz, Mishler and Chasanov,[49] and Fredrickson and Chasanov.[50]

Also plotted at 1000, 2000 and 3000°K on Figure 463-12 are elipses showing ± 1% limits of heat content and temperature.

The comparison of these results has been discussed in the reports mentioned. However, a realistic assessment of the accuracy and precision of the experiments may not have been considered. In medium-temperature calorimetry (300 to 1400°K) the experimental methods are such that a precision and perhaps accuracy of ± 0.1% could be expected. However, as illustrated in the papers of King and Grover,[51] Macleod,[52] and West and Churney[53] differences of ± 0.2% can exist for the same data due only to the mathematical method of data treatment without any consideration for experimental error. At temperatures from 1400 to 3000°K the differences due to the method of data treatment can become even larger. This is a result of the larger amounts of heat involved, the larger non-uniformity of temperature of the calorimeter block after the drop of the capsule, and larger thermal heads or ΔT of the calorimeter block. In addition, the calibration of the optical pyrometer for high temperature measurements is good to only ± 0.5% and temperature measurement is involved twice in drop calorimetry, i.e., measurements on the empty and loaded capsules. Therefore, it is difficult to expect an accuracy in high-temperature calorimetry that is better than ± 1%. In Figure 463-12 it can be said that all the sets of results agree within ± 1% and therefore there are no trends on differences between these sets of data.

7. Transport Properties

(K. W. R. Johnson, J. F. Kerrisk)

A. Thermal Conductivity

The thermal conductivities of a number of different specimens were measured in the comparative type thermal conductivity apparatus. The following is a discussion of the individual sets of measurements. The numerical results are listed in Table 463-XVII.

LASL "Round Robin" Armco Iron - A thermal conductivity specimen was fabricated from LASL "Round Robin" Armco Iron so that measurements with the comparative type apparatus could be compared with other thermal conductivity and/or thermal diffusivity measurements at Los Alamos. The measured values were within 2% of values calculated from independent thermal diffusivity measurements.

JUZ 98071-A - This metallic specimen consisted of 90% dense U-15 w/o Pu-6.8 w/o Zr. At 600°C, the temperature of a solid phase transformation, the material became soft and deformed. Data points above this temperature were corrected to take into account this change in shape.

JUZ 98071-B - This metallic sample had the same composition as the material described above. The measurements were made with the pressure on the thermal conductivity stack reduced by an order of magnitude. Deformation occurred above 600°C but to a lesser degree than on the previous specimen.

HNL 8-32-2 - Chemical analyses of this carbide sample indicated a composition $U_{0.81}Pu_{0.19}C_{0.983}O_{0.008}N_{0.007}$. Although the material was 93.2% of theoretical density, the thermal conductivity did not increase with temperature as rapidly as single phase material of similar density. Metallographic examination of the specimen after measurements were complete showed that the top half of the specimen was essentially single phase and high density whereas the lower half contained a large number of

Table 463-XVII

THERMAL CONDUCTIVITY MEASUREMENTS

Temp., °C	Thermal Conductivity cal./sec. cm. °C
LASL "Round Robin" Armco Iron	
71	0.168
220	0.143
325	0.121
477	0.103
674	0.082
589	0.090
321	0.124
322	0.124
190	0.144
110	0.162
75	0.166
JUZ 98071-A	
110	0.030
252	0.040
492	0.056
764	0.067*
891	0.080*
477	0.058*
JUZ 98071-B	
111	0.030
342	0.046
769	0.073*
HNL 8-32-2	
119	0.0295
497	0.0329
835	0.0352
HNL 8-50-1A	
108	0.0268
237	0.0283
595	0.0333
763	0.0341
970	0.0359

*Value corrected for specimen deformation.

*Value corrected for specimen deformation.

platelets and many larger type pores. This probably was introduced during the measurement period.

HNL 8-50-1A - The specimen composition was $U_{0.81}Pu_{0.19}C_{0.97}O_{0.028}N_{0.013}$. Metallographic examination showed the presence of both M_2C_3 tangles and large platelets. As with the previous specimen the thermal conductivity did not increase as rapidly with temperature as single phase carbide of comparable density.

During the course of the thermal conductivity measurements, oxidation of sample surfaces occurred in several instances at the higher temperatures. Effluent gas from the apparatus was analyzed in a gas chromatograph. The presence of water was positively indicated. Re-examination of the apparatus with a He leak detector showed a very slow diffusion of gas from the water channel in the baseplate through the metal of the baseplate. A new baseplate was designed and fabricated and is awaiting installation.

B. Electrical Resistivity

A high temperature electrical resistivity system has been designed and is being built. The initial objective of the system is to make dc resistivity measurements on plutonium containing ceramic or metal specimens between room temperature and 2700°C. Resistivities will be measured using a four point method. Samples will be passively heated in a vacuum or inert atmosphere furnace with a tungsten mesh heater.

The electrical equipment (potentiometer with its power supply, null detector, constant currect dc supply and standard resistors) has been assembled, and the resistivities of samples of standard materials have been measured at room temperature (23 to 25°C). The samples were right circular cylinders varying from 1/4 to 1/2 in. in diameter, and 1/2 to 2 in. long. The results of the resistivity measurements are shown in Table XVIII. The high temperature furnace has been received and is awaiting installation.

Table 463-XVIII

ROOM TEMPERATURE ELECTRICAL RESISTIVITY OF STANDARD MATERIALS

Material	Resistivity, μ Ω cm
Inconel 702	124
Alloy A-286	95
Armco Iron	10.6
Tungsten	5.7
Molybdenum	5.6

A method of measuring electrical resistivity of disc shaped samples has been investigated at room temperature.[54] The method requires four contacts on the periphery of a thin slab of uniform thickness but arbitrary shape. The actual location of the contacts around the periphery is not important. The method will allow

electrical resistivity measurements to be made on thermal diffusivity disc samples. Room temperature measurements on discs of Inconel 702 and Armco Iron gave results in good agreement with those noted in Table 463-XVIII.

Since the electrical equipment necessary for electrical resistivity measurements is available but the furnace is not, an interim method is being investigated for making electrical resistivity measurements above room temperature on materials containing plutonium. A minor modification of the comparative thermal conductivity apparatus allowed electrical resistivity and Seebeck coefficient measurements to be made during a thermal conductivity run. A current flow through the sample-meter bar stack produces a voltage drop across the sample which can be measured using the Pt legs of the sample thermocouples. Samples are 1/2 in. diameter by 1/2 in. long. The thermocouple spacing is 3/8 in. The current is introduced and removed through leads which contact Pt discs at each end of the stack. This current is measured as the voltage drop across a standard resistor in series with sample-meter bar stack. Seebeck coefficients relative to Pt are determined from the voltage across the two platinum legs of the sample thermocouples with no current flow and the same temperature gradient used for the thermal conductivity measurements. Absolute Seebeck coefficients are calculated from the relative values and the absolute Seebeck coefficient of Pt.

Preliminary tests indicated that the resistivities are particularly sensitive to the alignment of the sample-meter bar stack since the voltage probes (thermocouples) are close to the sample-meter bar interface and misalignment causes a non-uniform current distribution through the sample. To assure alignment the room temperature resistivity of the sample in the thermal conductivity apparatus is compared with a previous room temperature measurement of the resistivity outside the apparatus using a voltage probe spacing of approximately 0.06 inch. This smaller voltage probe spacing eliminates most of the end effects due to a non-uniform current distribution at the ends of the sample.

To date one run has been made on $U_{0.80}Pu_{0.20}C$ sample HNL 8-50-1A (described in the thermal conductivity section). The resistivity and Seebeck coefficient results are shown in Table 463-XIX.

Table 463-XIX

ELECTRICAL PROPERTIES OF $U_{0.80}Pu_{0.20}C$
(HNL 8-50-1A)

Temp., °C	Resistivity μ Ω cm	Absolute Seebeck Coefficient μv/°K
2.3	110	—
108	128	+ 36.5
237	145	+ 35.4
595	241	+ 31.8
763	287	+ 29.2
970	312	+ 26.1

C. Thermal Diffusivity

A system for measuring the thermal diffusivity of plutonium containing ceramic materials between room temperature and 2700°C is being constructed. The diffusivity measurements will be made using a flash technique in which a laser (Korad Model K-2, 125 joule laser) pulse will heat the front surface of a disc shaped sample while the back surface temperature is monitored with thermocouples or optical sensors. The sample will be heated passively in a vacuum or inert atmosphere furnace using a tungsten mesh heater.

The laser with its associated auxiliary equipment has been received and set up for preliminary operation. A circulating water system, which supplies cooled, constant temperature, distilled water to the laser head was constructed. Preliminary tests included an examination of the laser pulse shape and duration using a photo diode detector and of the laser energy output using a laser calorimeter. The pulse duration of approximately 1/2 m sec was short enough to be considered instantaneous for most materials. The energy output can be varied between approximately 1 joule and 125 joules. Problems with decreasing energy output with time were traced to scale on the aluminum flash lamp reflector in the laser head, thus reducing its reflectivity. Modifications in the cooling water system and a new reflector have eliminated this problem. The high temperature furnace has been received and is awaiting installation.

A series of room temperature thermal diffusivity measurements on samples of five different materials (Armco Iron, Inconel 702, Alloy A-286, tungsten, and molybdenum), were started. The initial measurements indicated that the time-temperature curve at the back of the sample, sensed with thermocouples and recorded on an oscilliscope, was extremely sensitive to the exact location of the thermocouples on the back of the sample. This was attributed to a non-uniform energy density in the laser beam. Two techniques were employed to examine the beam energy distribution: (1) photographing a magnified image of the beam with infrared film, and (2) flashing a thin sheet of copper with the laser and recording the temperature rise as a function of location. Both methods give indications of a significantly non-uniform energy distribution in the beam over the sample face (0.4 inch diameter). Subsequent work with the photographic technique indicated that a uniform energy distribution could be achieved by imaging a plane of the beam within the laser cavity onto the sample face.

8. Mechanical Properties

(M. Tokar)

A. Hot Hardness

A microindentation hardness tester has been used to determine the hardness as a function of temperature of several uranium-plutonium carbides and of PuN. The hardness indentations were made in vacuum at temperatures up to 1000°C. A diamond indentor was used with a load of 200 g.

The mean hardness numbers obtained on some carbides are shown in Figure 463-13. (As a basis of comparison, type 316 stainless steel has a DPH of app approximately 215 at room temperature and DPH 35 at 1000°C.) At temperatures above 500°C, it may be seen that plutonium monocarbide is considerably softer than plutonium sesquicarbide and the solid solution uranium-plutonium monocarbides. The $U_{0.47}Pu_{0.53}C_{1.03}$ solid solution was harder at elevated temperatures than the $U_{0.79}Pu_{0.21}C_{0.95}$ composition. Apparently some solid solution strengthening similar to that encountered is metal alloys (such as Cu-Ni) is obtained on alloying UC with PuC. Future work will be concerned with determining the effects of the solid solution carbides. These

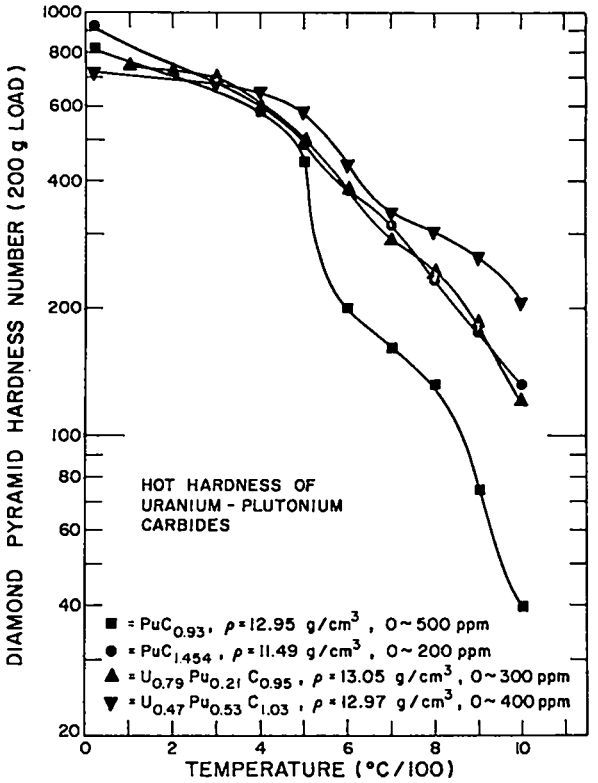

Figure 463-13. Hot hardness of uranium-plutonium carbides

tests provide a relatively quick means of obtaining a measure of high temperature mechanical strength as a function of composition.

The hot hardness of PuN, UN, and $U_{0.7}Pu_{0.3}N$ are shown in Figure 463-14. It is apparent that a strenghening or hardening effect is obtained from alloying UN with PuN, since the PuN-UN solid solution is harder than

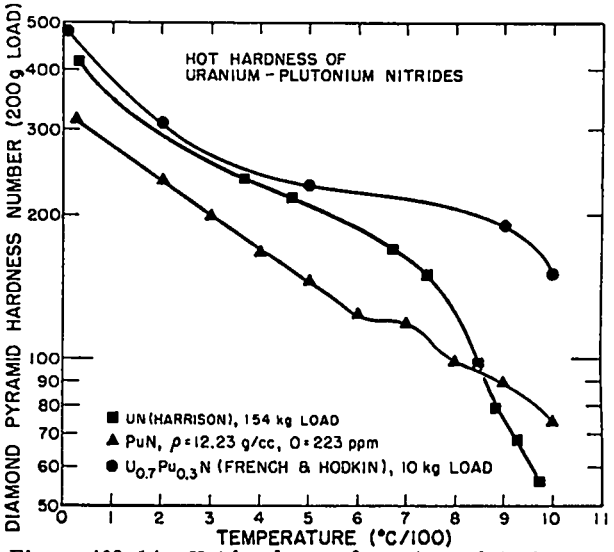

Figure 463-14. Hot hardness of uranium-plutonium nitrides.

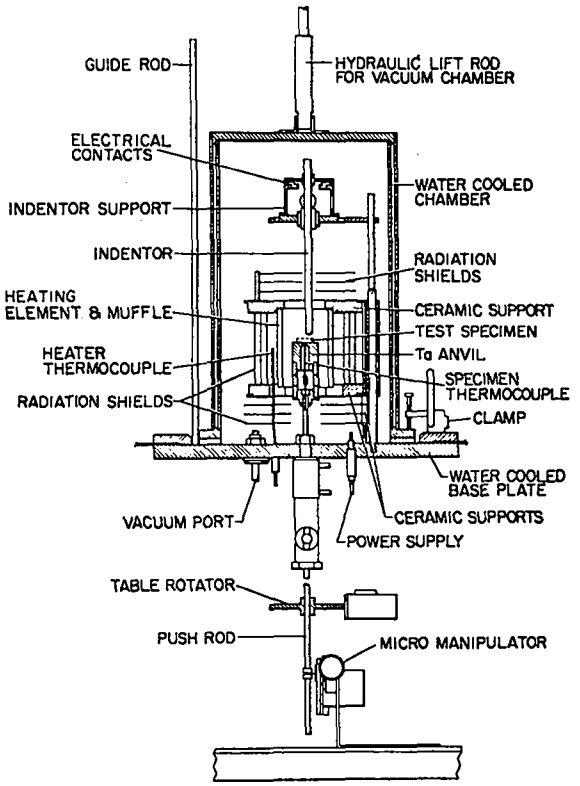

Figure 463-15. Schematic diagram of hot hardness apparatus.

either component alone. Future work will include investigation of the effects of U/Pu ratio on the hardness of the mononitrides.

Figure 463-15 is a schematic diagram of the hardness tester as modified for use at temperatures above 1000°C. The radiation shields, anvil, and metallic supports are made of tantalum. The ceramic parts are Al_2O_3 and the indentor is B_4C. The higher temperature capability provided by the use of these materials in place of less refractory ones, should make it possible to obtain some useful correlations between hot hardness and creep, since creep tests on $U_{0.80}Pu_{0.20}C$ are being conducted at temperatures between 1300-1500°C.

B. Compressive Creep

The compressive creep of solid solution carbides is being studied at temperatures from 1300 to 1500°C and pressures of 2000 to 6000 psi. The effects of microstructural variables such as porosity, grain size, and secondary phases on the creep rate are of particular interest. An effort is also being made to gain a better understanding of the fundamental mechanisms of creep in this material.

Specimens currently being tested have a sintered density of 11.5 g/cm^3 with an analyzed composition of $U_{0.79}Pu_{0.21}C_{1.02}$. Hence, the specimens contain a small amount of sesquicarbide. During creep testing these specimens increase in density; for example a specimen deformed 33.8% at 1500°C and 2000 psi had a final density of 12.2 g/cm^3.

Creep rates measured to date are compiled in Table 463-XX. These creep rates are higher than those reported for UC under similar test conditions. This result may be related to the relatively low sintered density of the solid solution test specimens. Hot hardness tests conducted to 1000°C have shown that the hardness of the solid solution U-Pu carbide is greater than that of UC.

Table 463-XX

COMPRESSIVE CREEP RATES OF $U_{0.79}Pu_{0.21}C_{1.02}$

Temp., °C	Pressure, psi	Creep Rates hr^{-1}
1300	4000	7.24×10^{-5}
1400	2000	3.29×10^{-4}
1400	4000	1.39×10^{-3}
1500	2000	2.64×10^{-3}

Microstructure studies indicate that the major portion of creep can be attributed to grain boundary sliding, although the evidence is of an indirect nature. The amount of grain boundary sliding can be inferred from measurements of the average grain shape, defined in terms of the parameter (L/B) where L is the average grain length and B the width, referred to the compressive stress direction. Sample areas in the sectioned, polished, and etched specimens are photographed and individual grains are measured. The change in interior grain shape is compared with the change in specimen shape (total specimen deformation). The amount of grain-boundary sliding is then deduced from the difference. For example, the L/B ratio for a specimen deformed 23.6% was 0.99, indicating very little change in grain shape. This indicates that most of the creep resulted from grain boundary sliding. Studies of changes

in pore shape agree with the grain shape studies. That is, while the pores in the as sintered condition are generally round, in specimens which are severely deformed the pores are elongated in a direction parallel to the compressive stress direction and have serrated edges. Plastic flow, i.e., dislocation glide, would on the other hand, not only cause changes in grain shape but would also flatten the pores in the compressive stress direction.

C. Elastic Constants of $U_{0.80}Pu_{0.20}C$
(A. W. Nutt)

Room temperature longitudinal and transverse sound velocities of polycrystalline single phase $U_{0.80}Pu_{0.20}C$ have been measured by employing a conventional ultrasonic pulse-echo technique. The isotropic elastic moduli and Poisson's ratio were calculated from the measured sound velocities (Table 463-XXI) and were evaluated as a function of material density. The Debye temperature of the single phase carbide solid solution was computed from the extrapolated sound velocities for fully dense carbides.

The results of this investigation are presented in Table 463-XXII. Since there have been no published

Table 463-XXI

EQUATIONS USED TO CALCULATE THE ROOM TEMPERATURE ISOTROPIC ELASTIC CONSTANTS AND THE DEBYE TEMPERATURE OF OF SINGLE PHASE $U_{0.80}Pu_{0.20}C$

Technique: Pulse-Echo
Frequency: 10 MHz
Specimen Size: Approx. 3/8" Dia x 1/2" Length

$$V_L = \frac{2L}{t} \qquad \text{(Longitudinal Velocity)}$$

$$V_s = \left[\left(\frac{\Delta t}{D}\right)^2 + \left(\frac{1}{2L}\right)^2\right]^{-1/2} \qquad \text{(Shear Velocity)}$$

$$\bar{V}_m = \left[\frac{1}{V_L^3} + \frac{2}{V_s^3}\right]^{-1/3} \qquad \text{(Average Velocity)}$$

$$\nu = \frac{2-2\left(\frac{V_L}{V_s}\right)^2}{2-\left(\frac{V_L}{V_s}\right)^2} \qquad \text{(Poisson's Ratio)}$$

$$G = V_s^2\rho \qquad \text{(Shear Modulus)}$$

$$E = 2G(1+\nu) \qquad \text{(Young's Modulus)}$$

$$B = V_L^2\rho - 4/3\,G \qquad \text{(Bulk Modulus)}$$

$$\theta = \frac{h}{k}\left[\frac{3N_o\rho}{4\pi M}\right]^{-1/3} \qquad \text{(Debye Temperature)}$$

where
t = time of longitudinal flight
Δt = time between longitudinal and transverse flight
ρ = sample density
D = sample diameter
L = sample length
h = Planck's constant
k = Boltzmann constant
N_o = Avogadro's number
m = molecular weight of sample

Table 463-XXII

ROOM TEMPERATURE ISOTROPIC ELASTIC CONSTANTS FOR SINGLE PHASE $U_{0.8}Pu_{0.2}C_{1-x}$

U = 75.09 w/o
Pu = 19.20 w/o
C = 4.71 w/o
a_o = 4.9651 ± 0.0003 Å
ρ_o = 13.576 gms/cm³
Grain size = 20 microns
Oxygen Content: 260 ppm
Nitrogen Content: 265 ppm
Metallic Impurities: < 400 ppm

Elastic Constant	Porosity Dependence (P = volume fraction porosity)	Standard Deviation
Young's Modulus, kilobars	E = 2023 (1-1.54 P)	54.4
Shear Modulus, kilobars	G = 785 (1-1.52 P)	26.1
Bulk Modulus, kilobars	B = 1603 (1-1.73 P)	110.7
Poisson's Ratio	ν = 0.290 (1-0.21 P)	0.018

elastic data to date for this compound, 100% dense elastic moduli of single phase $U_{0.80}Pu_{0.20}C$ cannot be directly compared. Table 463-XXIII is a comparison of the data obtained in this investigation with the elastic data of UC obtained by French workers.[55] The extrapolated elastic moduli of $U_{0.80}Pu_{0.20}C$ are slightly smaller than the extrapolated elastic moduli for UC. Poisson's ratio for theoretically dense $U_{0.80}Pu_{0.20}C$ was calculated to be 0.29, which is in good agreement with the 0.295 for UC reported by BMI,[56] and the 0.286 reported by Padel and DeNovion. Poisson's ratio decreased with increasing porosity, which corroborates data found in other elastic constant investigations.[55,57,58] Although the data of this investigation are of a preliminary nature (estimated accuracy of ± 5%), they appear to be in agreement with results obtained on UC.

The Debye temperature of this material, calculated from the theoretically dense sound velocities, is approximately 323°K. The standard deviation of this computation was 5°K. From data available on the elastic and thermodynamic properties of UC and PuC, Kempter[59] calculated the Debye temperature of PuC to be 271°K. This estimate, combined with the 330°K Debye temperature for UC,[59] allows one to estimate the Debye tem-

Table 463-XXIII

COMPARISON OF $U_{0.8}Pu_{0.2}C$ ELASTIC CONSTANTS WITH UC ELASTIC CONSTANTS*

	$U_{0.80}Pu_{0.20}C_{1-x}$	UC†
Young's Modulus (kilobars)	E = 2023 (1-1.54 P)	E = 2249 (1-2.30 P)
Shear Modulus (kilobars)	G = 785 (1-1.52 P)	G_o = 873 (1-1.92 P)
Bulk Modulus (kilobars)	B = 1603 (1-1.73 P)	B_o = 1768 (1-2.49 P)
Poisson's Ratio	ν = 0.290 (1-0.21 P)	ν = 0.288 (1-0.59 P)

*P = volume fraction porosity
†Calculated from 1st order P Mackenzie equation

perature of $U_{0.80}Pu_{0.20}C$ compositions to be 318°K, which is in good agreement with the data obtained in this investigation.

IV. ANALYTICAL CHEMISTRY

1. Determination of O_2 in Refractory Oxides, Carbides, and Nitrides

(M.E. Smith and J.E. Wilson)

Modifications to improve the method for measuring O_2 in ceramic-type Pu fuel materials are being investigated because of the great effects caused by this element on the properties of refractory oxides, carbides, and nitrides. One promising modification is the use of a microwave-excited, emissive detector system to measure the O_2 evolved as CO from the sample as it is inductively heated to 2000°C in a graphite crucible. A known fraction of the CO is swept by Ar through a fused-silica cell where a discharge is produced by microwave excitation of the CO. The discharge is monitored photometrically, and the O_2 concentration is calculated from the time-integrated signal from the photometer. Apparent advantages possible with this modification are rapidity of analysis, applicability to small (10- to 60-mg) samples, and continuous recording of CO evolved which aids greatly in selection of optimum operating conditions.

Repeated analyses of several refractory oxides used as standin materials for oxide fuels, show that the precision (1σ) ranges between 0.6 and 1.6 relative percent (Table 463-XXIV). The calculations are based on a standard curve prepared from data obtained for various amounts of U_3O_8. These precisions are smaller than the 10 relative percent of the capillary trap-micromanometric measurement of O_2,[60] but not as small as the 0.2 relative percent of the inert gas fusion-gravimetric method.[61] There is not a significant bias except for the determination of O_2 in Ta_2O_5, in which case an apparent bias of -1.8 relative percent exists. Additional analyses of Ta_2O_5 are planned for the purpose of finding the cause of the small bias. Data are being obtained to extend the range of the calibration curve and to determine if calibration for each specific oxide is necessary for better precision.

A second modification being investigated is substitution of impulse heating for induction heating of the sample. In the impulse heater fabricated at LASL, the sample in a small covered graphite crucible is heated within 1 to 2 sec to about 3000°C by a large direct current of short duration. The O_2 in the sample is evolved as CO which is trapped on SiO_2 gel cooled in liquid N_2 and then measured on a gas chromatograph. Apparent advantages of impulse heating over induction heating include: high sample temperatures rapidly attained, little outgassing from the small capsules, short analysis time, and elimination of sample loss by using covered capsules.

Table 463-XXIV

DETERMINATIONS OF O_2 IN REFRACTORY OXIDES

Oxide	Calculated O_2 Content, %	No. of Determinations	Av. O_2 Found, %	Recovery %	Rel. Std. Dev., %
U_3O_8	15.18	5	15.12	99.6	0.8
ZrO_2	25.73	5	25.81	100.3	1.6
ThO_2	12.16	5	12.19	100.2	0.9
Nb_2O_5	30.10	5	30.16	100.2	1.1
Ta_2O_5	18.10	5	17.77	98.2	0.6

Following initial tests that showed some pitting on the electrode surfaces contacting the graphite crucible, changes were made in the shapes of the electrodes and capsules which greatly reduced the amount of pitting and increased the temperature attained to slightly above 3400°C, as verified by the fact that W metal melted in two test capsules. Analyses of prepared U_3O_8-TaC mixtures, each weighing about 5 mg, for O_2 showed that the precision (1σ) of the method was about 10 relative percent. Air trapped in the capsule during loading of the sample was found to contribute significantly to the high reagent blanks and to affect the precision of the method adversely. The heater and sample-loading systems were redesigned to make the apparatus more compact, and to permit loading of samples in a He atmosphere. Testing of the modified equipment was started to determine if the apparatus blank was reduced and the precision was improved.

V. PUBLICATIONS

1. "Mass Spectrometric Studies of Plutonium Compounds at High Temperatures. V. The Plutonium-Carbon System", R.A. Kent, presented at the International Conference on Mass Spectroscopy, Kyoto, Japan, September 8-12, 1969.

2. "Ceramic Plutonium Fuel Materials Research at Los Alamos Scientific Laboratory", J.A. Leary and R.A.

Kent, invited paper presented at the Japan Atomic Energy Research Institute, Tokai-Mura, Japan, September 17, 1969.

3. "The Thermal Conductivity of Uranium-Plutonium Carbides", K.W.R. Johnson and J.A. Leary, Trans. Amer. Nuc. Soc., 12, 591 (1969).

4. "Determination of Oxygen in Refractory Oxides: Gas Chromatographic Method", D.E. Vance, M.E. Smith, and G.R. Waterbury, LA-4439, 1970.

5. "Crystallographic and Magnetic Ordering Studies of Plutonium Carbides Using Neutron Diffraction", J.L. Green, G.P. Arnold, J.A. Leary, and N.G. Nereson, J. Nucl. Mat., 34, 281-289 (1970).

6. "Present Status of the Uranium-Plutonium-Carbon Phase Diagram", J.A. Leary, Ceramic Nuclear Fuels Symposium, pp 38-50 (1969), publ. by American Ceramic Society, Columbus, Ohio.

7. "Mechanical Properties of Carbide and Nitride Reactor Fuels", M. Tokar, A.W. Nutt, and J.A. Leary, presented at American Nuclear Society Winter Meeting, San Francisco (Dec. 1969).

8. "The Thermal Conductivity of Uranium-Plutonium Carbides", K.W.R. Johnson and J.A. Leary, presented at American Nuclear Society Winter Meeting, San Francisco (Dec. 1969).

9. "The Thermal Diffusivity of Heterogeneous Materials by the Flash Method", J.F. Kerrisk, J. of Appl. Phy. (1970, in press).

10. "EMF Cells Containing Electroactive Ions in More than One Oxidation State: Properties of Pu_2C_3, $PuCl_3$, and $PuCl_4$ in LiCl-KCl", G.M. Campbell, submitted to J. Phys. Chem. (1970, in press).

11. "Differential Thermal Analysis Apparatus for Observation of Refractory Plutonium Compounds", J.G. Reavis, J.F. Buchen, and J.A. Leary, Los Alamos Scientific Laboratory Report LA-4103 (1969).

12. "Synthesis and Fabrication of Pure Single Phase Uranium-Plutonium Monocarbide Pellets", M.W. Shupe, A.E. Ogard, and J.A. Leary, Los Alamos Scientific Laboratory Report LA-4283 (1969).

13. "Plutonium Carbides", A.E. Ogard and J.A. Leary, Los Alamos Scientific Laboratory Report LA-4415 (1970).

VI. REFERENCES

1. Annual Status Report on the Advanced Plutonium Fuels Program, July 1, 1968 to June 30, 1969, Los Alamos Scientific Laboratory Report LA-4284-MS, p. 74.

2. L.S. Levinson, J. Chem. Phys. 38, 2105 (1963).

3. J.T. Dalton, E.A. Harper, H.J. Hedger, and R.W. Stannard, U.K.A.E.A. Report AERE-R 5948 (1969).

4. E.A. Harper, H.J. Hedger, and J.T. Dalton, Nature 219, 151 (1968).

5. M.H. Rand and R.S. Street, U.K.A.E.A. Report AERE-M 973 (1962).

6. P.G. Pallmer, U.S.A.E.C. Report HW-72245 (1962).

7. A.L. Bowman, J. Inorg. Nucl. Chem., 19, 111 (1966).

8. J.G. Reavis, M.W. Shupe, C.W. Bjorklund, and J.A. Leary, Transactions of the American Nuclear Society 10, 111 (1967).

9. U.S. A.E.C. Report ORNL-4480, pp 130 (1969).

10. H.K. Clark and J.L. Hoard, J. Am. Chem. Soc. 65, 2115-2119 (1943).

11. G. Zdanov and N. Sevastyanov, Compt. rend. (Doklady) Acad. Sci. U.S.S.R. 32, 432 (1941).

12. R. Kranz, Hamburger Beitr. Angew, Mineral. Kristallphy, Petrogen. 2, 99-115 (1959).

13. U.S.A.E.C. Report ARF-2200-12 (1961).

14. R.D. Allen, J. Am. Chem. Soc. 75, 3582 (1953).

15. C.E. Lowell, J. Am. Ceram. Soc. 50, 142 (1966).

16. Zhdanov, Zhuravlev and Zevin, Doklady Akad. Nauk S.S.S.R. 92, 767 (1953).

17. A.H. Silver and P.J. Bray, J. Chem. Phys. 31, 247 (1959).

18. C.W. Tucker and P. Senio, Acta Cryst. 8, 371 (1955).

19. W.M. Olson and R.N.R. Mulford, "Thermodynamics of Nuclear Materials", IAEA, Vienna, 1968, p. 467.

20. P.S. Harris, B.A. Phillips, M.H. Rand, and M. Tetenbaum, UKAEA Report AERE-R 5353 (1967).

21. R.A. Kent, "Mass Spectrometric Studies of Plutonium Compounds at High Temperatures. V. The Plutonium-Carbon System", presented at the International Conference on Mass Spectrometry, Kyoto, Japan, September, 1969.

22. G.M. Campbell, J. Phys. Chem. 73, 350 (1969).

23. Ref. 4 cited by R.S. Nicholson, Analytical Reviews, 1970, Fundamentals, Anal. Chem. 42, 132R (1970).

24. L. M. Atlas, et al., unpublished results, ANL 1967.

25. J. O'M. Bockris and S. Srinivasan, "Fuel Cells: Their Electrochemistry", McGraw Hill Book Co., New York, N.Y., 1969, p. 471.

26. G.M. Campbell, R.A. Kent, and J.A. Leary, "Thermodynamic Properties of the Pu-C System", to be presented at the Fourth Int. Conf. on Pu and Other Actinides, Santa Fe, N.M., Oct. 5-9, 1970.

27. Quarterly Status Report on the Advanced Plutonium Fuels Program, April 1 to June 30, 1969, Los Alamos Scientific Laboratory Report LA-4284-MS (1969), p 77.

28. Quarterly Status Report on the Advanced Plutonium Fuels Program, July 1 to September 30, 1969, Los Alamos Scientific Laboratory Report LA-4307-MS (1969), p 23.

29. R.A. Kent, "Mass Spectrometric Studies of Plutonium Compounds at High Temperatures. V. The Plutonium-Carbon System", presented at the International Conference on Mass Spectrometry, Kyoto, Japan, September 8-12, 1969.

30. Quarterly Status Report on the Advanced Plutonium Fuels Program, October 1 to December 31, 1969, Los Alamos Scientific Laboratory Report LA-4376-MS (1970), p 21.

31. Quarterly Status Report on the Advanced Plutonium Fuels Program, January 1 to March 31, 1970, Los Alamos Scientific Laboratory Report LA-4437-MS (1970), p 12.

32. R.A. Kent and J.A. Leary, Los Alamos Scientific Laboratory Report LA-3902 (1968).

33. R.A. Kent, High Temperature Science 1, 169 (1969).

34. M.H. Rand, "Thermochemical Properties", in Atomic Energy Review, Vol. 4, Special Issue No. 1, IAEA, Vienna (1966).

35. R.C. Feber and C.C. Herrick, Los Alamos Scientific Laboratory Report LA-3184 (1965).

36. JANAF Thermochemical Tables, The Dow Chemical Co., Midland, Mich., 1965 and Supplements.

37. M.H. Rand, "A Thermochemical Assessment of the Plutonium Carbon System", presented at IAEA, Vienna, Sept. 1968.

38. F.L. Oetting, Chem. Rev. 67, 261 (1967).

39. G.K. Johnson, Argonne National Laboratory, private communication, 1970.

40. U.S. National Bureau of Standards, Gold Standard Reference Material 745.

41. J.W. Tester, R.C. Feber and C.C. Herrick, J. Chem. Eng. Data 13, 419 (1968).

42. R. Hultgren, R.L. Orr, P.D. Anderson and K.K. Kelley, Selected Values of Thermodynamic Properties of Metals and Alloys, J. Wiley and Sons, Inc., New York, N.Y., 1963.

43. O.L. Kruger and H. Savage, J. Chem. Phys. 49, 4540 (1968).

44. A.E. Ogard and J.A. Leary, "Thermodynamics of Nuclear Materials, 1967", IAEA, Vienna, 651 (1968).

45. A.C. Macleod, Trans. Far. Soc. 63, 300 (1967).

46. P.B. Kantor, L.S. Lazareva, V.V. Kandyba, and E.M. Fomichev, Ukra, Fiz. Zhur. 7, 205 (1962).

47. G.E. Moore and K.K. Kelley, J. Am. Chem. Soc. 69, 2105 (1947).

48. R.A. Hein, L.H. Sjodahl and R. Szwarc, J. Nucl. Mater. 25, 99 (1968).

49. L. Leibowitz, L.W. Mishler, and M.G. Chasanov, J. Nucl. Mater. 29, 244 (1969).

50. D.R. Frederickson and M.G. Chasanov, in press.

51. A. King and H. Grover, J. Appl. Phys. 12, 557 (1941).

52. A.C. Macleod, Trans. Far. Soc. 63, 289 (1967).

53. E.D. West and K.L. Churney, J. Appl. Phys. 39, 4206 (1968).

54. L.J. van der Pauw, Phillips Research Reports, 13, No. 1, 1 (1958).

55. T.A. Padel and C.H. DeNovion, "Constantes Elastiques des Carbures, Nitrures, et Oxides. D'Uranium et D'Plutonium", J. Nucl. Mater. 33, 1, pp 40-51 (1969).

56. E.O. Speidel, D.E. Kizer, and D.E. Keller, "Preparation and Properties of UO_2, UN, and UC Cermet Fuels", BMI-1842, June 1968.

57. S. Spinner, F.P. Knudsen, and L. Stone, "Elastic Constant - Porosity Relations for Polycrystalline Thoria", J. of Rec. of the NBS, Vol. 67C, 1 (1963).

58. R.F. Brenton, C.R. Saunders, and C.P. Kempter, "Elastic Properties of Niobium Monocarbide to High Temperatures", J. Less Common

59. C. P. Kempter, "Debye Temperature of Some Metal Monocarbides", Short Note to be published in Phys. Stat. Sol.

60. W. G. Smiley, Anal. Chem. 27, 1098 (1955).

61. C. S. MacDougall, M. E. Smith, and G. R. Waterbury, Anal. Chem. 41, 372 (1969).

PROJECT 464

STUDIES OF Na-BONDED (U, Pu)C LMFBR FUELS

Person in Charge: D. B. Hall
Principal Investigator: J. C. Clifford

I. INTRODUCTION

Sodium-bonded (U, Pu)C is an attractive LMFBR advanced fuel concept because of its potential for operation at high specific power and moderate temperature, and for rather straightforward accommodation of fuel swelling. The object of this project has been to investigate, by out-of-pile experimentation, major uncertainties associated with the use of Na-bonded carbides, and to develop adequate equipment and procedures for handling these reactive materials. Of prime concern have been the compatibility of high purity, single phase (U, Pu)C with potential cladding materials in the presence of sodium, and the effects of fuel and sodium variables on overall compatibility.

Funding for this program was withdrawn at the end of FY 1970 and work has been terminated except where required for direct support of fuel irradiation experiments. Topical reports are being prepared covering phased-out activities.

II. LOADING FACILITY FOR TEST CAPSULES
(D. N. Dunning, J. O. Barner, J. A. Bridge)

A. General

A prerequisite to compatibility and irradiation programs involving (U, Pu)C and sodium is a satisfactory capsule loading and bonding facility. There is little point to obtaining well-characterized materials for testing if these materials are subject to contamination by impurities before they are placed in test. Sodium and (U, Pu)C are sufficiently reactive that all operations must be performed either in vacuum or in a high quality inert atmosphere. A loading facility for handling these materials has been constructed and is operational. The facility consists of inert-atmosphere gloveboxes equipped with gas cleanup systems to provide an environment for handling fuel pellets and bonding sodium with a minimum of contamination.

B. Results During FY 1970

During FY 1970 the EBR-II capsules were loaded utilizing modified sodium bonding procedures necessitated by the persistent occurrence of significant discontinuities in sodium bonds and by fuel pellet chipping. The following procedures were found effective:

1. Evacuate the loaded capsule to less than 10 microns pressure while the sodium is molten. Cool the capsule from the bottom up, back-fill with helium, and weld the top closure plug in place.
2. Place the sealed capsule in the centrifuge and heat, impressing an axial temperature gradient along the 14-1/2-in. fuel stack (150°C at the bottom and 280°C at the top).
3. Cool the centrifuge to room temperature while spinning at 150 rpm.
4. Heat the capsule to 600°C for 1 h and then cool to room temperature. Maintain a temperature gradient during heating and cooling so that the sodium melts from the top down and freezes from the bottom up.
5. Repeat Steps 2 and 3.

Use of this procedure has resulted in only minor bonding problems which are relieved by repeating steps 4 and 5.

Major impurities in the sodium loaded into test capsules are 7 to 16 ppm oxygen, < 10 ppm carbon, and < 1 ppm nitrogen. The sodium-handling box atmosphere during loading has been maintained at oxygen and water vapor levels of 1 to 2 ppm, as determined by on-line measuring devices. Similar levels have been confirmed for the fuel loading box.

Approximately 125 capsules were loaded with plutonium-bearing fuels during FY 1970. This includes EBR-II capsules containing $(^{235}U_{0.8}Pu_{0.2})C$ or $(^{233}U_{0.8}Pu_{0.2})C$, OWR capsules containing $(^{235}U_{0.8}Pu_{0.2})C$ and U-Pu-Zr alloys, and compatibility capsules containing all the above fuels, plutonium, and uranium.

III. SODIUM-BOND HEAT TRANSFER STUDIES
(K. L. Meier)

A. General

The purpose of this project is to evaluate the effects of fuel-pin defects on heat transfer properties of the sodium bond. Such defects could arise in a number of ways. For example, a void in the sodium bond could:

1. Be present before insertion in the reactor.
2. Come from dewetting of the pellet due to change in composition as fission products are formed.
3. Form from a hot spot on the pellet and consequent local vaporization of the sodium, and/or
4. Be produced from desorbed or fission-product gases.

Of these, probably the most serious defect would be presence of fission gas bubbles in the bond region.

One method of obtaining the high heat fluxes necessary for "defect analysis" consists of utilizing a central, high-heat-flux heater. This method is being utilized at LASL in sodium-bond heat transfer studies.

B. Results During FY 1970

All components of the apparatus for out-of-pile testing of sodium bonds utilizing a central high-heat-flux heater have been fabricated. Final assembly was begun but has not been completed. The components have been stored and a report describing the apparatus is being prepared.

IV. CARBIDE FUEL COMPATIBILITY STUDIES
(F. B. Litton, H. A. O'Brien, L.A.Geoffrion)

A. General

The objective of this research was to determine the out-of-pile metallurgical reactions affecting the integrity of sodium-bonded uranium-plutonium carbide in Type 316 stainless steel and vanadium alloy containers. The behavior of vanadium alloys in hot-trapped sodium and the carburization of Type 316 stainless steel in static sodium were phases of this investigation which were reported elsewhere.[1,2]

The transfer of carbon through static sodium is a diffusion controlled process in which the differences in chemical activity between the source and the reaction product in the solid components is the primary driving force. Long time periods are required to establish equilibria in a given system, and the chemical activities of the components may change during a carburizing process.[3] This, of course, implies that the rate-controlling steps may change. Carbon is assumed to be soluble in sodium to some small but finite amount,[4] but the reaction products are independent of the transferring species.

Alexander, Ward, Ogden and Cunningham reviewed the chemical thermodynamics for the reaction of uranium carbides with refractory metals in the temperature range of 1000^{o} to $2000^{o}C$.[5] They predicted that metal claddings of niobium, tantalum, titanium, zirconium and hafnium would react with uranium carbides in this temperature range. Their calculations indicated that tungsten and, possibly, molybdenum should not react below $1700^{o}C$ with stoichiometric uranium monocarbide, but would react with the dicarbide and sesquicarbide phases over the entire temperature range. In a study conducted by Katz, uranium monocarbide was stable in contact with molybdenum and vanadium, but reacted with Type 304 stainless steel, at temperatures below $1000^{o}C$.[6]

French and Hodkin studied the reaction of sodium bonded hyperstoichiometric uranium and uranium-plutonium carbides of equivalent carbon contents in Type 316 stainless steel containers.[7] They observed that the carbide specimens reacted similarly during a three-month period at temperatures up to $800^{o}C$. Stability of the monocarbide and sesquicarbide phases was reported, but the dicarbide phase was depleted in their specimens. Plutonium addition to hyperstoichiometric uranium

carbide is known to stabilize the sesquicarbide phase, but complete conversion of the carbon in excess of the monocarbide composition to the sesquicarbide phase in the $(U_{0.8}Pu_{0.2})C_{1+X}$ system is an extremely slow reaction, and a minor quantity of the dicarbide phase is generally present in the hyperstoichiometric composition.[8]

Sowden, Hodge, Moreton-Smith and White observed that hyperstoichiometric actinide carbides were reduced by hydrogen to the monocarbide phase at temperatures in the order of 800°C.[9] This observation proved to be a major advance in carbide technology, permitting an adjustment in carbon content of hyperstoichiometric carbide fuels during their fabrication.

B. Results During FY 1970

The metallurgical reactions affecting the results of the carbide fuel compatibility study are complex and subtly interdependent. The transfer of carbon from the fuel to the cladding alloy was of prime consideration in this study. However, in the absence of a carbon activity gradient within the capsule, external reactions within the system components may occur to render a particular configuration of dubious engineering acceptability; for example, the reaction of vanadium alloys with impurities in the coolant sodium, and the formation of Sigma phase in Type 316 stainless steel. The correlation of the metallurgical reactions observed in the experimental results with the mechanical properties of the cladding alloys was beyond the scope of this investigation.

The compatibility program consisted of the examination of Type 316 stainless steel and vanadium alloy capsules containing sodium bonded stoichiometric and hyperstoichiometric fuel carbides after heating for 1000, 3000, 4000 and 8000 h at a temperature of 750°C. The tests were conducted in capsules whose dimensions were 0.30 in. (7.6 mm) o.d. by 0.28 in. (7.1 mm) i.d. by 3.0 in. (76 mm) long. The capsules contained three fuel pellets, 0.26 in. (6.7 mm) o.d. by 0.25 in. (6.4 mm) high, and 1.0 g of sodium. The tests were conducted in triplicate in zirconium-gettered, forced-convection sodium loops.

After testing, the capsules were opened and the sodium removed by vacuum distillation at 500°C.[10] The carbide fuel and clad materials were prepared for microscopic examination by standard techniques. Selected metallographic specimens were used for electron microprobe and x-ray diffraction analyses, and for microhardness measurements to aid in identification of reaction products.

The results of tests with single-phase uranium-plutonium carbides, $(U_{0.8}Pu_{0.2})C$, synthesized and fabricated as part of the Advanced Fuels Program at Los Alamos Scientific Laboratory,[11] showed that carbon was not transferred to either Type 316 stainless steel or V-15Cr-5Ti alloy cladding materials for time periods of 1000, 3000, 4000 and 8000 h at 750°C. Mixed carbide fuels were intentionally "over-tested" in order to accelerate diffusion and reaction processes, and were not tested at temperatures lower than 750°C. Typical views of the cladding wall are shown after the 8000 h test period in Fig. 464-1 and 464-2, respectively.

After each test period investigated, the vanadium alloy was structurally stable, but the Sigma phase was formed in Type 316 stainless steel. Sigma phase formation in stainless steel is known to be time, temperature and composition dependent.[12]

A reaction layer was observed on the surface of the end-closure of Type 316 stainless steel in contact with the bottom fuel pellet. The reaction layer was not observed previous to the 8000 h test period and, then, on two of the three stainless steel capsules. The reaction layer is shown in Fig. 464-3. Electron microprobe analyses indicate an interdiffusion of plutonium from the carbide with nickel from the stainless steel. An explanation may be that, as Sigma is formed in the Type 316 stainless steel, the matrix is depleted in chromium and iron and enriched in nickel. The nickel-rich matrix then becomes incompatible with single-phase carbide, possibly forming complex intermetallic compounds, such as $(U,Pu)Ni_3$. The surface structure of the single-phase $(U_{0.8}Pu_{0.2})C$ test pellets was not affected by sodium contact. A typical view of the surface structure of a single-phase pellet is shown in Fig. 464-4.

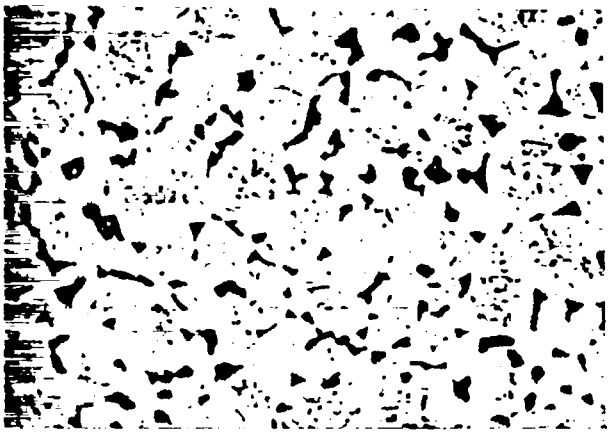

Fig. 464-1. Type 316 stainless steel showing Sigma phase formation and carbide precipitation. The microstructure indicated that carbon was not transferred to the capsule wall $(U_{0.8}Pu_{0.2})C$ in test periods up to 8000 h at 750°C. Etched, 300X.

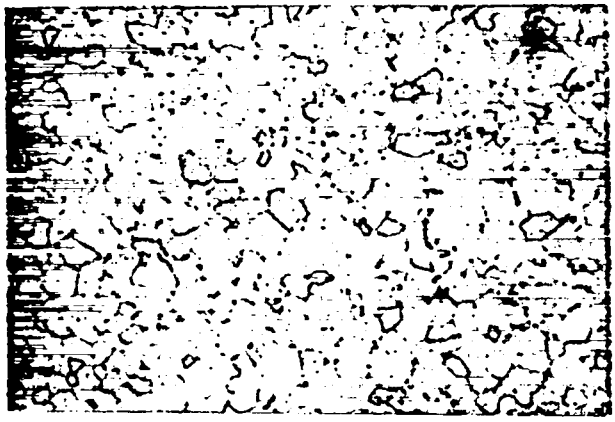

Fig. 464-2. V-15Cr-5Ti alloy showing structural stability with single-phase $(_{0.8}Pu_{0.2})C$ after an 8000 h test period at 750°C. Etched, 300X.

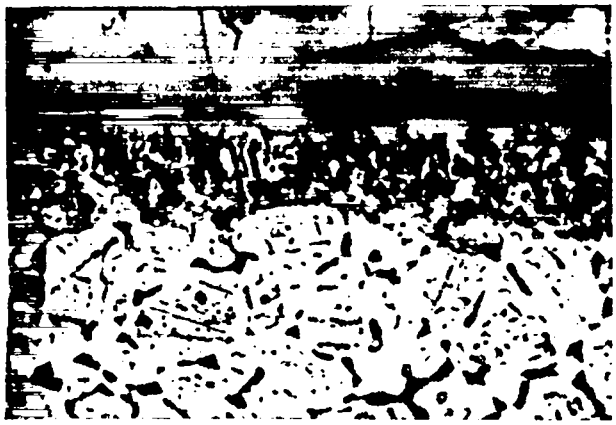

Fig. 464-3. Type 316 stainless and cap showing a reaction layer with single-phase (U, Pu)C after 8000 h at 750°C. Etched, 300X.

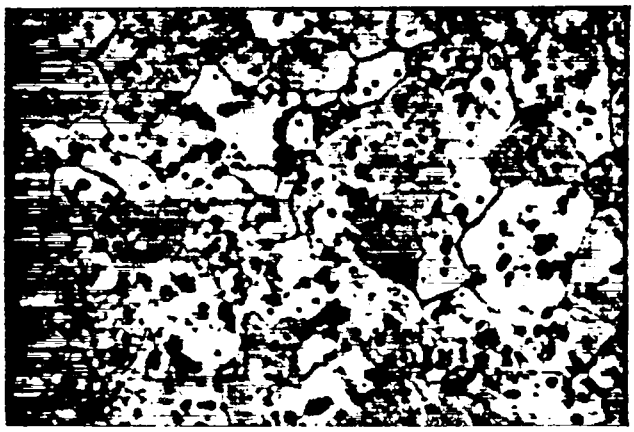

Fig. 464-4. Surface of a single-phase carbide fuel pellet after sodium contact for 8000 h at 750°C. Etched, 300X

Hyperstoichiometric uranium-plutonium carbide fuel, prepared by United Nuclear Corporation to contain ~ 10% sesquicarbide and trace amounts of the dicarbide phase, carburized Type 316 stainless steel and vanadium alloy capsule materials. The carbon transfer occurred in two sequential steps:

1. Depletion of the dicarbide phase, usually associated with sodium attack and fuel disintegration, and

2. The diffusion of carbon from the sesquicarbide phase.

The depletion of the dicarbide phase from hyperstoichiometric uranium-plutonium carbide is shown by comparing Fig. 464-5 and 464-6, showing typical microstructures before and after testing, respectively. A view indicating sodium attack and depletion of the sesquicarbide phase is shown in Fig. 464-7. Depletion of the sesquicarbide phase from fuel was observed after 4000 h in V-15Cr-5Ti alloy capsules and after 8000 h in Type 316 stainless steel capsules.

The metallographic structures of carburized cladding materials are shown in Figures 464-8, 464-9 and 464-10. The Type 316 stainless steel showed the absence of the Sigma phase in the microstructure and $Cr_{23}C_6$-type carbide precipitation along the grain boundaries and within the matrix. The V-15Cr-5Ti alloy showed carbide precipitation throughout the cross section. The amount of precipitate increased toward the fuel/sodium contact surface. The contrast, the Vanstar-7 alloy (9.4% Cr,

Fig. 464-5. Distribution of dicarbide phase in hyperstoichiometric uranium-plutonium carbide prepared to contain the sesquicarbide phase. Etched, 300X.

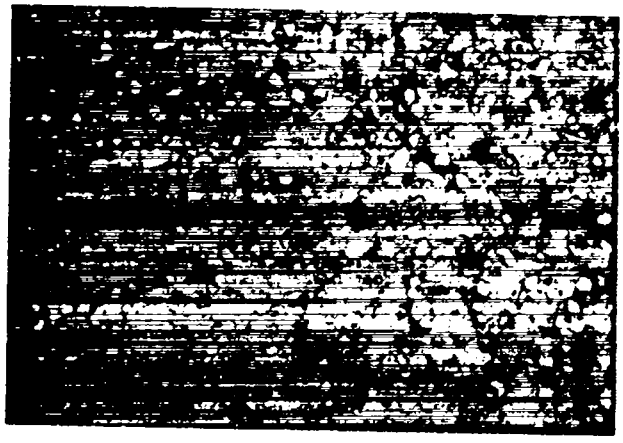

Fig. 464-6. Hyperstoichiometric uranium-plutonium carbide after testing for 4000 h at 750°C. The dicarbide phase was depleted from the pellet. Etched, 300X.

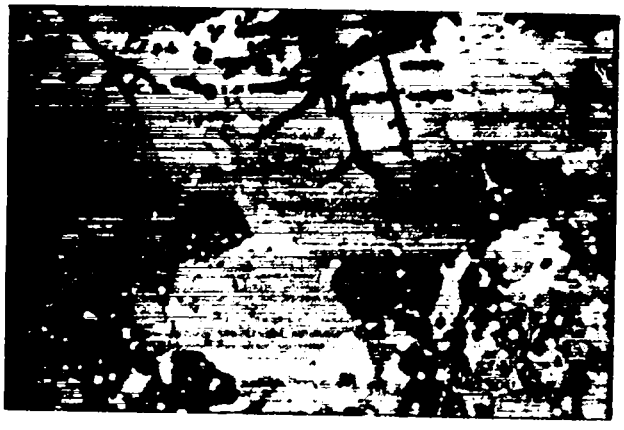

Fig. 464-7. Attack by sodium and depletion of the sesquicarbide phase near the surface of hyperstoichiometric carbide fuel. Type 316 stainless steel capsule was tested for 8000 h at 750°C. Etched, 300X.

Fig. 464-8. Type 316 stainless steel after heating with hyperstoichiometric uranium-plutonium carbide for 4000 h at 750°C. Etched, 300X.

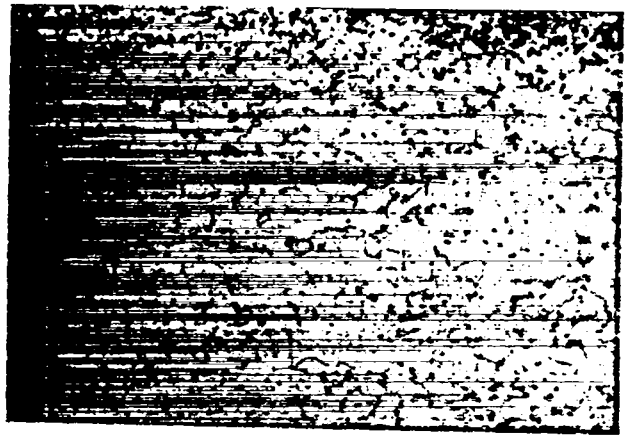

Fig. 464-9. V-15Cr-5Ti alloy after heating with hyperstoichiometric uranium-plutonium carbide for 8000 h at 750°C. Etched, 300X.

Fig. 464-10. Vanstar-7 alloy after heating with hyperstoichiometric uranium-plutonium carbide for 1000 h at 750°C. Etched, 1000X.

3.3% Fe, 1.2% Zr, 0.6% C) showed a carburized surface layer. The layer was 10 μm thick after 1000 h at 750°C. Reaction other than carburization was not observed between hyperstoichiometric carbide fuel and the cladding materials investigated.

The uniformity of the uranium and plutonium distribution between the phases in hyperstoichiometric mixed carbide fuel was determined by electron microprobe analysis. Confirming the results of Potter,[13] a heterogeneous distribution was observed. The relative standard deviations for x-ray intensities were approximately 5 and 20% for uranium and plutonium, respectively, between grains of the monocarbide in the matrix, and 1.2 and 2% within single grains. The plutonium x-ray intensity from the sesquicarbide phase was approximately 60% greater and the uranium x-ray intensity was approximately 12% less than the average intensities of these elements in the monocarbide phase.

V. REFERENCES

1. F. B. Litton, J. H. Bender, and L. A. Geoffrion, Met. Trans., AIME, 1, 441 (1970).
2. F. B. Litton and A. E. Morris, "Carburization of Type 316L Stainless Steel in Static Sodium," to be published in J. Less-Common Metals.
3. C. S. Campbell and C. Tyzack, Alkali Metal Coolants, IAEA, Vienna (1967).
4. C. Luner, A. Cosgarea, Jr., and H. M. Fader, Alkali Metal Coolants, Vienna (1967).
5. C. A. Alexander, J. S. Ward, J. S. Ogden, and G. W. Cunningham, Carbides in Nuclear Energy, 1, Macmillan and Co., Ltd., London (1964).
6. Seymour Katz, J. Nucl. Mat., 6, 2 (1966).
7. P. M. French and D. J. Hodkin, Plutonium 1965, Chapman and Hall, London (1967).
8. M. W. Shupe, A. E. Ogard, R. L. Nance and D. Kelly, Los Alamos Scientific Laboratory, LA-4114-MS.
9. R. G. Sowden, N. Hodge, M. J. Moreton-Smith, and D. B. White, Carbides in Nuclear Energy, 1, Macmillan and Co., Ltd., London (1964).
10. F. B. Litton and J. H. Bender, Nucl. Appl., 5 299 (1968).
11. R. Honnell, S. McClanahan, R. Walker, G. Moore, and C. Baker, Los Alamos Scientific Laboratory, LA-3993-MS.
12. Max Hansen, Constitution of Binary Alloys, p. 527, McGraw-Hill Book Co., Inc., New York (1958).
13. P. E. Potter,"The Plutonium-Uranium-Carbon System," Panel on the Thermodynamics of Uranium and Plutonium Carbide, IAEA, Vienna (1968).

PROJECT 465

REACTOR PHYSICS

Person in Charge: D. B. Hall
Principal Investigator: G. H. Best

I. INTRODUCTION

Basic to the evaluation of various fast breeder concepts and proposals are the analytical techniques and physical data used in the analyses. Valid comparisons between different concepts and proposals depend on minimization of differences in results due to methods of analyses. To this end, the Los Alamos Scientific Laboratory is cooperating with other AEC laboratories and contractors in the development of evaluated cross-section data and associated processing codes. In addition, the Laboratory is working on the development and maintenance of digital computer programs pertinent to the nuclear analysis of fast breeder concepts. The Laboratory is also adapting, modifying, and evaluating modular programming systems for comprehensive nuclear analysis. Finally, the Laboratory is evaluating the performance characteristics of various fast breeder reactor concepts.

II. CROSS-SECTION PROCUREMENT, EVALUATION, AND TESTING (M. E. Battat, D. J. Dudziak, R. J. LaBauve, R. E. Seamon)

A. General

Accurate predictions of reactor design parameters, such as critical mass, material worths, and spectral response, require the development and maintenance of up-to-date basic microscopic nuclear data files. To meet this end, a national cooperative program is in progress to provide an evaluated nuclear data file (ENDF/B). The large amount of experimental data which is becoming available, together with theoretical data, makes the maintenance of ENDF/B a continuing task. In addition, a large effort is needed in evaluating and testing the microscopic data prior to use in reactor calculations.

B. Data Revisions and Procurement

Revisions of the ^{6}Li and ^{7}Li data sets have been prepared and submitted to the Cross-Section Evaluation Working Group (CSEWG) for inclusion in the ENDF/B Version II library which is presently undergoing Phase II data testing. Minor changes made in 1967 and 1968 by the United Kingdom Atomic Energy Authority (UKAEA) have been incorporated in these data sets. There have been major changes made in the form used to describe the secondary neutron energy distributions. Instead of describing the secondary energy distributions as a discrete energy loss ($E' = E - \theta$), it was found that these distributions, except for the $(n,n'\gamma)$ reaction can be equally well approximated by Maxwellian distributions. Wherever possible, the Maxwellian form has been used with a concomitant 25% reduction in the size of the files.

C. Procurement and Testing of Re-evaluated ENDF/B Data

Proposed re-evaluations of the ENDF/B data for ^{235}U, ^{238}U, ^{239}Pu, ^{240}Pu, ^{241}Pu, iron, chromium, niobium, molybdenum, and ^{232}Th were distributed at the first of the year by the National Neutron Cross-Section Center (NNCSC) at Brookhaven National Laboratory (BNL) for testing by members of CSEWG. The re-evaluated data included several format options which are allowed in the ENDF/B specifications but which had not been implemented in the data processing codes. Revised versions of the ENDF/B processing codes DAMMET and CHECKER were provided by BNL. However, several changes in the data as received had to be made before they could be processed.

In connection with changes in the data format, two codes called MAKE4 and PUNCH were written. For some materials, there was no total inelastic cross

section (MT=4) given in File 3, but only the cross sections for discrete levels ($5 \leq MT \leq 14$, $51 \leq MT \leq 80$) and the continuum (MT=15). The code MAKE4 combines the cross sections and calculates the probability distributions, viz.,

$$\sigma_{MT=4}(E) = \sum_i \sigma_{MT=i}(E) \quad ,$$

and

$$P_i(E) = \frac{\sigma_{MT=i}(E)}{\sigma_{MT=4}(E)} \quad ,$$

where

$$5 \leq i < 15, \quad 51 \leq i \leq 80 \quad .$$

Program PUNCH was written to prepare cards for ETOE from File 2 unresolved resonance data given under the LRU=2, LRF=2 option. The two codes were sent to the NNCSC.

A binary input tape for the MC^2 cross-section data processing code was prepared using re-evaluated data wherever possible. Copies of this tape were supplied to all CDC-6600 users in CSEWG.

Successful MC^2 runs have been made with all re-evaluated data, except molybdenum and niobium. Additional changes in MC^2 will be required before these data can be processed.

The experimental fast critical assemblies JEZEBEL and GODIVA were used as the calculational models for the initial testing of the re-evaluated data files. In order to minimize uncertainties in the model specifications, the geometry and material specifications for these assemblies were based on a recent re-evaluation by Hansen and Paxton,[1] which resulted in modest changes in the critical masses of homogeneous spheres of the appropriate alloys.

Multigroup constants were generated from the microscopic data using MC^2. The criticality calculations assumed spherical geometry and used isotropic transport theory. The effects of higher-order anisotropic scattering and quadrature order were taken into account in arriving at the final comparison. Central reactivity worths were computed using a perturbation theory calculation.

Certain physics parameters are calculated better with the re-evaluated data, but the general lack of agreement between measured and calculated parameters indicates that deficiencies remain in the cross-section data.

These results and a comparison with values obtained using the ENDF/B data have been incorporated in a paper[2] presented at the Conference on Nuclear Data for Reactors in Helsinki, Finland, June 15-19, 1970.

D. Processing Codes

1. MC^2, ETOG, SUPERTOG. Work has continued on the comparison of the three versions (BNLMC2, WAPMC2, and BAWMC2) of the MC^2 code described in Ref. 3. The differences between these versions are well understood for the P_1 fundamental mode calculation (IOPT=1), both fine- and ultrafine-group options, for the consistent P_1 isotropic option (IOPT=3) and for the consistent B_1 anisotropic option (IOPT=4). Comparisons between the three versions of the code and with another ENDF/B multigroup processing code,[4] SUPERTOG, were presented[3] at a conference on Multigroup Nuclear Cross Section Preparation held at Oak Ridge, Tennessee, October 1-3, 1969.

In response to a request from the Reactor Physics Division at Argonne National Laboratory, recommendations were submitted for additions to and improvements in the MC^2 code. Also, the code and the current ENDF/B library tape were sent to Kirtland AFB.

A version of the ETOG code was received from Westinghouse (Atomic Power Division) and was activated on the CDC 6600. This code is used to generate multitable group-averaged cross sections directly from the ENDF/B data file. It differs from MC^2 in that a computation on an "ultrafine" mesh is not available, and only one material at a time can be processed. However, it will use a fine mesh with up to 99 points (vs 70 for MC^2) and will produce up to four-table (P_0, P_1, P_2, P_3) cross sections (vs P_0 and P_1 for MC^2). A routine was written to convert the ETOG output to the DTF-IV format and also to combine the P_0 and P_1 tables to obtain single-table isotropic transport multigroup cross sections in DTF-IV format.

A study was made of the effect of using multitable cross sections for ^{239}Pu (ENDF/B Version I data) in calculations of the JEZEBEL assembly. Multitable cross sections were obtained with ETOG using 0.5 lethargy widths from 10 MeV, infinite dilution, and a fission spectrum with a "1/E" tail as a weighting function. The DTF-IV results are shown

in Table 465-I, where it can be seen that, as the number of tables increases, the value of k_{eff} converges to 1.009 (P_∞). It can be concluded that the correction from isotropic transport to P_∞ is about 0.003 for JEZEBEL.

TABLE 465-I

SENSITIVITY OF JEZEBEL CALCULATION TO ^{239}Pu MULTITABLE CROSS SECTIONS

Tables Used in Run	k_{eff}	Running Time (CP) (sec)
One-table, isotropic transport	1.01229	107.7
One-table, P_0	1.09514	113.1
Two-table, P_1	1.00342	150.3
Three-table, P_2	1.00930	209.2
Four-table, P_3	1.00913	256.8

Note: The value for k_{eff} using all cross sections (single-table, isotropic transport) derived from MC^2 is 1.01021.

Some comparisons were made with ^{239}Pu cross sections obtained with WAPMC2 and ETOG for infinitely dilute concentration. The differences with MC^2 averaged over all groups are given in Table 465-II. Also shown are similar results obtained with the SUPERTOG code; no large discrepancies have been noted.

TABLE 465-II

COMPARISON OF SUPERTOG AND ETOG RESULTS WITH MC^2 RESULTS [^{239}Pu (MAT=1051) Cross Sections]

	% Difference	
	SUPERTOG	ETOG
Unresolved resonance		
Capture	0.6	0.4
Fission	0.5	0.4
Resolved resonance		
Capture	2.5	2.5
Fission	2.5	1.8
Total capture	1.4	1.2
Total fission	1.5	0.7

2. GLEN, FLANGE2. Work on a code to generate multigroup-multitable (MULTAB) cross sections from ENDF/B thermal data has continued. The GLEN code has been linked to the FLANGE2 code, and ENDF/B thermal data for H_2 bound in H_2O has been used for checking of results. The FLANGE2 code is used for generating fine-group cross sections, including an inelastic scattering kernel for the ENDF/B material being processed. GLEN is used for generating an infinite-medium spectrum used in collapsing to broad-group cross sections, which the code outputs in the DTF-IV format.

FLANGE2 also makes a very accurate calculation of the total inelastic cross sections directly from the $S(\alpha,\beta)$ data on the ENDF/B tape. As an option in the code, these total cross sections can be used to normalize the scattering kernels output by the code.

Further tests of the cross sections will be made by using them in the DTF-IV code to calculate an H_2O-^{235}U (300:1) system.

E. Shielding Methods

1. Photon Data Format Revision. At its September meeting, the Codes and Formats Subcommittee of CSEWG tentatively adopted a new format for storage of photon production data. The acceptance of the new format was contingent upon the submission of a detailed format and procedures document to supersede LA-3801,[5] as well as on commitments by other laboratories to revise the CHECKER and PLOTFB codes. The Los Alamos Scientific Laboratory undertook the task of retranslating photon production data for sodium, magnesium, chlorine, potassium, and calcium into the new format, as well as rewriting the LAPH and PHOX codes. The new format is logically equivalent to the old but is restructured into new file numbers; it had not yet been carefully documented at the time of the Codes and Formats Subcommittee meeting. The revision of LA-3801 contains the equivalent of a Procedures Manual, with a section for procedures being included in each ENDF/B photon production data file, as well as in each photon interaction data file. The document has been written, reviewed by contributors at other laboratories, and modified based upon their comments; it will soon be sent to the entire CSEWG Shielding Subcommittee for review prior to issuance as an LA report. The sodium data presently in the ENDF/B Data File in the original photon production data format has been translated to the revised format. These translated data will be included in an appendix of the report as a sample case.

2. Codes. The photon production matrix and source vector code, LAPH, has been published,[6] and an abstract appeared in the May 1970 issue of Nuclear Science and Engineering. A code package has been prepared and sent to the Radiation Shielding

Information Center (RSIC) at Oak Ridge. Several modifications were made in the tape handling parts of the code to reduce the long execution time when there are several materials on the ENDF/B tape, as is the case with the sample problem included with the documentation. The central processor time was reduced about a factor of two, as was the peripheral processor time.

The ENDF/B data tape read by the LAPH code is an abbreviated tape containing only neutron cross sections from File 3 and photon production information from File 15. An auxiliary code, ETOL, was written at LASL to prepare the abbreviated tape. However, the revised version of DAMMET (Version 70-1) received in January from NNCSC included changes that allow processing of photon production data. We have found that DAMMET can be used to produce the abbreviated tape for input to LAPH and that there is, therefore, no need to maintain ETOL.

The "physics" checking code[7] for photon production data in the ENDF/B format, PHOX, has been revised and extended and is now designated PHOXE. It has undergone final debugging and has been submitted to RSIC Computer Code Collection. PHOXE was debugged by processing sodium, magnesium, silicon, chlorine, potassium, and calcium data. Special emphasis was placed on the silicon and calcium data, because these data are being provided for some LASL test calculations of photon production in concrete.

Specifications for a new "physics" checking code, VIXEN, are being formulated, based upon experience with PHOXE and upon comments from CSEWG Shielding Subcommittee Task Force 1 members. The new code will use the revised photon production format and will delete some format syntax checks which BNL will incorporate into the CHECKER code.

Several utility codes for use in translating photon production data to the revised format have been written or made operational at LASL. Both LUTE and LATEX have been documented in University of Virginia (UVa) Report No. NE-3383-102-694, which will be distributed by BNL to the ENDF/B distribution list under the document number ENDF-128. FIXLUTE is a code written at UVa to check normalization of photon secondary angular and energy distributions, renormalize to unity, and produce a corrected ENDF/B tape. FIXUKTP is a code, also written at UVa, to correct data which is in the UKAEA format. It is analogous to the ENDF/B code CRECT.

3. Meeting. A meeting of the CSEWG Shielding Subcommittee Task Force 1 was held at LASL on May 12-13, 1970. The Task Force resolved many questions of formats and procedures required for placing evaluations in the new photon production format and determined responsibilities for conversion of data and codes into the new format. (These responsibilities are divided among Brookhaven, Oak Ridge, and Los Alamos Laboratories.) The Task Force then set up a Phase I review procedure, appointed a review coordinator, and obtained reviewers for all presently available or scheduled evaluations of photon production (including neutron interaction) data. Logistic procedures for data collection, plotting, distribution, etc., were set up, and coordination on a Formats and Procedures Manual was established between BNL and LASL. User interests in cross sections related to shielding, as well as existing or projected evaluations, were discussed and summarized. A report on the Phase I review of the photon interaction data in ENDF/B led to a recommendation by the Task Force that the data be approved for public release by NNCSC.

III. REACTOR ANALYSIS METHODS AND CONCEPT EVALUATIONS

A. General

A continuing task in fast reactor analysis and evaluation is the improvement of computer programs and the development of new computational methods. In addition to new methods, advances are constantly being made in computer technology which make possible the extension of existing calculational techniques.

B. Modular Programming Systems (F. McGirt)

1. LAMPS. A modified version of the Knolls Atomic Power Laboratory (KAPL) DATATRAN System[8] is fully operational on the LASL CDC-6600 computers. This has resulted in the Los Alamos Modular Programming System[9] (LAMPS) which preserves the basic features of DATATRAN. Some examples of these features are:

a. Series of functional program units (modules) may be easily linked to perform a specific task,

b. Free-standing codes may be executed and linked in the environment of the LAMPS system with almost no additional user programming effort, and

c. Data lists generated by free-standing codes and modules (as well as the modules and free-standing codes themselves) may be saved in a cataloged fashion on user-supplied tapes for later recall and use.

Since most of the work with LAMPS has been directed toward making the system operational at LASL, only a few of the above features of LAMPS have been employed. Free-standing codes have been linked using LAMPS with very little modification of these codes.[10] Geometry-processing modules from the KAPL iterative transport package have been compiled and added to the system. Modules that generate cross-section sets from ENDF/B data tapes are being obtained from KAPL.

LAMPS is also available to users of the LASL remote terminal systems. Due to a shortage of permanent disk files, a magnetic tape containing the LAMPS system programs must be assigned for each job.

Experience gained through use of this LAMPS system should show that program units (modules) can easily be shared between groups, thus eliminating the need for costly duplicate programming. Better program documentation can also be promoted with simplified module input-output lists which are standardized.

The feasibility of using components of the Argonne modular system[11] (ARC) on the LASL computers is being investigated. Instead of trying to load the complete modular system, as with DATATRAN, the one-dimensional transport theory standard path PTR1D is being used. One of two possible approaches in loading PTR1D will be tried. The first possibility is to use the PTR1D standard path as a structured overlay system. The second is to use only the computational module NUC003 of PTR1D and supply the input-output requirements using LAMPS data lists. A choice of method will be made after more extensive examination of the ARC system. If it proves possible to include ARC modules in the LAMPS system without extensive reprogramming, the computational capability for reactor development can be further enhanced.

C. Preparation and Maintenance of Code Packages

1. Improvement of Existing S_n Methods (B. M. Carmichael). The UPDATE program[12] and the CDC-6600 control cards provide facilities for linking free-standing codes. One advantage to UPDATE linking is that no modifications to the codes are required; consequently, the free-standing capabilities are preserved. In the linking procedure, input and output data files, as well as program files, are stored on the UPDATE tape.

The DTF-IV S_n code and the DAC1 perturbation code have been linked by this method. The files on the UPDATE tape for this case are:

DTF-IV program
DAC1 program
Regular flux
Adjoint flux
Regular angular flux
Adjoint angular flux
DTF-IV input
DAC1 perturbation input

The steps involved in solving a complete problem are:

a. Read DTF-IV input from regular input stream and store same on UPDATE tape.
b. Solve regular DTF-IV problem and store regular flux and regular angular flux on UPDATE tape.
c. Repeat Step b for adjoint problem.
d. Read DAC1 perturbation input from regular input stream and store same.
e. Recall all data files, except regular and adjoint total flux files from UPDATE tape for input to DAC1.

The UPDATE facilities may be used to modify any of the input data files for subsequent runs. For example, n might be varied in successive DTF-IV runs, or the convergence criterion might be varied. Where appropriate, the total flux, either regular or adjoint, would be recalled from the UPDATE tape to restart a problem. Once the DTF-IV problems for a given configuration are solved and the results are stored on tape, any number of different perturbation runs might be executed in which the same DTF-IV flux data are recalled from the UPDATE tape.

2. Computer Code Coordination (B. M. Carmichael, J. C. Vigil, R. E. Seamon). LASL participated actively in the work of the *de facto* Committee on Computer Code Coordination. This committee consists of representatives from several laboratories selected by the AEC to study the problems of adapting reactor codes to various types of computers and the problems of interfacing reactor codes from different organizations in linked calculations. During the past year, a set of codes was selected for use in a study of the interfacing and adaptation problems. Standard interface files for linking these codes were defined, and work on the adaptation of the codes to these interfaces was, for the most part, completed.

LASL participants are currently heavily engaged in the work of adapting the revised interfaced codes to LASL computers.

The set of codes adopted by the Committee are listed below. The organizations assigned to the work of adapting the codes to the standard interfaces are also listed.

MC^2 (cross-section processing)
Argonne National Laboratory (ANL)

ETOX-1DX (cross-section processing)
Battelle Northwest Laboratory (BNWL)

ANISN (one-dimensional S_n)
Brookhaven National Laboratory (BNL)

DOT2DB (two-dimensional S_n and diffusion)
General Electric - Sunnyvale, California (GE-Sunnyvale)

DAC (one-, two-, or three-dimensional perturbation)
Los Alamos Scientific Laboratory (LASL)

CITATION (fuel management)
Oak Ridge National Laboratory (ORNL)

The standard interface files adopted by the Committee for linking the above codes are:

ADMNSTR (administration and control file containing dimension and option control data)

GEO DIST (geometry and material distributions)

SN CONS (SN constants)

INTQUANT (integral quantities, such as zone volumes and zone-averaged fluxes)

MIX DATA (mixture data)

MULTIGRP (multigroup cross-section file)

GRP FLXS (group fluxes)

Computers at the various installations are CDC 6600 at LASL and BNL, IBM 360 at ANL and ORNL, UNIVAC 1108 at BNWL, and GE 635 at GE-Sunnyvale.

The one-dimensional DAC1 code[13] was generalized locally to calculate perturbations in one, two, or three dimensions using standard data files. The theoretical basis and general structure of the interfaced DAC code are similar to those described in Ref. 13. All of the interface files are required as input to DAC, including both perturbed and unperturbed versions of MULTIGRP and regular and adjoint versions of GRP FLXS. To make it possible to use generalized reading routines on the standard files, all files are first preprocessed to place Hollerith, fixed-point, and floating-point data in separate records containing no more than one vector per record. Next, the flags, IREAD(I), are read from cards for each File I.

IREAD(I) = 1 denotes all File I data to be read from cards,

IREAD(I) = 2 denotes all File I data to be read from the standard file, and

IREAD(I) = 3 signals File I data to be read from both cards and a file.

If Option 3 is exercised, then additional flags IRD(I,J) are read from cards to signify that the data of type J in File I are to be read from cards (IRD(I,J)=0) or are to be read from an existing file (IRD(I,J)=1). If any data are to be read from cards, then both an old and new version of the given file will exist. The new version will contain the updated data read from cards.

The limited amount of Hollerith information contained in the files is read by special read statements provided for each Hollerith record. Fixed-point and floating-point data are read, respectively, by the generalized read subroutines, REAFXP and REAREL. The argument list in these routines contains ARRAY, NWDS, IFG, (HOLL(K),K=1,6), IRD(I,J), and IPRIN. The vector ARRAY containing NWDS words is read by the subroutine. The array IFG contains these five items:

IFG(1) specifies the input file for card data,
IFG(2) specifies the output print file,
IFG(3) identifies the old standard file,
IFG(4) identifies the new standard file, and
IFG(5) = IREAD(I).

ARRAY and its Hollerith description contained in (HOLL(K),K=1,6) are printed only if IPRIN = 1.

DAC uses 21 files; nine of the files are input standard files, and allowance is made for nine output or modified files. In addition, three scratch files are required. To avoid allocating the excessive core memory space (21,525 words) for buffering all 21 files simultaneously, a COMPASS subroutine obtained from Knolls Atomic Power Laboratory (KAPL) is used which permits the reassignment of buffer areas during execution. By using this COMPASS subroutine, the number of buffers required is reduced to seven.

Test problems in one and two dimensions were successfully executed with the interfaced DAC code. Tapes containing DAC and a sample problem, along

with operating instructions for the code, were sent to ANL, BNWL, BNL, and GE-Sunnyvale.

As a result of the experience gained in adapting DAC to the interface files, three basic recommendations are made for improving the files. First, Hollerith, fixed-point, and floating-point data should be placed in separate records to simplify reading of the files. Second, subject to the preceding limitation and to the limits imposed by the definition of records in the codes, records should be made as large as possible to promote reading efficiency. Finally, all dimension data should be placed at the head of a file or in the ADMNSTR file to facilitate the application of variable dimensioning techniques to the storage of the data. The MULTIGRP file in particular needs revision, since it contains a large number of very small records containing a complicated mixture of Hollerith, fixed-point, floating-point, and dimension data.

All of the interfaced codes, except the CITATION code[14] have been received at LASL. However, since CITATION requires repeated passes through the cross-section and flux codes, the latter codes must be activated first before CITATION can be tested.

Interfaced versions of the ETOX code[15] and the 1DX code[16] along with sample problems were received from BNWL. Both ETOX and 1DX were compiled on the CDC-6600 computer after making modifications and additions to the codes. The sample problems provided with the codes were successfully executed. In the process of executing the ETOX sample problem, several bugs were discovered and corrected.

The original ETOX program was in overlay structure. However, the interfaced version, as received, did not contain overlays. As a result, the ETOX object program required $67{,}000_{10}$ words of central memory and thus had to be run on the 130K machine. Work is in progress to convert ETOX to overlay structure.

The interfaced version of the MC^2 code[17] was received from ANL. A considerable amount of work will be required to adapt this code to our computing environment. This work is in progress.

The interfaced version of the ANISN code[18] and sample problems were received from BNL. Also included in the package was an auxiliary code, UPTON, and associated sample problems. The UPTON code produces a standard MULTIGRP file from cross-section data in the ANISN format. UPTON and ANISN were compiled on the CDC 6600, and the sample problems for UPTON were successfully executed. Testing of the ANISN code is in progress.

The DOT2DB code[19] was received recently from GE-Sunnyvale.

It appears, thus far, that codes written in standard FORTRAN-IV for the UNIVAC 1108, GE 635, and for the CDC 6600 at other installations can be adapted to LASL's CDC 6600's fairly readily. Codes written for the IBM 360's, however, present a more serious problem. Extensive revisions are required particularly to eliminate the double precision and variable word-length specifications in the IBM 360 codes. A code for performing the necessary translations would be useful.

3. Three-Dimensional Diffusion Theory Code, 3DDT (J. C. Vigil). A three-dimensional diffusion theory code (3DDT) was programmed, compiled, and tested. The 3DDT code is an extension to three space dimensions of the two-dimensional 2DB code.[20] All of the 2DB features were retained in 3DDT, except that the geometry options are X-Y-Z and R-θ-Z. Briefly, some of the features are:

- Multigroup calculations of k_{eff} or criticality searches on reactor composition, reactor dimensions, or time absorption (α) by means of either the regular or the adjoint flux equations,
- Computation of material burnup and fission product buildup,
- Variable dimensioning for maximum use of available fast memory,
- Group rebalancing and successive overrelaxation with line inversion,
- Searches on compositions or dimensions with values of α or k_{eff} as parametric eigenvalues (user selected),
- DTF-IV input format,[21] and
- Restriction to downscattering.

Both Extended Core Storage (ECS) and disk storage are utilized in 3DDT. In general, four-dimensional arrays [e.g., $\phi(x,y,z,E)$] are stored on disk; three-dimensional arrays [e.g., $\phi(x,y,z)$ for a particular energy group] are stored in ECS; and two-dimensional arrays [e.g., $\phi(x,y)$ for a particular group and axial mesh point] are stored in the fast central memory. Thus, central memory storage requirements are insensitive to the number of energy groups and the number of axial mesh points.

Calculations with 3DDT in R-θ-Z and X-Y-Z geometries, with homogeneous compositions in one of the dimensions, were compared with corresponding two-dimensional calculations with the 2DB code. The 3DDT-2DB comparisons served as a check on the various options in 3DDT. A true three-dimensional problem in X-Y-Z geometry was also calculated with 3DDT and compared with results obtained with the 3DB code[22] developed recently at Battelle Northwest Laboratory. The results of the various calculations are summarized below.

The first series of 3DDT calculations consisted of two-group k_{eff} (both regular and adjoint), alpha, concentration, and delta computations of a two-region cylindrical reactor in R-θ-Z geometry. For these problems, material compositions were constant in the θ direction. Thus, the reactor could be represented exactly in an R-Z calculation with 2DB. Only a 15° sector of the θ dimension was represented in the R-θ-Z calculation. Periodic and reflective boundary conditions on the θ boundaries are equivalent in this configuration and should give the same results. This was indeed found to be the case.

All common input data (mesh intervals, cross sections, convergence parameters, initial flux guess, etc.) for the R-Z and R-θ-Z calculations were identical. The meshes contained 21 intervals radially, 15 axially, and five in the θ direction. Thus, the R-θ-Z problem contained five times more mesh points than the R-Z problem.

The regular k_{eff} computation was followed automatically by a burnup interval of 30 days at 3 MWT total power, and a computation of the k_{eff} for the depleted inventory. Results of the two- and three-dimensional calculations are shown in Table 465-III.

TABLE 465-III

REGULAR k_{eff} CALCULATIONS
WITH 30-DAY BURNUP AT 3 MWT

Two-Group, R-θ-Z Problem

	2DB	3DDT	3DDT/2DB
Initial k_{eff}	1.0557	1.0553	0.9996
Final k_{eff}	1.0502	1.0499	0.9997
Reactivity change (Δk/k)	-0.0052	-0.0051	0.98
^{235}U depletion (g)	112.8	112.8	1.000
Breeding ratio	0.0045	0.0045	1.000
Computation time (sec)	15.3	83.2	5.4

In absolute magnitude, the initial and final k_{eff}'s both agreed within 0.0004, and the reactivity changes due to burnup agreed within 0.0001. The amounts of ^{235}U depleted were in complete agreement, as were the breeding ratios (the core contained only small amounts of fertile material). Both before and after depletion, group fluxes from 2DB and 3DDT were in agreement within 0.2% at all mesh points. The computing time, defined as Central Processor (CP) time, exclusive of compilation time, was 5.4 times longer for the 3DDT calculation than for the 2DB calculation. Thus, the ratio of 3DDT to 2DB computing time was approximately the same as the mesh point ratio.

The results of the adjoint k_{eff} calculation and of the eigenvalue searches on alpha and critical fuel concentration are shown in Table 465-IV. For both

TABLE 465-IV

TWO-GROUP, R-θ-Z CALCULATIONS

	2DB	3DDT	3DDT/2DB
Adjoint k_{eff}			
k_{eff}	1.0557	1.0553	0.9996
Computing time (sec)	13.9	78.3	5.6
Alpha Search			
Alpha (sec^{-1})	116.3	115.7	0.995
Prompt neutron generation time (sec)	4.79×10^{-4}	4.78×10^{-4}	0.998
Computing time (sec)	17.6	113	6.4
Concentration Search			
Eigenvalue	0.8461	0.8475	1.002
Computing time (sec)	16.8	98.7	5.9

3DDT and 2DB, the k_{eff} computed in the adjoint problem was identical to that obtained in the regular problem (Table 465-III). Adjoint group fluxes from 3DDT and 2DB agreed within 0.3% at all mesh points. For the alpha calculation, 3DDT and 2DB agreed within 0.5% in the eigenvalue and group fluxes agreed within 0.2% at all mesh points. Since k_{eff} and α were obtained from separate calculations, the prompt neutron generation time could be derived from $\Lambda = (k_{eff} - 1)/\alpha$. The values of Λ derived from 3DDT and 2DB calculations agreed within 0.2%. For the concentration search, the eigenvalue is the factor by which the fuel atom densities in the core must be multiplied to yield a critical system. In this case, 3DDT and 2DB agreed within 0.2% in the eigenvalue and within 0.4% in the group fluxes.

Results of the delta calculations are summarized in Table 465-V. Three separate calculations were made. In the first, the core height was held

TABLE 465-V

CRITICAL DIMENSIONS SEARCH CALCULATIONS

Two-Group, R-θ-Z Problem

	2DB	3DDT	3DDT/2DB
Search on:			
Core radius (core height held constant at 99.06 cm)			
Eigenvalue	- 0.1137	- 0.1139	1.002
Critical radius (cm)	76.12	76.10	0.9997
Computing time (sec)	17.8	110	6.2
Core height (core radius held constant at 85.88 cm)			
Eigenvalue	- 0.1519	- 0.1508	0.993
Critical height (cm)	84.02	84.12	1.001
Computing time (sec)	17.2	138	8.0
Both height and radius			
Eigenvalue	- 0.0703	- 0.0707	1.006
Critical height (cm)	92.10	92.06	0.9996
Critical radius (cm)	79.85	79.81	0.9995
Computing time (sec)	18.1	118	6.5

constant, and a search was made on the core radius. In the second, the core radius was held constant, and the core height was varied to achieve a critical system. Finally, both the core radius and height were varied by the same factor to achieve criticality in the third calculation. In the delta calculations, the adjusted dimension, say L, is given in terms of the initial dimension, L_o, by $L = L_o(1 - EV)$ where EV is the eigenvalue. Critical core dimensions computed with 3DDT and 2DB agreed within 0.1% or better. Group fluxes in these calculations agreed within 0.4% or better.

The second series of 3DDT calculations consisted of two- and three-group regular k_{eff} computations of a two-region parallelepiped in X-Y-Z geometry. For these calculations, material compositions were homogeneous in the Z direction. Furthermore, the top and bottom boundaries in the X-Y-Z calculation were reflected to simulate an infinite height. Thus, the configuration could be represented exactly in an X-Y calculation with 2DB. As in the previous calculations, all common input data for the X-Y and X-Y-Z calculations were identical. The meshes contained 21 intervals in the X direction, 20 in the Y direction, and five in the Z direction. Thus, the X-Y-Z problem contained five times more mesh points than the X-Y problem.

Results of the X-Y-Z calculations are summarized in Table 465-VI. For the two-group calculations, the k_{eff}'s computed with 3DDT and 2DB agreed within 0.09% and group fluxes typically agreed within 0.3% with a maximum disagreement of 0.6%. For the three-group case, the k_{eff}'s computed with 3DDT and 2DB agreed within 0.12% and group fluxes typically agreed within 0.4% (maximum disagreement was 1%).

TABLE 465-VI

REGULAR k_{eff} CALCULATIONS

X-Y-Z Problem

	2DB	3DDT	3DDT/2DB
Two-Energy Groups			
k_{eff}	1.0084	1.0075	0.9991
Computing time (sec)	15.1	91.4	6.1
Three-Energy Groups			
k_{eff}	1.0138	1.0126	0.9988
Computing time (sec)	17.5	124	7.1

The true three-dimensional test problem was a two-group, two-region, one-step burnup calculation in X-Y-Z geometry. The reactor consisted of a cubical core region surrounded on all sides by a blanket region. Because of symmetry, only one octant of the reactor was represented in the calculational model, which contained ten intervals in each dimension. The initial k_{eff} calculation was followed by a burnup interval of 50 days with the reactor at 800 MWT total power. Following the burnup interval, a final k_{eff} was computed for the new material compositions resulting from fuel depletion, breeding, and fission-product buildup.

Results obtained with 3DDT on a CDC 6600 computer are shown in Table 465-VII, along with results obtained at BNWL with the 3DB code on a UNIVAC 1108 computer. As seen in the table, results obtained with 3DDT and 3DB agree very well. However, the

TABLE 465-VII

SUMMARY OF 3DDT AND 3DB RESULTS

	Initial System	
	3DB	3DDT
Converged lambda	0.999998	0.999996
Multiplication factor	1.02172	1.02172
Total		
Flux at K=J=I=1	2.02526×10^{16}	2.02524×10^{16}
Flux at K=1, J=I=10	2.84968×10^{13}	2.84935×10^{13}
Outer iterations	10	10
Z iterations	84	84
X-Y iterations	3638	1679
Running time (min)	2.13	0.35
	Depleted System	
Converged lambda	0.999991	0.999990
Multiplication factor	0.99959	0.99961
Breeding ratio	1.6764	1.6765
Total		
Outer iterations	6	9
Z iterations	51	37
X-Y iterations	2022	1669
Running time (min)	1.28	0.34

running time with 3DDT was about five times shorter than with 3DB. This is due to the differences in the CDC and UNIVAC computing systems, and the fact that 3DDT used fewer X-Y iterations.

All of the 3DDT test problems described above were run with the object program produced by the standard RUN compiler on the CDC 6600. The FORTRAN extended (FTN) compiler for the CDC 6600 produces a more efficient object program than the RUN compiler, at a cost of increased compilation time. In order to investigate possible savings of computer time, the 3DDT code was compiled with the FTN compiler. A sample k_{eff} problem in X-Y-X geometry (14 x 14 x 14 mesh points), three energy groups, and three material zones was executed using the object programs from both the FTN and RUN compilers. The running time (exclusive of compilation time) was 20% shorter using the FTN object program. For problems that require large amounts of running time, this difference represents a significant savings.

By extrapolating from the test problems, it is estimated that a six-group 3DDT problem, containing 30 x 30 x 30 mesh points, would require 30 to 60 min of computing time on the CDC 6600 computer. The low estimate applies to a k_{eff} calculation, and the high estimate applies to an implicit eigenvalue search calculation.

A document that describes the 3DDT code was written and will be issued as a Los Alamos Scientific Laboratory report. Also, an abstract of the 3DDT code was submitted for publication in Nuclear Science and Engineering.

4. Two-Dimensional Perturbation Code DAC2 (G. C. Hopkins). DAC2, a two-dimensional S_n perturbation code, was written and successfully tested with a sample problem.

The code was built up from parts of two other codes: the two-dimensional S_n transport code[23] 2DF, and the one-dimensional perturbation code DAC1. First, the input and data preparation subroutines from 2DF were set up. Then, a subroutine SORT was added to reorder and combine the angular fluxes put out by a revised version of 2DF. Finally, the computational subroutines of DAC1 were added and modified for two dimensions.

For a JEZEBEL fast critical assembly problem with a 2% increase in the ^{235}U fuel density in the core region, the reactivity calculated by DAC2 was within 0.2% of the reactivity as calculated from k_{eff} differences in the associated 2DF problems.

Additional testing is continuing, and a Los Alamos report on DAC2 is being written.

In addition, both the revised version of 2DF and DAC2 have been linked together in the LAMPS system, thereby enabling a variable number of problems to be executed in a predetermined "path" in one run, without any of the load times normally associated with each problem when executed separately. As an example, one such run consisted of: (1) A 2DF regular problem, (2) a 2DF adjoint problem, (3) a DAC2 problem which calculated perturbation results for a perturbed core region, using the regular and adjoint fluxes created in the first two problems, and (4) a third 2DF problem with a perturbed core region which provided a comparison with the DAC2 results.

5. Burnup Code PHENIX (T. J. Hirons). The LA report on the burnup-refueling code[24] PHENIX has been written and issued. PHENIX is a two-dimensional multigroup diffusion-burnup-refueling code for use with fast reactors. The code is designed primarily for fuel-cycle analysis of fast reactors and can be used to calculate the detailed burnup and refueling history of fast-breeder-reactor concepts having any generalized fractional-batch reloading scheme. Either ordinary k_{eff} calculations or searches on material concentration or region dimensions can be performed at any time during the burnup history. The refueling option of the code accounts for the spatial flux shifts over the reactor lifetime. Effects of this flux shift were presented recently,[25] and are discussed in detail in Ref. 26. For each burnup interval in the fuel-cycle history, the code performs the following operations:

a. Calculates, for each fuel isotope in each zone, both the atom density of the fuel fraction to be discharged and the atom density following the refueling,

b. Calculates, for each fuel isotope, the total charge and discharge (in kg) of the entire reactor,

c. Collapses the atom density data for any number of regions, e.g., all the radial or axial blanket regions, into a single total charge and discharge, and

d. Punches on cards the charge-discharge mass balances for input to a reactor economics code (if desired).

All of these calculations reflect the spectral and spatial flux shifts from one burnup interval to another.

An abstract of the PHENIX code was published in Nuclear Science and Engineering.[27]

The PHENIX code was modified during the latter part of FY 1970. Two principal additions were made to the original version of the code: (1) the capability of performing a series of burnup intervals in one run, and (2) a provision for a buckling correction to be used in X-Y and R-θ calculations. Each addition is discussed briefly below.

The capability of performing a series of burnup intervals allows an entire fuel-cycle analysis to be performed in one run. Thus, if the clean reactor configuration and the appropriate refueling fractions are specified, the equilibrium fuel-cycle parameters can be calculated in a single run. Data dump capabilities are also provided so that the problem can be restarted after any number of burnup intervals. This multi-interval modification requires only two additional input control words, but reduces the maximum allowable storage in the A Common Block from $30{,}000_{10}$ to $27{,}000_{10}$ words.

The buckling correction option is made available by use of the newly added control word BUCK (on control card 8). If BUCK is input as 0.0 (or left blank), no buckling correction is made. If BUCK > 0.0, and the geometry is X-Y or R-θ, BUCK is used in one of two ways:

a. If 0.0 < BUCK < 1.0, BUCK is used directly as $B^2_{g,I}$, the same for all groups g and regions I.

b. If BUCK > 1.0, it is assumed to be the buckling height of the reactor and the buckling for each group g and region I is computed as

$$B^2_{g,I} = \left[\frac{3.1416}{\text{BUCK} + 2\left(0.71\ \lambda^{g,I}_{tr}\right)}\right]^2$$

to give the group/region-dependent buckling.

In both cases, the buckling correction consists of adding the quantity $D_{g,I}\ B^2_{g,I}$ to the macroscopic absorption cross section in each region I for each group g. (This quantity is also subtracted from the macroscopic self-scatter cross section to maintain the correct total cross section.) $D_{g,I}$ is computed as $1.0/3\Sigma^{g,I}_{tr}$.

A supplement to the LA report on the code (Ref. 9) was issued in June 1970. A revised version of the code was sent to the Argonne Code Center.

D. Synthesis of Static Multigroup Transport Theory (R. E. Alcouffe)

As a continuing effort to account for two-dimensional transport effects without using time-consuming two-dimensional transport theory, a modification of the leakage term of the conventional diffusion equation has been developed. This modification consists of the utilization of the flux and current obtained from one-dimensional transport calculations on the system. In this way, the two-dimensional diffusion equation acts as a "synthesizing" equation for constructing a two-dimensional scalar flux from one-dimensional calculations. In order to effect this synthesis, the following procedure is used:

1. One-dimensional S_n calculations are performed in each of the transverse directions and for each of the important regions of the system,
2. Leakage coefficients applicable to two-dimensional diffusion theory are computed from the transport scalar fluxes and currents, and
3. The two-dimensional diffusion calculation is performed on the system to obtain the "synthesized" two-dimensional flux and eigenvalue.

In order to amplify Step 2, examine the leakage term from the two-dimensional cylindrical diffusion leakage expression around the mesh point (V_i, A_j):

$$\mathcal{L}_{i,j} = -2\pi \int_{z_{j-\frac{1}{2}}}^{z_{j+\frac{1}{2}}} dZ \int_{r_{i-\frac{1}{2}}}^{r_{i+\frac{1}{2}}} r dr \left[\frac{1}{r}\frac{\partial}{\partial r}\left(rD\,\frac{\partial\phi}{\partial r}\right) + \frac{\partial}{\partial z}\left(D\,\frac{\partial\phi}{\partial z}\right)\right]$$

$$\simeq -2\pi\left(z_{j+\frac{1}{2}} - z_{j-\frac{1}{2}}\right)\left[r_{i+\frac{1}{2}}\,D_{i+\frac{1}{2},j}\left(\frac{\phi_{i+1,j} - \phi_{i,j}}{r_{i+1} - r_i}\right) - r_{i-\frac{1}{2}}\,D_{i-\frac{1}{2},j}\left(\frac{\phi_{i,j} - \phi_{i-1,j}}{r_i - r_{i-1}}\right)\right]$$

$$- \pi\left(r_{i+\frac{1}{2}}^2 - r_{i-\frac{1}{2}}^2\right)\left[D_{i,j+\frac{1}{2}}\left(\frac{\phi_{i,j+1} - \phi_{i,j}}{z_{j+1} - z_j}\right) - D_{i,j-\frac{1}{2}}\left(\frac{\phi_{i,j} - \phi_{i,j-1}}{z_j - z_{j-1}}\right)\right] ,$$

where the normal finite difference approximation

$$\left.\frac{\partial\phi}{\partial r}\right|_{r_{i+\frac{1}{2}}} \simeq \frac{\phi_{i+1,j} - \phi_{i,j}}{r_{i+1} - r_i} \quad \text{etc.},$$

has been made. Equation 1 is the term normally used to estimate two-dimensional leakage, with the diffusion coefficients being estimated by

$$D_{i,j} = \left(\frac{1}{3\Sigma_{tr}}\right)_{i,j} ,$$

where Σ_{tr} is the transport cross section. Equation 1 may be summarized as

$$\mathcal{L}_{i,j} = R_{i,j}(\phi_{i+i,j} - \phi_{i,j}) - L_{i,j}(\phi_{i,j} - \phi_{i-1,j}) + T_{i,j}(\phi_{i,j+1} - \phi_{i,j}) - B_{i,j}(\phi_{i,j} - \phi_{i,j-1}). \quad (2)$$

When currents and fluxes are available from a transport calculation, the equations

$$j_{r,i+\frac{1}{2},j} = D_{i+\frac{1}{2},j}\left.\frac{\partial\phi}{\partial r}\right|_{i+\frac{1}{2},j}$$

$$j_{z,i,j+\frac{1}{2}} = -D_{i,j+\frac{1}{2}}\left.\frac{\partial\phi}{\partial z}\right|_{i,j+\frac{1}{2}} \quad (3)$$

may be used to more adequately represent the diffusion coefficients appearing in the leakage term. The leakage coefficients of Eq. 2 then become:

$$R_{i,j} = \frac{-2\pi\,\Delta z_j\; r_{i+\frac{1}{2}}\; j_{r,i+\frac{1}{2},j}}{\phi_{i+1,j} - \phi_{i,j}}$$

$$L_{i,j} = \frac{-2\pi\,\Delta z_j\; r_{i-\frac{1}{2}}\; j_{r,i-\frac{1}{2},j}}{\phi_{i,j} - \phi_{i-1,j}}$$

$$T_{i,j} = \frac{-\pi\left(r_{i+\frac{1}{2}}^2 - r_{i-\frac{1}{2}}^2\right) j_{z,i,j+\frac{1}{2}}}{\phi_{i,j+1} - \phi_{i,j}}$$

$$B_{i,j} = \frac{-\pi\left(r_{i+\frac{1}{2}}^2 - r_{i-\frac{1}{2}}^2\right) j_{z,i,j-\frac{1}{2}}}{\phi_{i,j} - \phi_{i,j-1}} . \quad (4)$$

This formulation is, therefore, consistent with the discrete two-dimensional diffusion leakage term.

The above procedure has been tested first by using the two-dimensional S_n code 2DF to calculate two-dimensional transport fluxes and currents. This information was formulated as leakage coefficients for the diffusion codes; the results of the subsequent diffusion calculation using these coefficients were virtually identical to the results from 2DF. The systems used as a test were described as examples #2 and #4 in Ref. 28. These are small fast, fully reflected cylindrical systems.

These calculations prove that when two-dimensional fluxes and currents are used in Eq. 4, then the resulting diffusion theory will reproduce the results of the S_n computation.

In order to see how well the procedure will do when one-dimensional information is used, the calculations were repeated using DTF-IV transverses of the system. In the first case, transverses through the main core region only were used. In the second, transverses in the reflectors were also employed. The results for the eigenvalues are shown in Table 465-VIII.

These preliminary results show that a significant improvement in the eigenvalue is obtained in this example, even though the leakage is more than 50% of the neutron losses.

TABLE 465-VIII

EIGENVALUES FROM VARIOUS ESTIMATES OF THE TWO-DIMENSIONAL LEAKAGE

Method of Calculation	Eigenvalue Case 2	Case 4
2DF	1.0425	1.0054
2DB[a]	1.1084	1.0226
2DB[b]	1.0412	1.0161
2DB unmodified	0.8782	0.9035
Contribution of leakage to neutron loss	52.5%	50.5%

[a] Using leakage coefficients calculated from core fluxes and currents.

[b] Using leakage coefficients calculated from both core and reflector fluxes and currents.

The next example furnishes a much more stringent test of this technique. Since this example is more complicated than the previous one, the DATATRAN system[29] has been employed to carry out efficiently the necessary steps. This system allows manipulation or linkage of existing codes by a FORTRAN program. The data computed or used by the separate codes can also be manipulated in the same way as FORTRAN variables and saved on a cataloged library tape for possible later use.

The system used to synthesize the two-dimensional transport flux again consists of the DTF-IV code,[21] which does the one-dimensional transport calculation and the 2DB code,[20] which performs the two-dimensional diffusion theory calculation. An experimental intermediate code was written to compute the leakage coefficients. This system was used to calculate the flux in the cell shown in Fig. 465-1. Region I is a beryllium oxide rod, Regions II and IV are ^{238}U rods, where the total cross section of ^{238}U is taken to be 1000 b to simulate a resonance, and Region III is sodium. Three one-group calculations were performed to compare the effects of different approximations to compute the flux; the zone-integrated flux is shown in Table 465-IX. These three computations are, respectively, two-dimensional transport (TWOTRAN-XY), two-dimensional synthesis (DTF+2DB), and two-dimensional diffusion (2DB). As can be seen from the table, there is a large error in the fuel regions when the results of the latter two approximate calculations are compared to the reference TWOTRAN-XY

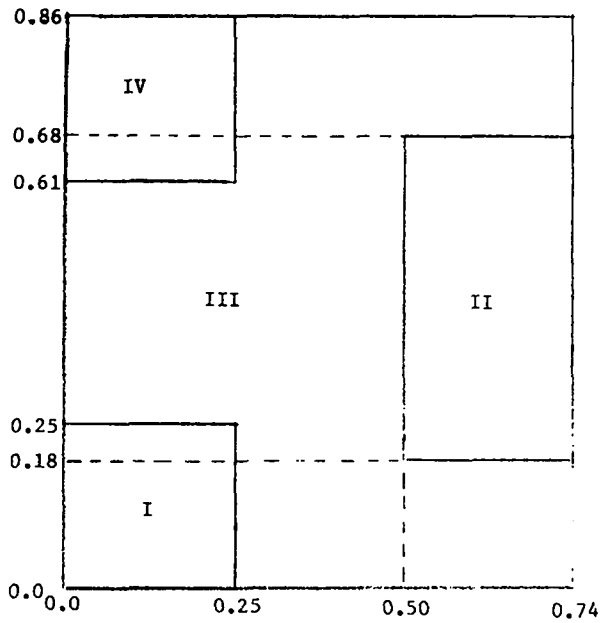

Fig. 465-1. Fast reactor calculational cell model.

TABLE 465-IX

AVERAGED CELL FLUXES FROM APPROXIMATE TWO-DIMENSIONAL CALCULATIONS

Zone	Reference Fluxes TWOTRAN-XY	% Deviation from Reference DTF + 2DB	2DB
I	1.424	- 3.4	+88.3
II	0.1479	+25.5	-99.1
III	1.332	- 1.0	- 9.5
IV	0.1557	+25.5	-99.1
CDC 6600 CP time (sec)	165	36	31

calculation. The reason for this is currently being investigated to correct the technique.

E. Fast Reactor Design Analysis

1. Fuel-Cycle Analysis (T. J. Hirons). A complete fuel-cycle analysis has been performed on a recent advanced LMFBR design.[30] This reactor has a core H/D of 0.44, an increase of a factor of 2.5 over the pancake design[31] analyzed previously. The two-dimensional diffusion-burnup-refueling code[24] PHENIX was used for the analysis. Several reactor characteristics at the midpoint of the equilibrium cycle were tabulated and compared with those given in the design report. Values for the core fissile loading, breeding ratio, and core conversion ratio agreed very closely with the design values, while the burnups were 15 to 20% higher than the specified 112,200 MWd/Te.

The mass balances from the above-mentioned analysis were processed through LAFF and the Los Alamos Reactor Economics Code (LAREC). LAFF takes the charges and discharges from the fuel-cycle analysis, along with the appropriate load history, and prepares a set of mass balances for input to LAREC. LAREC then performs the complete economic analysis for the given reactor system and calculates a power cost in mills/kWh.

Additional parametric studies are being performed on this reactor; quantities being varied include the length of the burnup time step, the load history, and the capital costs. Results of these parametric studies will be published at a later date.

2. Heterogeneous and Resonance Self-Shielding Effects on Fast Breeder Calculations (R. E. Alcouffe and T. J. Hirons). In a typical LMFBR, the neutron flux spectra extend into the resolved resonance region of the fertile and fissile elements. As a result, the multigroup cross sections in the resonance region should include the effects of heterogeneity and resonance self-shielding. This section presents results of an investigation of these effects on fast breeder reactor physics and fuel-cycle parameters.

A large pancake mixed-oxide LMFBR[31] was used in the analysis. The core fuel consists of UO_2-PuO_2, and the clean blanket fuel contains only UO_2. The ^{238}U atom density in a core fuel pin is 60% of the theoretical density of UO_2 and 16% of the theoretical density in the homogenized core mixture. The ^{238}U atom densities of the axial blanket are 90% and 24% of theoretical UO_2 density in the blanket fuel pin and homogenized blanket mixture, respectively.

The MC^2 code[17] was used to process ENDF/B cross sections into a 49-energy-group structure. The first 48 groups (10 MeV to 61 eV) are each of 0.25 lethargy width and correspond to the fine groups in MC^2. The 49th group was a broad group covering the energy range 61 to 8 eV. Since the resonance self-shielding is mixture-dependent, four different MC^2 analyses were performed to determine the effects of heterogeneity and resonance self-shielding. These four runs consisted of both homogeneous and heterogeneous MC^2 calculations, using both core and axial blanket atom densities. The heterogeneous or cell calculation in MC^2 is limited to two regions, and a modification of this cell model was required to include the effect of the beryllium oxide pins which are present in the mixed-oxide LMFBR being analyzed. The BeO pins have the same diameter as the fuel pins and are present in a ratio of approximately 1:3.5 (BeO to fuel). For the MC^2 cell runs, the appropriate volume fraction of BeO was smeared into the outer coolant region. Fine-energy mesh (49-group) MC^2 calculations were then performed for both core and axial blanket regions, using both the homogeneous and heterogeneous representations of the modified two-region cell described above.

In Table 465-X, the total capture cross section of ^{238}U as calculated from these four MC^2 runs is shown for the latter 12 groups of the 49-group structure; these groups cover the majority of the resolved resonance region. This parameter is of considerable

TABLE 465-X

σ_c FOR ^{238}U FROM HOMOGENEOUS AND HETEROGENEOUS MC^2 RUNS

	Core		Axial Blanket	
Group	Homog.	Heter.	Homog.	Heter.
38	1.94	1.85	1.57	1.48
39	1.78	1.68	1.35	1.26
40	1.85	1.75	1.40	1.31
41	1.65	1.58	1.30	1.21
42	1.76	1.63	1.21	1.11
43	2.38	2.19	1.59	1.44
44	2.57	2.34	1.70	1.54
45	1.61	1.54	1.35	1.27
46	5.45	4.96	3.41	3.10
47	2.85	2.71	2.02	1.88
48	4.19	3.83	3.06	2.78
49	1.11	1.07	1.36	1.27

importance in the calculation of breeding ratio and other fuel-cycle parameters. The results indicate that the heterogeneous shielding effects lower the ^{238}U σ_c by anywhere from 4 to 10% in both the core and axial blanket regions. The cross section values given are lower in the axial blanket because of the greater resonance self-shielding caused by the higher ^{238}U content in the blanket. Using cross sections from both the homogeneous and heterogeneous MC^2 runs, 49-group two-dimensional diffusion theory calculations were performed on the pancake LMFBR. The breeding ratios for the clean reactor are given in Table 465-XI. For the homogeneous and heterogeneous MC^2 analyses, criticality calculations were performed

TABLE 465-XI

BREEDING RATIOS FOR CLEAN REACTOR

	Two Cross-Section Sets[a]		One Cross-Section Set	
	Heter.	Homog.	Heter.	Homog.
Initial breeding ratio	1.100	1.115	1.124	1.137
% error		1.4	2.2	3.4

[a]Reference case.

using two sets of cross sections (both core and axial blanket), and core cross sections alone. The effect of heterogeneity decreases the reactor breeding ratio by 1.4% for the two-set cross-section case (about a 1.2% decrease when core cross sections only are used). The effect of resonance self-shielding on the breeding ratio can be seen by comparing either heterogeneous or homogeneous calculations for the one- and two-set cross-section cases (2.2% error for heterogeneous, 2.0% error for homogeneous).

A Monte Carlo calculation of the actual reactor cell is presently being formulated. Results of this calculation will provide a check on the validity of the modified two-region cell used in the MC^2 runs.

3. Calculational Models (T. J. Hirons). The paper, "Calculational Models for Fast Reactor Fuel-Cycle Analysis," by Thomas J. Hirons and R. Douglas O'Dell has been revised and accepted for publication in Nuclear Applications and Technology. It will appear in the July 1970 issue.

F. Effect of Energy and Space Collapse Upon Fast Breeder Fuel-Cycle Analyses (R. E. Alcouffe and T. J. Hirons).

A technique has been developed that employs a consistent condensing of cross-section data used in the fuel-cycle analysis of fast breeder reactors. This makes possible an accurate analysis while using very few energy groups and spatial mesh points. The technique itself makes use of an extension of the ideas presented in Ref. 32, which is based upon a functional representation of the equations describing the fuel-cycle behavior. In this case, it is possible to develop a reference condition of the reactor system. This equation which resembles a conventional collapsed equation in space and energy is then used to extend the calculation of the system in time. To demonstrate the usefulness of such a technique, two sets of calculations have been performed. In the first, only the effects of the energy collapse are examined; in the second, both space and energy collapse effects are shown.

1. Comparison of Fuel-Cycle Parameters Obtained from Using Space-Dependent and Fundamental-Mode Collapsing Spectra. This comparison of fuel-cycle parameters was performed using the LMFBR design[31] mentioned in Sec. E.2. The use of the initial two-dimensional fine spectrum as the reference calculation is profitable, if the changes in the spatial and energy distribution of the flux in time are such that the resultant spectrum is not very different from the reference calculation. If these changes are small or if the group structure is chosen to be consistent with the expected changes, the initial investment in the reference calculation will yield fuel-cycle results which are accurate throughout the burnup history of the reactor. This is verified below for the reactor system chosen.

To begin the calculation, a 49-fine-group reference calculation was performed using ENDF/B cross-section data processed by MC^2 but with no broad-group collapsing performed by MC^2. The fine-group cross sections and leakage coefficients were condensed to eight and four broad groups, using the two-dimensional space-dependent spectrum. Burnup analyses, using these broad-group structures, were then carried out over the first six burnup intervals. Refueling was performed between burnup intervals according to the prescribed fuel management schedule. The 49-group reference calculation was performed through the first burnup interval. Parallel burnup analyses, using eight- and four-group cross sections generated directly from MC^2, were also performed to compare the effects of using space-dependent and fundamental-mode collapsing spectra. All fine- and broad-group criticality and fuel-cycle calculations were performed using two-dimensional diffusion theory.

The results of the collapsed analyses (eight from 49 and four from 49) were virtually identical and differed from the 49-group calculation by less than 0.2% in k_{eff}, breeding ratio, and plutonium content in the blankets at the end of the first burnup interval. A 2-from-49 analysis was also performed, resulting in less than 1% error in all parameters. The 49-fine-group calculation was rerun at

the beginning of the fifth burnup interval, but the resultant collapse yielded no significant changes from the broad-group cross sections calculated at beginning-of-life. This indicates that the changes in the time-dependent spectrum have been adequately accounted for by both the eight- and four-group structures.

For the eight-group analysis using cross sections averaged over a fundamental core spectrum generated by MC^2, errors in the breeding ratio (compared with the collapsed analyses) over the first six burnup intervals ranged from -2.9 to -1.6%, while for the four-group case, this range was -11.1 to -8.3%. The errors in the ^{239}Pu discharge from the axial blankets for the eight-group analysis ranged from -4.1 to -2.2%, while for the four-group case the range was -16.4 to -11.8%. The error decreases in time due to a compensation of larger errors in effective ^{238}U and ^{239}Pu cross sections used for the burnup equations. All of the results given above are based on a single set of cross sections from MC^2 calculated using core atom densities only. The burnup analyses were also performed using two sets of cross sections from MC^2, one based on the core and the other on the axial blanket atom densities and spectrum. Results of these fuel-cycle analyses showed a slight reduction in the range of errors incurred relative to the use of core cross sections only. For example, errors in the breeding ratio using four-group cross sections generated directly from MC^2 ranged from -10.3 to -7.1% with two sets as compared with -11.1 to -8.3% when one cross-section set was used.

The main conclusion to be drawn from these results is that, when cross-section data is averaged over a representative two-dimensional fine-group spectrum, the fuel-cycle parameters are relatively insensitive to the number and distribution of energy groups used. This success is due to the fact that the neutron spectrum changes very little from the beginning-of-life spectrum during the entire reactor lifetime. This is not true of the same analysis performed on the same system using parameters derived from fundamental-mode or infinite-medium spectra. The results are very sensitive to the number of groups and their distribution in the energy domain. Confidence in the results can be obtained only by increasing the number of groups to show that the results have not changed. Therefore, before performing a fuel-cycle analysis on a given system, it is recommended that as detailed a calculation as is possible be performed at the beginning-of-life and from this few-group parameters appropriate for the time-dependent analysis be derived.

2. Space Collapsing for Fast Breeder Fuel-Cycle Analysis. The technique described above is applied here in space collapsing the appropriate finite difference equations to perform the fuel-cycle analysis. The trial solution is taken as the fine-group (49), fine-spatial-mesh (1462) computation of the initial condition. In order to determine the effectiveness of this procedure, three fuel-cycle computations were performed through six burnup intervals and compared with the reference calculation. This reference computation utilized all 1462 spatial mesh points but was collapsed to eight energy groups. The test calculations also used the same eight energy groups, but with 49, 225, and 342 spatial mesh points for Cases 1, 2, and 3, respectively. In these latter calculations, the 225 and 342 mesh problems differ fundamentally from the 49-mesh calculation in that, in the 49-mesh case, both the cross sections and leakages were energy collapsed at each mesh point. In Cases 2 and 3, the cross-section data used is the same as that used in Case 1, but the leakage coefficients were collapsed for each of the mesh points. The effect of this approximation will be tested at a later date.

The effect of space collapsing on certain fuel-cycle parameters was examined at three time points: (1) beginning-of-life, (2) third burnup interval, and (3) equilibrium value, and for three regions—the core, the inner axial blanket, and the outer axial blanket. For each of the cases, the distribution of mesh points throughout the reactor is shown in Table 465-XII.

TABLE 465-XII

MESH POINT DISTRIBUTION

	Core	Blankets	Total
Reference	250	772	1462
Case 1	3	20	49
Case 2	9	145	225
Case 3	22	228	342

As seen from the table, the bulk of the mesh points added to those of Case 1 were added in the blankets. The reason is that the core flux distribution changes very little in time, while that of the blanket changes significantly, especially in the outer regions. The results of the calculations are shown in Table 465-XIII. As can be seen from this data, mesh points do significantly improve the calculation. Also, it is seen that satisfactory fuel-cycle parameters may be obtained, even when the number of space points used is reduced by a factor of thirty as long as the data is collapsed correctly.

TABLE 465-XIII

EFFECT OF A SPACE-COLLAPSED ANALYSIS ON SOME FUEL-CYCLE PARAMETERS

BREEDING RATIOS (% error)

Time	Reference	Case 1	Case 2	Case 3
1	1.1471	0.1	0.1	0.1
2	1.1883	-1.9	-1.4	-0.8
3	1.1852	-2.5	-1.7	-0.9

^{239}Pu ATOM DENSITIES (% error)

a. Core

Time	Reference	Case 1	Case 2	Case 3
1	9125	0.0	0.0	0.0
2	8396	-0.2	-0.1	-0.1
3	8284	-0.3	-0.2	-0.2

b. Inner Axial Blanket

1	658	0.0	0.2	0.2
2	1465	-1.7	-1.3	-0.9
3	1693	-2.3	-1.8	-1.2

c. Outer Axial Blanket

1	318	0.0	0.0	0.0
2	745	-3.8	-2.4	-1.2
3	883	-5.1	-3.3	-1.6

G. Review of Synthesis Methods for Fast Reactors (R. E. Alcouffe)

A topical review of synthesis methods for the LMFBR program has been completed and a report is being prepared. The emphasis of this review is in the area of flux synthesis, where the object is to obtain an accurate flux solution to the equations describing an aspect or approximation of neutron behavior by utilizing some approximate solutions to the problem and blending or synthesizing them together.

The techniques for accomplishing this for the diffusion approximation in the areas of neutron kinetics and statics have been well developed and documented. This documentation includes numerous applications to thermal systems and some on fast multigroup systems. The comparable situation for the neutron transport equation is much less developed. Techniques have yet to be developed with which it is possible to perform a synthesis of a transport solution from lower-order approximate solutions to the problem.

One of the main areas of concern in this field is the lack of documented synthesis codes. At present, there is one two-dimensional diffusion code published,[34] and one two-dimensional and one three-dimensional diffusion codes are in preparation. These codes are structured primarily for fast reactors. There is also a two-dimensional fast reactor kinetics code written at Karlsruhe.[35]

The main areas indicated by this review that require more development are:

a. The development of a versatile space-time diffusion kinetics code for performing three-dimensional transient analyses,

b. Development of techniques to do transport synthesis utilizing lower-dimensional calculations, and

c. Demonstrating the feasibility and usefulness of space-energy synthesis in fast reactors.

An extensive bibliography[36] has also been prepared on synthesis methods.

H. Computational Techniques for Repetitively Pulsed Reactors (G. C. Hopkins)

In a repetitively pulsed reactor excited by some form of accelerator and synchronously pulsed reactivity, a problem arises in determining the neutronic response in a computationally efficient manner. The quasi-stabilized time-dependent solution to the monoenergetic point kinetics equations is sought with equal, but unknown, initial and final boundary conditions. Pulse characteristics and typical system parameters have been described previously.[37]

Previous studies of this problem have involved: approximating the precursor density as a constant;[38] computationally long asymptotic approaches to the quasi-stabilized state;[39] and considering the power pulse as a delta function.[40] None of these restrictions are contained in the present formulation.

Two basic cases are being investigated: 1) the linear problem associated with either constant or a priori known time-dependent reactivities and

sources, both during the pulse and off-pulse; and 2) the nonlinear problem arising from consideration of feedback-dependent reactivity.

For the first of these cases, then, the problem is to obtain the neutronic response over the cycle $t = 0 \rightarrow T$, starting from the point kinetics equations:

$$\frac{dN(t)}{dt} = \frac{\rho(t) - \beta}{\Lambda} N(t) + \lambda C(t) + S(t) \qquad (5)$$

$$\frac{dC(t)}{dt} = \frac{\beta}{\Lambda} N(t) - \lambda C(t), \qquad (6)$$

where

$$S(t) = \bar{S} \qquad t = 0 \rightarrow t = t_p$$
$$= 0 \qquad t = t_p \rightarrow t = T$$

and, for illustrative purposes

$$\rho(t) = \rho_0 + \rho_1 \sin\left(\frac{\pi}{t_p}\right)t \qquad t = 0 \rightarrow t = t_p$$
$$= \rho_0 \qquad t = t_p \rightarrow t = T$$

Most numerical techniques for solving this equation set are iterative, based on dividing the entire cycle into many time intervals, during each one of which two approximations are made: 1) approximating the derivatives and 2) approximating the reactivity, as constants during the interval. The size of the time interval is then dependent upon how well both approximations are satisfied. For a problem such as this, with rapidly varying neutron behavior, the derivative approximation leads to a much more stringent time-interval determination than does the reactivity approximation.

The Laplace transform-residue method, however, is not only noniterative but also involves only one approximation--that for the reactivity from $t = 0 \rightarrow t = t_p$, which is only a thousandth of the entire cycle. The portion of the cycle from $t = t_p \rightarrow t = T$ can be treated as one time interval without any approximation, in contrast to most other techniques.

The solution is obtained by starting with the Laplace transform of Eqs. 5 and 6, treating $\rho(t)$ and $S(t)$ as constants. After some algebraic manipulations and inverse transforming, the equation set reappears in the form:

$$N_0 = N_n$$
$$C_0 = C_n$$

$$N_{i+1} = a_{1i} N_i + a_{2i} C_i + a_{3i} \bar{S}_i$$
$$C_{i+1} = b_{1i} N_i + b_{2i} C_i + b_{3i} \bar{S}_i \qquad i = 1, n - 1$$

In matrix form, this is

$$\underline{M}\underline{N} = \underline{S},$$

where

$$\underline{N} = \begin{bmatrix} N_0 \\ C_0 \\ N_1 \\ C_1 \\ \cdot \\ \cdot \\ \cdot \\ N_n \\ C_n \end{bmatrix} \qquad \underline{S} = \begin{bmatrix} 0 \\ 0 \\ a_{31}\bar{S}_1 \\ b_{31}\bar{S}_1 \\ \cdot \\ \cdot \\ \cdot \\ a_{3n}\bar{S}_n \\ b_{3n}\bar{S}_n \end{bmatrix}$$

and

$$M = \begin{bmatrix} 1 & 0 & \cdot & \cdot & \cdot & 0 & -1 & 0 \\ 0 & 1 & & & & & & -1 \\ a_{11} & a_{21} & 1 & & & & & \cdot \\ b_{11} & b_{21} & & 1 & & & & \\ 0 & & & & & & & \cdot \\ \cdot & & & & & & & \\ \cdot & & & & & & & \cdot \\ \cdot & & & & a_{1n} & a_{2n} & 1 & 0 \\ 0 & \cdot & \cdot & \cdot & b_{1n} & b_{2n} & 0 & 1 \end{bmatrix}$$

The solution, $\underline{N} = M^{-1}\underline{S}$, is going to depend either explicitly or implicitly, on some form of inversion of the matrix M. But for 1000 time intervals, typical for the reactivity approximation, and the two variables N(t) and C(t), the matrix M is 2000 x 2000, too bulky for efficient manipulation as such. However, a quick examination reveals that no row contains more than three elements, thereby reducing the matrix to two 2000 x 3 arrays: one for the coefficients and one for the indices. The straight inversion is still out of the question, however, because each row of the inverse would contain many more than three elements.

A method well suited to this matrix, though, is Gaussian elimination. Because of the nature of the method and the matrix, plus the fact that the diagonal already consists of only 1's, a single array of 2000 x 2 and 2 sec of CP time are all that is required to effect a solution.

For the nonlinear case involving feedback-dependent reactivity, the solution was necessarily iterative. However, a convergence-acceleration technique was employed between sets of iterations, resulting in a convergence time still much less than that possible with other published techniques.

The solution over the entire cycle at quasi-stabilization is equivalent to knowing only the initial values at quasi-stabilization. Therefore, analytic continuation was used to generate twenty successive initial values. A curve, consisting of these initial values, was then fed into a spline extrapolation routine, which extrapolated out in time a factor of five and returned a new set of initial values. This process was then repeated until all variables became quasi-stabilized.

Comparative studies demonstrated that this method was approximately twice as efficient as Runge-Kutta or Milne Difference methods.

REFERENCES

1. G. E. Hansen and H. C. Paxton, "Re-evaluated Critical Specifications of Some Los Alamos Fast-Neutron Systems," LA-4208, Los Alamos Scientific Laboratory (1969).

2. G. H. Best, M. E. Battat, R. J. LaBauve, and R. E. Seamon, "Calculations of JEZEBEL and GODIVA with Recent ENDF/B Microscopic Data," Paper CN-26/92 presented at IAEA/CN-26, Conference on Nuclear Data for Reactors, Helsinki, Finland, June 15-19, 1970.

3. M. E. Battat, R. J. LaBauve, and R. E. Seamon, "Comparison of Several Versions of the MC^2 Code, Code," ORNL-RSIC-27, p. 73, Proc. Conf. on Multigroup Cross Section Preparation - Theory, Techniques, and Computer Codes, Oak Ridge, Tennessee, October 1-3, 1969.

4. R. Q. Wright, N. M. Greene, J. Lucius, and C. W. Craven, Jr., "SUPERTOG: A Program to Generate Fine Group Constants and P_n Scattering Matrices from ENDF/B," ORNL-TM-2679, Oak Ridge National Laboratory (1969).

5. Donald J. Dudziak (ed.), "ENDF/B Format Requirements for Shielding Applications," LA-3801, Los Alamos Scientific Laboratory (1967).

6. Donald J. Dudziak, Alan H. Marshall, and Robert E. Seamon, "LAPH, A Multigroup Photon Production Matrix and Source Vector Code for ENDF/B," LA-4337 (ENDF-132), Los Alamos Scientific Laboratory (1969).

7. Donald J. Dudziak, "Translation to ENDF/B and 'Physics' Checking of Cross Sections for Shielding," DASA-2379 (ENDF-130), University of Virginia (1969).

8. H. J. Kopp, J. D. Morris, and W. E. Schilling, "DATATRAN Modular Programming System for Digital Computers," KAPL-M-6997, Knolls Atomic Power Laboratory (1968).

9. F. McGirt, "LAMPS, Los Alamos Modular Programming System," LA-4371, Los Alamos Scientific Laboratory (1970).

10. F. McGirt, "Linking the DTF-IV and DAC1 Free-Standing Codes with LAMPS," Los Alamos Scientific Laboratory report (in preparation).

11. B. J. Toppel, "The Argonne Reactor Computation (ARC) System," ANL-7322, Argonne National Laboratory (1967).

12. "Control Data Scope Reference Manual," Publication No. 60189400, Control Data Corporation (1969).

13. B. M. Carmichael, "DAC1, A One-Dimensional S_n Perturbation Code," LA-4342, Los Alamos Scientific Laboratory (1970).

14. T. B. Fowler and D. R. Vondy, "Nuclear Reactor Core Analysis Code: CITATION," ORNL-TM-2496, Rev. 1, Oak Ridge National Laboratory (1970).

15. R. E. Schenter, J. L. Baker, and R. B. Kidman, "ETOX, A Code to Calculate Group Constants for Nuclear Reactor Calculation," BNWL-1002, Pacific Northwest Laboratory (1969).

16. R. W. Hardie and W. W. Little, Jr., "1DX, A One-Dimensional Diffusion Code for Generating Effective Nuclear Cross Sections," BNWL-954, Pacific Northwest Laboratory (1969).

17. B. J. Toppel, A. L. Rago, and D. M. O'Shea, "MC^2, A Code to Calculate Multigroup Cross-Sections," ANL-7318, Argonne National Laboratory (1967).

18. W. W. Engle, Jr., "A Users Manual for ANISN: A One-Dimensional Discrete Ordinates Transport Code with Anisotropic Scattering," K-1693, Union Carbide Corporation (1967).

19. R. Protsik and E. G. Leff, "Users Manual for DOT2DB: A Two-Dimensional Multigroup Discrete Ordinates Transport/Diffusion Code with Anisotropic Scattering," GEAP-13537, General Electric Sunnyvale, (1969).

20. W. W. Little, Jr. and R. W. Hardie, "2DB User's Manual," BNWL-831, Pacific Northwest Laboratory (1970).

21. K. D. Lathrop, "DTF-IV, A FORTRAN-IV Program for Solving the Multigroup Transport Equation with Anisotropic Scattering," LA-3373, Los Alamos Scientific Laboratory (1965).

22. R. W. Hardie and W. W. Little, Jr., "3DB, A Three-Dimensional Diffusion Theory Burnup Code," BNWL-1264, Pacific Northwest Laboratory (1970).

23. M. K. Butler, Marianne Legan, and L. Ranzini, "Argonne Code Center: Compilation of Program Abstracts," ANL-7411, Argonne National Laboratory (1968).

24. R. Douglas O'Dell and Thomas J. Hirons, "PHENIX, A Two-Dimensional Diffusion-Burnup-Refueling Code," LA-4231, Los Alamos Scientific Laboratory (1970).

25. Thomas J. Hirons and R. Douglas O'Dell, "Models for Fuel-Cycle Analysis in Large Fast Breeders," Trans. Am. Nucl. Soc. 12, 38 (1969).

26. Thomas J. Hirons and R. Douglas O'Dell, "Calculational Modeling Effects on Fast Breeder Fuel-Cycle Analysis," LA-4187, Los Alamos Scientific Laboratory (1969).

27. R. Douglas O'Dell and Thomas J. Hirons, "PHENIX, A Two-Dimensional Diffusion-Burnup-Refueling Code," Nucl. Sci. Eng. 39, 411 (1970).

28. "Quarterly Status Report on the Advanced Plutonium Fuels Program, October 1 to December 31, 1968," LA-4114-MS, Los Alamos Scientific Laboratory (1968).

29. Private Communication.

30. "Comparison of Two Sodium-Cooled 1000 MWe Fast Reactor Concepts; Task 1, Report of 1000 MWe LMFBR Follow-On Work," GEAP-3618, General Electric (1968).

31. "Liquid Metal Fast Breeder Reactor Design Study (1000 MWe UO_2-PuO_2 Fueled Plant)," GEAP-4418, General Electric (1963).

32. Raymond E. Alcouffe and Robert W. Albrecht, "A Generalization of the Finite Difference Approximation Method with an Application to Space-Time Nuclear Reactor Kinetics," Nucl. Sci. Eng. 37, 1 (1970).

33. Raymond E. Alcouffe, Thomas J. Hirons, and R. Douglas O'Dell, "Effect of Collapsing Cross-Section Data on Fast Breeder Physics Parameters," submitted to Nucl. Sci. Eng. (1970).

34. P. Greebler, "BISYN - A Two-Dimensional Synthesis Program," GEAP-4722, General Electric (1965).

35. G. Kessler, "RADYVAR, Programm zur Behandlung der raumabhängigin Dynamik schneller Brutreaktoren mit Hilfe des Variationsverfanrens von Kantorowitsch," KFK-781/II, Institut für Reaktorentwicklung, Kernforschungszentrum Karlsruhe, Germany (1970).

36. J. Furnish, "A Bibliography of Reactor Flux Synthesis Methods," LA-4461-MS, Los Alamos Scientific Laboratory (in preparation).

37. "Quarterly Status Report on the Advanced Plutonium Fuels Program, January 1 to March 31, 1969," LA-4193-MS, Los Alamos Scientific Laboratory.

38. Ing. T. Trombetti, "Cinetica di un Reattore Veloce Pulsato in Regime Periodico o Quasi Periodico," ARV(65)43, Comitato Nazionale Per L'Energia Nucleare, Bologna (1965).

39. M. S. Trasi, "Integration of the Point-Reactor Kinetic Equations with a Periodic Reactivity Input by Use of Quasi-Periodic Vector Solutions," B.A.R.C.-371, Bhabha Atomic Research Center, Bombay (1968).

40. G. Blaesser and J. A. Larrimore, Nucl. Sci. Eng. 37, 186 (1969).

PROJECT 467

FUEL IRRADIATION EXPERIMENTS

Person in Charge: D. B. Hall
Principal Investigator: J. C. Clifford

I. INTRODUCTION

The goal of this program is to examine the irradiation behavior of advanced fuels for LMFBRs. During the past fiscal year, the fuel concepts under study were sodium-bonded mixed carbides and metals. Metal fuel work has been terminated. Work on carbides will continue, but at a lower level.

Carbide investigations are concerned with the irradiation performance of high purity, single-phase $(U_{0.8}Pu_{0.2})C$ produced and characterized at the Los Alamos Scientific Laboratory (Project 463). Sodium-bonded, mixed-carbide pins are being irradiated in the EBR-II reactor at heat ratings of interest for fast reactor application. The experiments are designed to examine the degree of fuel swelling, gas release, fuel-sodium-clad interaction, and the migration of fissionable material and fission products as a function of burnup and fuel density. Thermal flux irradiations of LASL-produced carbides also are included to augment determination of the effects of high burnup on fuel-bond-clad compatibility.

II. EBR-II IRRADIATION TESTING
(J. O. Barner)

A. General

The purpose of the EBR-II irradiations is to evaluate candidate fuel/sodium/clad systems for the LMFBR program. In the reference design, fuel pellets of single-phase (U,Pu)C are separated by a sodium bond from a cladding of Type 316 stainless steel. Three series of experiments are planned and approval-in-principle has been received from the AEC.

The capsules are to be irradiated under the following conditions:

Condition	Series 1	Series 2	Series 3
1. Lineal power, kW/ft	~ 30	~ 45	~ 30
2. Fuel composition	$(U_{0.8}Pu_{0.2})C$, single-phase, sintered		
3. Fuel uranium	^{235}U	^{233}U	^{235}U
4. Fuel density	90%	95%	95%
5. Smear density	80%	80%	80%
6. Clad size	0.300-in. i.d. x 0.010-in. wall		
7. Clad type	316 SS	316 SS	316 SS
8. Max clad temp, °F	1250	1275	1250
9. Max fuel centerline temp, °F	2130	2550	2100
10. Burnup	3 a/o to 8 a/o		

The capsules are doubly contained.

B. Results During FY 1970

Two capsules from Series 1, designated K-42B and K-36B, are currently operating at ~ 29 kW/ft (maximum) in EBR-II. During July, 1970, they will be discharged from EBR-II at maximum burnups of 4.5 a/o and 3 a/o. They will be returned to LASL for destructive examination and evaluation.

Three capsules from Series 1, designated K-37B, K-38B, and K-39B, and two capsules from Series 3, designated K-43 and K-44, have been available at EBR-II for irradiation since the third quarter of FY 1970. They are expected to start irradiation in subassembly XO86 during the first quarter of FY 1971. The target burnup for these capsules is 6 to 8 a/o.

The three capsules from Series 2, designated K-49, K-50, and K-51, and two additional capsules from Series

3, designated K-45 and K-46, were completed during the fourth quarter of FY 1970 and shipped to EBR-II. It is expected that these capsules will commence irradiation during the first quarter of FY 1971 in a reconstituted subassembly with some oxide fuels from other experiments.

Improved eddy current testing for defects in the capsule sodium bonds was instituted during the year. Voids of 0.030 in. diam can be detected reliably and the limit of detection is 0.020 in. diam.

A program has been started in conjunction with the LASL's Nuclear Safeguards Group, N-6, to ensure that the pellets loaded into specific positions in the EBR-II capsules contained the proper isotopes and amounts of heavy metals. Capsules K-45, K-46, K-49, and K-51 were analyzed for ^{235}U, ^{233}U, ^{238}U and ^{239}Pu and were found to contain the proper amounts of the proper isotopes in the correct position in the capsules.

Two thermal control capsules are operating in an out-of-pile loop. Capsule external temperatures are approximately those of EBR-II in-pile temperature. These capsules will operate for several thousand hours.

III. THERMAL IRRADIATIONS OF SODIUM-BONDED MIXED CARBIDES (J. C. Clifford, R. L. Cubitt, D. C. Kirkpatrick)

A. General

Mixed carbides, sodium-bonded to Type 316 stainless steel cladding, are being irradiated in the LASL Omega West Reactor (OWR), a 6 MW MTR-type facility. The purpose of the experiments is to determine whether fuel, clad, and sodium remain mutually compatible as burnups of interest in the LMFBR program are approached. While fast-spectrum irradiations are preferred in order to produce the power densities and radial temperature gradients anticipated in LMFBRs, thermal irradiations appear acceptable in this instance because the fuel regions of prime interest (those in contact with sodium) for compatibility studies can be maintained at realistic temperatures. Fuel for the experiments is fully enriched in ^{235}U, minimizing the time required to reach significant skin burnup.

Experiments are conducted in instrumented environmental cells installed semipermanently in the OWR. The principal features of these cells are: (1) a heat removal and temperature control system consisting of a natural convection sodium loop, electrical heaters, and a variable conductivity heat leak, and (2) a sweep gas system for the rapid detection of leaking fuel capsules.

B. Results During FY 1970

Three sodium bonded mixed carbide experiments were assembled and irradiated in the OWR. The first was terminated, as planned, at an estimated skin burnup of 4 a/o and destructive examination is in progress. The second was terminated after a fission gas release which occurred one week short of the scheduled shutdown at 8 a/o skin burnup. The third experiment has reached approximately one-third of a planned exposure to 12 a/o skin burnup and is operating satisfactorily. Assuming no prior failure occurs, this experiment will be completed in December.

The experiments are identical except in capsule closure weld design and thermocouple placement. Fuel for the experiments is a single phase, uranium-plutonium carbide, fully enriched in ^{235}U. Fuel pellets are 0.265 in. diam, 0.250 in. thick, and approach 95% of theoretical density.

An experimental assembly contains two Type 316 stainless steel fuel capsules, each 2.5 in. long and 0.300 in. diam with a 10 mil wall. Each capsule contains three fuel pellets, a stainless steel insulator pellet to separate the fuel from the capsule lower closure weld, and approximately 0.3 g sodium. The capsules are stacked end on end in a 0.600-in.-diam stainless steel secondary container and are centered in the secondary by thin stainless steel disks at the top and base of each capsule. The annular volume between capsules and secondary container is filled with sodium. Each experiment contains eight, 31-mil diam thermocouples which pass through small holes in the centering disks and are wired to the fuel capsules. Figure 467-1 illustrates the method of assembly.

Neutron flux distributions and the corresponding power distributions were calculated for these experiments using a one-dimensional transport code approximating the fuel, environmental cell, and OWR as concentric, infinitely long cylinders. Hansen-Roach 16 group cross sections were used in the calculations. Prior

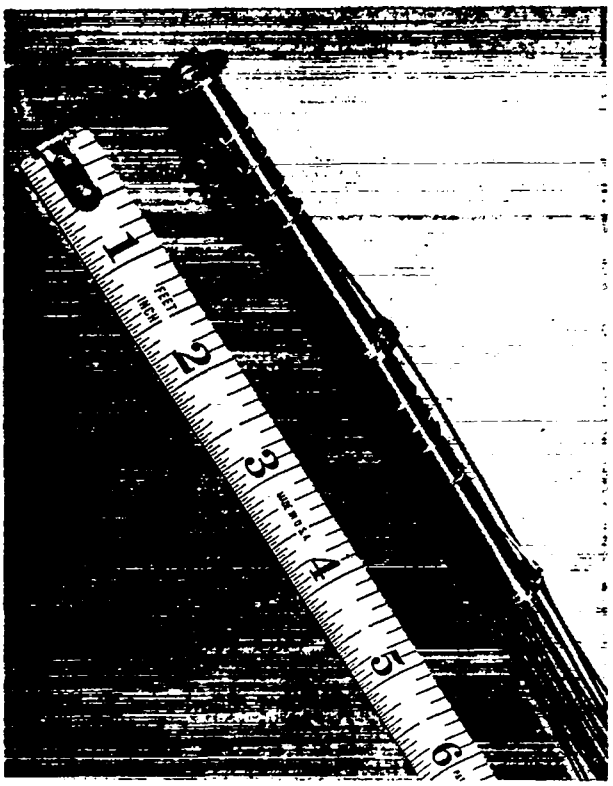

Fig. 467-1. Fuel capsules for OWR irradiation of sodium-bonded (U, Pu)C.

experience with this calculational technique for predicting power distribution in OWR-irradiated fuels has resulted in good agreement with experimentally determined distributions.[1]

Measurements of fission heating in the three experiments agree within 5% and indicate that each operated at a linear heat rating of 22 kW/ft. Fuel surfaces are maintained in the range 600-700°C and predicted centerline temperatures vary from ~ 775 to 875°C. Using the computed radial power distribution and normalizing this to measured total power, a specific power of 670 W/g of fuel was obtained for the fuel skin and 50 W/g, for the fuel centerline. The variation of specific power with radial position is shown in Fig. 467-2. An attempt will be made to verify this power distribution experimentally using a combination of pin-hole gamma scanning of fuel wafers[2] and burnup analysis.

OWREX-14, which was terminated at 4 a/o skin burnup, has been radiographed, gamma-scanned, and disassembled. Fuel, clad, and insulator pellet specimens

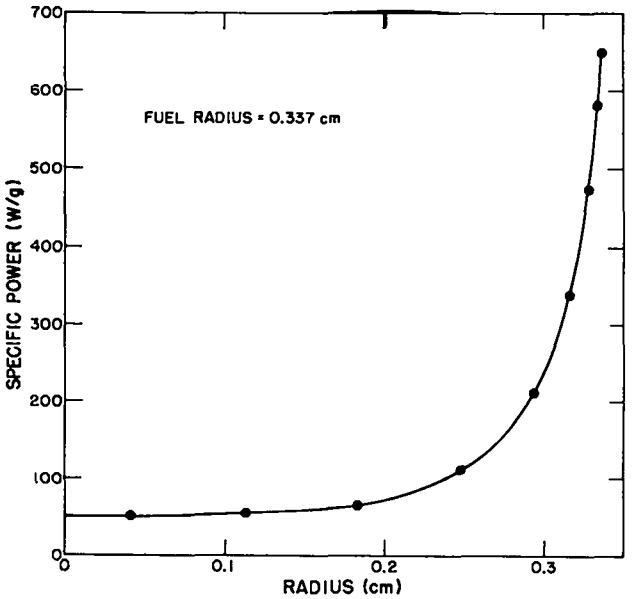

Fig. 467-2. Predicted radial power distribution in OWR-irradiated (U, Pu)C.

are awaiting metallographic examination. Because of the large radial variation in specific power no swelling or fission gas release estimates were made. OWREX-15, which failed a week before scheduled shutdown, has been removed from the reactor and radiographed. It will be disassembled as the hot cell schedule permits. No thermal irradiation experiments are planned past the present experiment, OWREX-16.

IV. THERMAL IRRADIATIONS OF SODIUM-BONDED U-Pu-Zr (J. C. Clifford, R. L. Cubitt, D. C. Kirkpatrick)

A. General

A program of thermal irradiations was initiated to evaluate the behavior of U-Pu-Zr alloys produced by the LASL. Irradiations were conducted at the OWR in an environmental cell presently being used for irradiations of mixed carbides (Section 467-III). Temperature changes accompanying reactor power level changes were minimized with electrical heaters and with a variable conductivity heat leak incorporated into the cell. In this manner it was possible to minimize thermal cycling of the fuel through phase transformations that affect its swelling behavior.

About the time the first U-Pu-Zr experiment was irradiated, interest in metal fuels waned. Rapid failure of this experiment, and of a second one late last summer,

led to abandonment of the program except for a small postmortem effort. This has been completed recently.

Complementary to the irradiations was an out-of-pile investigation of the compatibility of LASL-produced U-Pu-Zr alloys with Type 316 stainless steel and with a vanadium alloy. Of prime interest were the effects of zirconium and oxygen content of the fuel on reactions between fuel and stainless steel, and the effects of sodium on these reactions. The work has been terminated except for the examination of compatibility experiments completed during the past quarter. Results from these experiments will be summarized in a topical report.

B. Results During FY 1970

1. Irradiation Experiments

The metal fuel experiments were put together in the same fashion as the carbide experiments described in the previous section. Fuel for the experiments consisted of both as-cast and extruded U-15Pu-12Zr alloys machined to final dimensions of 1.00 in. long and 0.144 in. diam. Conical depressions in the ends of the fuel slugs matched conical protrusions in the lower end caps and in cruciform devices riding on top of the slugs (Fig. 467-3). The effect was to hold the fuel slugs in the approximate center of the capsules and away from the walls. Clearance between the cruciform device and the capsule wall was sufficient to allow axial movement of the fuel at operating temperature. Fuel capsules were 0.196 in. diam and 2.5 in. high, with a 15 mil wall. The 22 mil diametral gap between fuel and clad was filled with sodium.

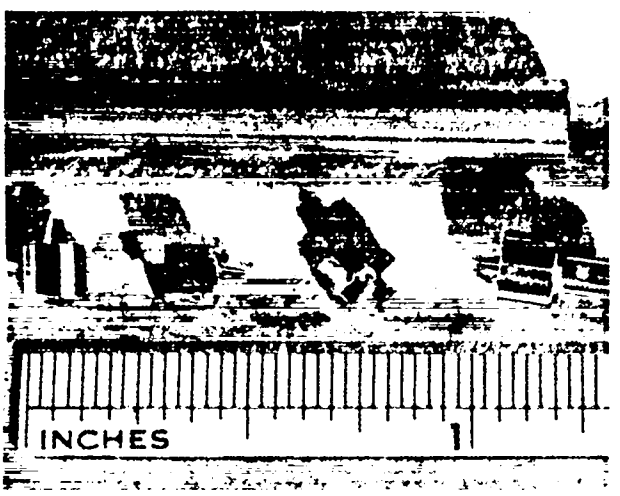

Fig. 467-3. Fuel capsule components for U-Pu-Zr thermal irradiations.

At startup of the first experiment (OWREX-12) a 45°C axial temperature gradient (because of the natural convection loop in the cell) and a maximum clad temperature of 630°C were measured. Using the measured fission heat and assuming no axial flux gradient, fuel skin operating temperatures of 605-650°C and fuel centerline temperatures of 665-710°C were calculated. Initially, then, all fuel surfaces appear to have operated in a three phase region of the ternary U-Pu-Zr system,[3] and all interiors in a higher temperature, single phase region. Shortly after startup, temperatures in the top capsule began rising and were permitted to increase to a maximum fuel surface temperature of 690°C. At this point, the assembly was cooled until the top pin operated at its start-up temperatures. The experiment was terminated a day later after a fission gas release. The total operating time was four days.

Visual and radiographic examination of the assembly indicated that the top pin had lost sodium and that the fuel had slumped. No distortion was detected in the other pins. An apparent crack was located in the heat affected zone of the lower closure weld, and the failure was attributed to capsule cracking, sodium bond expulsion, and fuel overheat.

With a reason for failure at hand, another experiment (OWREX-13) was assembled using three capsules and extruded fuel. At startup, the measured axial temperature gradient for this experiment was 50°C and the estimated maximum fuel skin and fuel centerline temperatures were 715 and 780°C, respectively. Average specific power, based on a fission heat measurement, was 150 W/g of fuel. Under these conditions the fuel specimens probably operated entirely in a single phase region which, at the composition of this fuel, exists above ~ 655°C. Shortly after startup, the temperatures of all three fuel capsules began fluctuating, and, three days

later, fission gas was released from the experiment. The experiment was terminated immediately. Examination of the assembly showed that all three fuel slugs had slumped and that fuel had penetrated the wall of the middle capsule. At that point, attempts to irradiate U-Pu-Zr were ended and the cell was diverted to mixed carbide experiments.

OWREX-12 and -13 capsules which showed evidence of fuel slumping were sectioned, autoradiographed, and examined metallographically. An axial section through the apparent crack in the capsule from OWREX-12 revealed only a normal microstructure. Alpha and beta-gamma autoradiographs of the section shown in Fig. 467-4 showed fraction of plutonium and fission products.

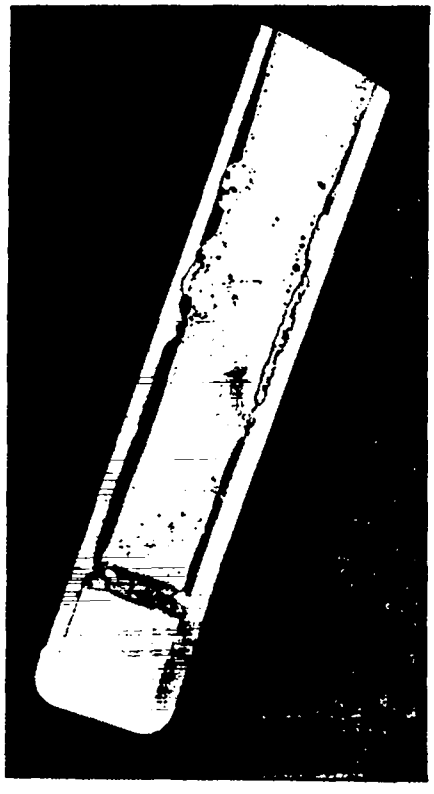

Fig. 467-4. Section from OWREX-12 fuel capsule.

Fuel-clad interaction, fuel distortion, and voids or bubbles are visible in Fig. 467-4. The fuel microstructures are complex, particularly in the regions of fuel-clad reaction, where several phases appear. No attempt was made to identify microstructural components. The OWREX-13 failures are more impressive. Figure 467-5 shows a transverse section through the middle capsule where fuel penetrated the clad. Figure 467-6 shows an axial section from the top capsule. Plutonium

Fig. 467-5. Transverse section from OWREX-13 fuel capsule showing extensive wall thinning and penetration of clad by fuel.

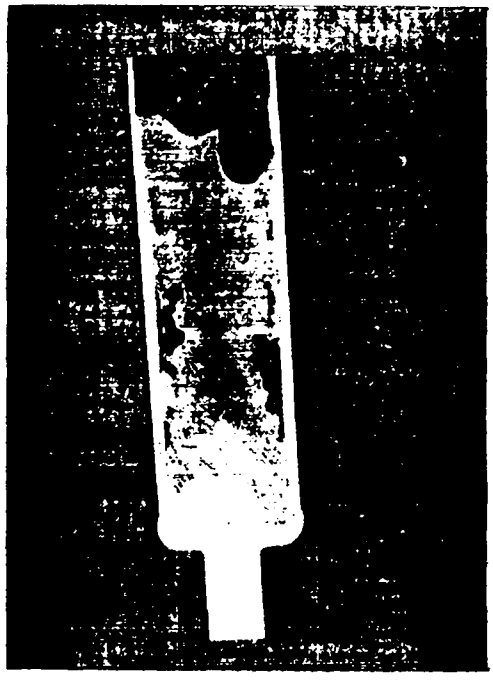

Fig. 467-6. Section from OWREX-13 highest temperature fuel capsule.

and fission products were distributed heterogeneously and fuel microstructures were complex. No evidence of cladding failure was found in the top and bottom capsules, although > 50% reductions in wall thickness were observed.

In view of the catastrophic nature of the failures, power and temperature measurements, stress calculations, fuel pin assembly procedures, and nondestructive testing procedures and results were reviewed. No anomalies were apparent. Particular attention had been given the assembly and inspection of OWREX-13 capsules after the OWREX-12 failure, but nondestructive examination of tubing stock, finished capsules, closure welds, and sodium bonds failed to reveal any significant flaws. With the failure of four out of seven capsules, it would appear that something more than random defects should be involved. The only obvious feature common to the four failures is a fuel minimum operating temperature of 650°C. Whether this is coincidence cannot be evaluated without additional experimentation.

2. Compatibility Experiments

Two types of compatibility tests have been conducted with U-Pu-Zr fuels: dry assemblies of fuel and clad, and sodium bonded fuel capsules. For the dry experiments, blank disks of fuel and cladding alloy, with nominal dimensions of 1/4 in. diam and 3/16 in. thick, were rough polished through 600 grit paper in an air atmosphere. The disks were transferred to a high purity inert gas glovebox train where final polishing was done by hand on 4/0 emery paper. Stacks of specimens, consisting of a fuel disk with a cladding disk on each side, were assembled in presses (Fig. 467-7). The presses were wrapped in zirconium foil and sealed in stainless steel capsules, using the glovebox atmosphere as the cover gas. The difference in thermal expansion between specimen stacks and presses at operating temperature was relied upon to maintain intimate contact between disks. Capsules were heated at 500, 650, and 750°C for periods of 250 to 4000 h, furnace cooled, and disassembled. Stacks of disks were sectioned axially and examined. In some cases electron beam microprobe examination and x-ray diffraction analysis were used to augment optical metallography. Several sodium bonded

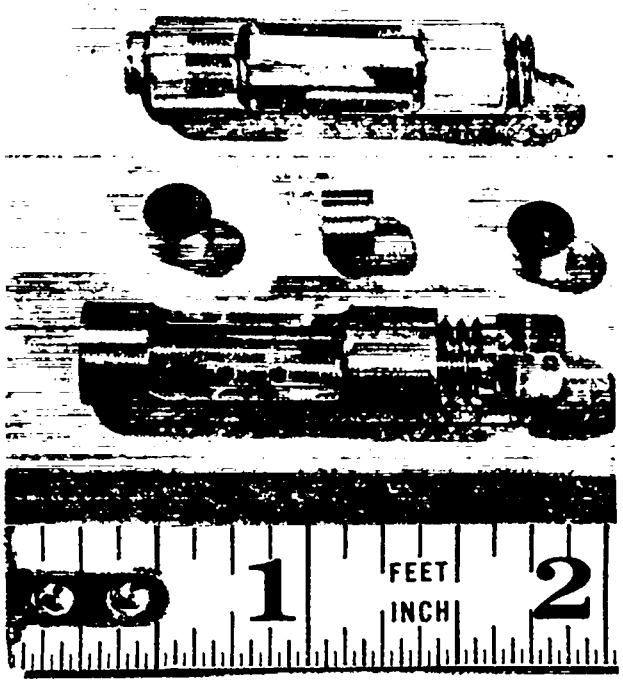

Fig. 467-7. Presses and stainless steel disks used for dry compatibility experiments.

fuel capsules, identical to those irradiated in the OWR, were heated out of pile at 605 and 750°C for 1000, 2000, and 4000 h. After test, bonding sodium was removed from these capsules by vacuum distillation.

The compatibility test schedule is shown in Table 467-I.

TABLE 467-I

TESTING SCHEDULE FOR METAL FUEL COMPATIBILITY EXPERIMENTS

	Materials	Temperature (°C)	Time (h)
(a)	Type 316 stainless vs U-15Pu-12.7Zr (180 ppm O)	650 750	1000-2000-4000 1000-2000-4000
(b)	Type 316 stainless vs U-15Pu-12Zr (820 ppm O)	650 750	1000-2000-4000 1000-2000-4000
(c)	Type 316 stainless vs U-14Pu-6Zr (125 ppm O)	650 750	1000-2000-4000 1000-2000-4000
(d)	Type 316 stainless vs U-15.6Pu-10.7Zr (650 ppm O)	650 750	1000-2000-4000 1000-2000-4000
(e)	V-15Cr-5Ti vs U-15Pu-12.7Zr (180 ppm O)	550 650 750	500-1000-2000 250-500-1000-2000 250-500-1000
(f)	Type 304 stainless vs U-15Pu-12Zr (170 ppm O) Na bonded	650 750	1000-2000-4000 1000-2000-4000

In the dry experiments, four fuel compositions and Type 316 stainless steel were used. The principal fuel variables of interest were zirconium and oxygen content. A

low oxygen fuel also was used with a V-15Cr-5Ti alloy to determine the temperatures and times required for transfer of significant amounts of Cr and Ti to the fuel alloy. A fifth fuel alloy, close in composition to that used in (a) of Table 467-I, was used in the sodium bond tests.

During dry tests at 750°C, plutonium moved from the fuel alloys into the stainless steel to a depth of a few microns. Nickel was depleted from the stainless steel surface, and a thin, zirconium-rich layer was formed at the fuel surface. At 650°C, and below, nothing much of interest has been observed in the dry fuel/stainless steel assemblies. At 650 and 750°C, vanadium and chromium moved rapidly into the fuel matrix from the V-15Cr-5Ti alloy, and all three fuel constituents moved into a thin layer at the vanadium alloy surface.

The stainless steel surface in contact with fuel during a 1000-h, 650°C sodium bond test is shown in Fig. 467-8. At the end of test the lower end of the capsule was badly contaminated with plutonium and although the composition of the badly overetched structure shown in Fig. 467-8 has not been determined, probably plutonium is present. The difference in behavior between dry and sodium-bond experiments has not been explained but it very likely is not attributable to composition differences between Types 304 and 316 stainless steel.

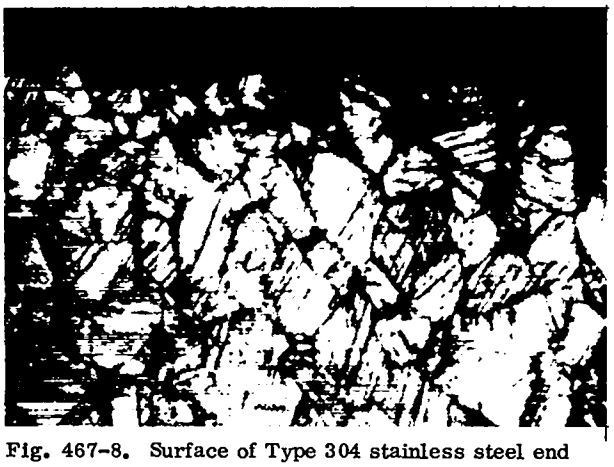

Fig. 467-8. Surface of Type 304 stainless steel end plug after contact with a U-15Pu-12Zr alloy for 1000 h at 650°C in the presence of sodium. Etched, 300X.

V. ANALYTICAL CHEMISTRY

Spectroanalysis of Na (O. R. Simi, R. T. Phelps)

Spectrographic measurement of contaminants in the bonding Na of reactor fuel elements provides important information about interactions and corrosion that have occurred within the element. For this reason, a spectrochemical method for determination of 26 impurity elements in Na was developed and tested for operation in a glovebox for unirradiated samples and in a hot cell for analyses of irradiated fuel elements. The method consisted of arcing the sample in a d.-c. arc following conversion of the Na metal to NaCl by dissolution in ethanol or n-butanol, addition of HCl, and evaporation to dryness. The NaCl residue was mixed with an equal weight of graphite powder containing 100 ppm of Ga to serve as an internal standard, and a 25-mg portion of the mixture was placed in a cratered electrode for arcing using a 12-amp arc. The exposures were continued as long as Na persisted in the arc, and the spectra were recorded either on a 2-m ARL spectrograph for the glovebox operation or a 3.4-m Ebert-mounting spectrograph for analyses in a hot cell. The densities of the analytical lines were measured photometrically and calculated by digital computer if optimum precision and accuracy were desired.

Calibration standards, prepared by adding 26 elements at concentrations of 0.3 to 300 ppm to NaCl and mixing in the dry state with a graphite powder-Ga_2O_3 mixture, were analyzed to determine the lowest concentration that could be detected reliably (Table 467-II).

TABLE 467-II

LIMITS OF DETECTION FOR ELEMENTS IN NaCl

Element	Limit of Detection, ppm Glovebox	Hot-cell	Element	Limit of Detection, ppm Glovebox	Hot-cell
Li	1	-	Co	2	1
Be	0.5	1	Ni	3	3
B	10	10	Cu	0.3	0.3
Mg	0.3	0.3	Zn	300	300
Al	1	1	Sr	0.3	1
Si	3	3	Mo	1	0.3
K	10	-	Ag	0.3	0.3
Ca	0.3	3	Cd	10	20
Ti	3	3	Sn	3	3
V	0.3	0.3	Sb	30	60
Cr	0.3	0.3	Ba	1	1
Mn	0.3	0.3	Pb	3	3
Fe	1	1	Bi	3	3

To evaluate the method further, four test samples containing 10 to 300 ppm of Al, Mo, Si, Cr, Fe, and Ni in NaCl (Table 467-III) were prepared, and each sample was analyzed in duplicate five times, thus providing ten spectra on five separate films for each impurity concentration. The calculations were made using a computer program to obtain the mean value of each set. The relative standard deviations (RSD) of each set of ten analyses at each concentration were calculated and averaged (Table 467-III). The test results were generally slightly lower than the nominal values, an effect ascribed to the presence of more elements (26) in the calibration standards than the six present in the test samples. The RSD of the measurements were 9% for determining Cr, Fe, and Ni and ranged between 13 and 22% for determining Al, Mo, and Si. Results from a set of analyses completed in the hot cell on these test samples were similar in precision and accuracy to the values obtained in the glovebox operations, showing that the method was satisfactory for analysis of either unirradiated or irradiated samples.

During preliminary tests of the method in a glovebox, several contaminating elements (Al, Cr, Cu, Fe, Mg, Pb, and Si) appeared randomly at concentrations as high as 20 ppm. The main source of the contaminants was impurities in the electrodes. Chloride in the electrode charge enhanced the detection of the impurities. Use of a larger electrode sample and careful selection of more-pure electrodes having a smaller diameter, thinner wall, and deeper crater reduced the effect of the impurities to acceptable levels of 1 or 2 ppm. Initial tests of the hot cell operations showed that contamination of the samples with several elements at concentrations up to 100 ppm occurred. Thorough cleaning of the hot cells reduced the contaminants to acceptable levels. The satisfactory results shown in Tables 467-II and -III were obtained following the changes made to eliminate the difficulties discovered in these preliminary tests.

VI. REFERENCES

1. R. L. Cubitt, G. L. Ragan, and D. C. Kirkpatrick, Los Alamos Scientific Laboratory, LA-3557-MS.
2. Quarterly Status Report on the Advanced Plutonium Fuels Program, April 1 to June 30, 1969, and Third Annual Report, FY 1969, LA-4284-MS.
3. W. N. Beck, R. J. Fousek, and J. H. Kittel, Argonne National Laboratory, ANL-7388.

TABLE 467-III

ANALYSIS OF TEST SAMPLES

	Nominal Conc. PPM		Concentrations Found, PPM in NaCl					
Sample	Al, Mo, Si	Cr, Fe, Ni	Al	Mo	Si	Cr	Fe	Ni
A	10	300	9.0	7.7	9.3	308	295	295
B	30	100	28	30	24	99	97	93
C	100	30	94	109	77	27	26	26
D	300	10	284	343	267	8.8	9.1	8.7
RSD, Average for 4 samples (40 spectra)			13	22	19	9	9	9

PROJECT 501

STANDARDS, QUALITY CONTROL, AND INSPECTION OF PRODUCTS

Person in Charge: R. D. Baker
Principal Investigator: C. F. Metz

I. INTRODUCTION

A major factor in the development of a successful reactor fuel is a high degree of technical competence for doing the required chemical analysis and related measurements necessary to characterize thoroughly the raw materials, the manufactured fuel, and the irradiated fuel. This project is identified with the mixed fuel development phase of the LMFBR/FFTF Program.

This project is directed toward (1) developing an analytical chemistry and measurements program, thereby ensuring high quality and uniformity of raw materials, (2) establishing and conducting a statistically designed quality control program of chemical analyses and other measurements that can be used to assure continuing adequate analytical competence of the fuel producers during the fuel fabrication stage, and (3) doing correlated chemical analyses and related measurements on irradiated fuel as a means of studying fuel behavior during core life; specifically involved will be burnup studies correlated with microprobe and metallography studies, gas release studies as related to cladding corrosion, and gas retention studies as related to porosity, particle size, and other properties of the fuel.

II. FFTF ANALYTICAL CHEMISTRY PROGRAM

A statistical analysis of data obtained in a program (Phase I), that was designed and executed to uncover the problems that existed in adequately characterizing FFTF mixed oxide fuel, clearly indicated the needs for common standards for calibration of methods, standardization of certain methods, updating some equipment, and developing better analytical methods in some cases. To meet these needs an analytical program (Phase II) was formulated, as described in LASL document CMB-1-870, and largely completed during the previous fiscal year. The remainder of the data for Phase II was received from participating laboratories, and all data were statistically analyzed. The results, including evaluation of the methods used, the capabilities of each participating laboratory, and the analytical problems remaining to be solved, were published in LA Report No. 4407, entitled, "LMFBR/FFTF Fuel Development Analytical Chemistry Program, (Phase II)". The report also showed that close control will be required of the sampling and analytical methods used to assure complete and adequate characterization of the high quality fuels.

Based upon these findings, plans were formulated for the qualification runs and for product quality control throughout the production of the first FFTF core loading. These plans were set forth in a proposed RDT Standard "Qualification of Analytical Chemistry Laboratories for FFTF Fuel" which prescribes the course of action by which analytical laboratories establish their technical competence to do the chemical and physical measurements required to characterize FFTF fuel. It also provides a quality control program for the continual evaluation of analytical data obtained during fuel production.

During a recent visit at AEC Headquarters, RDT personnel concurred with the conclusions given in LA Report No. 4407 and the evaluation of the Phase II results. Endorsement was received for the program of sampling and analyses, and also for the quantities of test materials for the qualification runs and the product quality control. A LASL document CMB-1-908 was prepared to provide additional technical information to guide the planning for

the work to be done in implementing the program outlined in the Proposed RDT Standard.

Purchases of two mass spectrometers were completed following evaluation of the bids received, and scheduled deliveries were made during the second quarter of FY 1971. One of these instruments will be used on burnup studies, and the other mainly on fission gas analyses with some work on gas retention problems. Standards were prepared for mass spectrometer calibrations. Plans were completed and requests processed for laboratory remodeling to house the mass spectrometers, and to provide space and equipment for the burnup and gas retention studies and for the fission gas analyses. The remodeling of the laboratories and installation of equipment were scheduled for completion early in the second quarter of FY 1971.

III. INVESTIGATION OF METHODS

An important part of the analytical chemistry program is the investigation and improvement of analytical methods, and development of new methods. The following analyses of sintered $(U,Pu)O_2$ were investigated:

A. Determination of F^- in Sintered $(U,Pu)O_2$

(T. K. Marshall and G. R. Waterbury)

Reliable measurements of F^- at low concentrations were required because traces of this element may significantly affect corrosion rates of stainless steel cladding materials and fuel-cladding behavior. A method was developed in which F^- was measured with a fluoride ion specific electrode following pyrohydrolytic separation in an all-nickel apparatus from the sintered oxides. Results obtained for 1 to 10 μg of F^- added to 1-g portions of U_3O_8, used as a stand-in for $(U,Pu)O_2$, showed that recovery of fluoride was 97% and the relative precision (1 σ) was 4% for a single determination.

Testing of the method was completed by making repeated measurements of 1 to 9 μg of F^- added as a solution of KF to 1-g portions of $(U,Pu)O_2$. The $(U,Pu)O_2$ used in preparing these samples was freed of traces of F^- by a pyrohydrolysis treatment before addition of the KF. Results for the repeated analyses showed an average recovery of 104% of the F^- and relative standard deviations (1 σ) of 5% for a single measurement of 2 to 9 μg of F^- and 6% for 1 μg of F^-. The reliability was considered adequate for the small quantities determined, and the method was used to measure F^- in several sintered $(U,Pu)O_2$ samples.

B. O/M Atom Ratios in Sintered $(U,Pu)O_2$

(G. C. Swanson, J. W. Dahlby, T. K. Marshall, and G. R. Waterbury)

The O/M atom ratio is an important chemical property that has significant effects on oxide reactor fuel behavior, and therefore, this ratio is included in the tentative FFTF fuel specifications. Two thermogravimetric methods were developed for the quantitative measurement of this property. These methods, as for all thermogravimetric measurements of this type, were based upon proper selection of conditions to convert the initial oxide quantitatively to the stoichiometric dioxide. The O/M ratio was calculated from the initial and final weights. Earlier work by Lyon[1] and by Chikalla[2] was extended in developing the two methods which differ only in the conditions to produce the stoichiometric dioxides.

In the first method, the change in weight of a 3- to 5-g sample as it was oxidized in air and then reduced for 6 h at 1000°C in a 1 ℓ/min flow of He-6% H_2 was used to calculate the O/M atom ratio of the original oxide. These reduction conditions were established as a result of repeated tests on 3 : 1 mixtures of UO_2 and PuO_2 prepared with known oxygen contents from the pure metals (>99.99% pure). In these tests, the temperature of the reduction, the length of the reduction period, and the rate of flow of He-6% H_2 were varied individually. The O/M ratios of the oxides produced at temperatures between 700 and 1000°C in He-6% H_2 (Table 501-I) showed that stoichiometry was not attained below 1000°C. Plots of sample

Table 501-I

Effect of Reduction Temperature on O/M Ratio
(2 ℓ/min flow of He-6% H_2; 6 h)

Temperature, °C	Avg O/M Ratio of Product
700	2.016
800	2.011
900	2.005
1000	2.001

weight versus temperature obtained for small UO_2 samples by an automatic microthermogravimetric analysis apparatus showed also that O/M ratios near 2.000 were obtained at 1000°C in dry He-6% H_2.

The length of the reduction period at 1000°C also was found to be critical. The O/M ratios obtained for initially hyperstoichiometric oxides reduced in He-6% H_2 at 1000°C for 2 to 18 h showed that a 6-h reduction period was optimum. Decreasing the flow of reducing gas from 2 ℓ/min to 1ℓ/min did not affect the results. Using the optimum reduction conditions of a 1 ℓ/min flow of He-6% H_2 for 6 h at 1000°C, the final O/M ratios of 12 prepared oxides, each weighing 3 to 5 g, averaged 2.001 with a standard deviation (1 σ) of 0.002. The product stoichiometry was 2.002 ± 0.003 for 17 high purity U_3O_8 samples, each weighing 300 mg, that were reduced under these optimum conditions in an automatic microthermogravimetric analyzer.

In concluding the investigation of this method, determinations were made of the effects on the O/M measurement caused by impurities either commonly found in sintered mixed oxide fuels or included in the tentative FFTF fuel specifications. Portions of an unsintered $(U_{0.75}Pu_{0.25})O_2$ powder made from the pure metals with known O_2 content were well mixed with the added impurities, and the O/M ratio was determined as described. It was found the 500 to 1300 ppm of Fe, Fe_2O_3, CaO, Ni, or Ni_2O_3, when added individually, did not affect the O/M by as much as 0.005, but similar amounts of C, Al, Al_2O_3, Ca, or Na_2SO_4 caused errors as large as + 0.094 (Table 501-II). Six impurity elements (Al, Cr, Fe, Ni, Si, and Ti) included in the specifications did not affect the method when added collectively as oxides at metal concentrations ranging between 160 and 240 ppm, but similar amounts of the metals caused a large negative bias. An investigation is in progress to determine the effects of impurities on the O/M ratios of samples prepared from ground, sintered $(U_{0.75}Pu_{0.25})O_2$ pellets.

In the second method, the O/M ratio was calculated from the change in weight as a 3- to 5-g sample was heated in Ar-8% H_2 containing 4 mm partial pressure of H_2O at 1250°C for 20 h. Preliminary tests showed that

Table 501-II

Effects of Selected Impurities on the Thermogravimetric Determination of O/M Ratio (Unsintered mixture of UO_2 and PuO_2)

Element	Form	Concentration, ppm[a]	Effect on O/M Ratio[b]
Fe	metal	967	-0.004
	Fe_2O_3	655	-0.001
Ni	metal	1,048	-0.012
	Ni_2O_3	625	-0.003
Ca	metal	1,000	-0.012
	CaO	799	-0.003
C	elemental	964	+0.013
Al	metal	997	-0.023
	Al_2O_3	536	-0.007
		900	
Na, S	Na_2SO_4	700	+0.094
Al,Cr,Fe, Ni,Si,Ti	metal	160 to 240 mg each	-0.032
	oxides	140 to 280 mg each	-0.001

[a] ppm of the element whether added as metal, oxide, or compound.

[b] average of duplicate determinations.

hyperstoichiometric oxides were produced at lower temperatures, or for shorter reaction times at 1250°C, from unsintered UO_2, PuO_2, or a UO_2-PuO_2 mixture, prepared from the pure metals. The O/M ratios were between 2.016 and 2.019 for the oxides reacted at 800°C, and about 2.008 for oxides produced at 1000°C. It was also found that the product oxide had to be cooled in dry Ar-8% H_2 to prevent weight increases due to moisture pickup. The oxides produced by this method were essentially stoichiometric when U_3O_8 was heated for 20 h at 1250°C (Table 501-III), or when $(U_{0.75}Pu_{0.25})O_2$ mixtures were heated for 16 h at 1250°C in this gas mixture.

Table 501-III

O/M Ratios of Oxides Heated at 1250°C in Ar 8% He -- 4 mm H_2O Pressure

Oxide	Time at 1250°C, h	No. of Determinations	Avg. O/M[a] of Product
U_3O_8	7	4	2.004
	15	4	2.002
	20	4	2.000
$(U,Pu)O_2$	8	6	2.003
	16	5	2.002
	24	3	2.002

[a] Each oxide cooled in dry Ar-8% H_2 before weighing.

Plots of sample weight versus temperature obtained for 300- to 350-mg samples of U_3O_8 using an automatic microthermogravimetric analyzer showed also that the

O/M ratio was 2.002 following heating of the oxide in dry Ar-6% H_2 at 1000°C until constant weight was attained. This required about 2 h. The O/M ratio of the oxide produced by heating at 1000°C in Ar-8% H_2-4 mm H_2O pressure was 2.017 which is in agreement with the value obtained with the macrothermogravimetric apparatus for 3- to 5-g samples in this temperature range.

Based on these investigations, the method in which the sample is oxidized in air and then reduced in dry He-6% H_2 at 1000°C was selected for further use. A final report is being prepared describing this development work and the modified method.

C. Gas Evolution from Sintered $(U,Pu)O_2$
(D.E.Vance, M.E.Smith, G. R. Waterbury)

The internal pressures developed in sealed reactor fuel capsules are dependent to a significant extent on the quantities of gases, including H_2O vapor, evolved from the fuel at operating temperatures. To determine the amount of gases obtained from sintered mixed-oxide pellets, the H_2O released at 800°C was measured separately from the other gases evolved at 1600°C. The sintered mixed-oxide pellet was heated in a fused-silica furnace tube at 800°C, and the evolved H_2O was swept by Ar to a moisture monitor. Integration of the monitor signal gave a quantitative measure of the H_2O. To determine if 800°C was adequate to evolve the H_2O quantitatively, pellets that had been heated to 800°C were reheated to 950°C. Additional gas was not collected at the higher temperature. The H_2O contents of several sintered mixed-oxide pellets were measured without known difficulty, but estimation of the accuracy of the method was impossible because of the lack of standard samples. Further work on this method was deferred pending agreement on a generally acceptable temperature for the moisture release.

Gases other than H_2O were evolved by heating the sintered mixed-oxide inductively in a W crucible to 1600°C. These gases were dried over anhydrous $Mg(ClO_4)_2$ and measured manometrically. A decrease in the apparatus blank and an improvement in the reliability of the method were obtained by installing a new type of induction furnace and an all-stainless steel manifold in the apparatus. A sample-loading device was fabricated which alternately removed the sample pellet from the crucible and then replaced it without breeching the vacuum system. This device permitted the determination of apparatus blanks at each of several temperatures prior to the evolution of gases from a pellet at that temperature. The quantity of gas evolved was measured manometrically, and in many cases its composition was determined on a mass spectrometer.

Data obtained for several fuel pellets showed that each pellet was unique in its outgassing behavior. Outgassing of $(U,Pu)O_2$ sintered oxide generally was almost complete (> 98%) at 1300°C, but a very small volume of gas was collected at 1900°C. The major constituent of the gases evolved at 1300°C usually was H_2. At higher temperatures, CO was the primary gas. The other gases found were CO_2, N_2, and very small quantities of He and NO. At temperatures greater than 1900°C, a large fraction of the sample vaporized and coated the inside of the furnace tube. The apparatus performed satisfactorily in measuring the small total quantities (0.02 to 0.06 cc/g) of gases evolved from several sintered mixed oxide pellets.

D. Measurement of N_2 in $(U,Pu)O_2$
(G. C. Swanson, N. L. Koski, T. K. Marshall, G. R. Waterbury)

Measurement of N_2 at low concentrations in $(U,Pu)O_2$ was necessary to ensure that the maximum concentration included in the specifications for FFTF fuel was not exceeded. In the first method tested for this analysis, the N_2 was separated by a Kjeldahl distillation as NH_3 and measured spectrophotometrically following reaction with Nessler's reagent.

The most tedious operation in this method was the dissolution of the sintered mixed oxide. This was done best in about 2 h in 12M HCl at 3000 to 4000 lb/sq. in. pressure and 300°C by a sealed tube method.[3] As facilities for this dissolution method were not available in many laboratories, dissolutions at lower temperatures were tried by refluxing the sample in various solvents, including H_2SiF_6-$CuSeO_4$, HCl-HNO_3-HF, HNO_3-HF, H_2SO_4, H_2SO_4-H_3PO_4, H_3PO_4-HF, and H_3PO_4. The samples were finely ground sintered $(U,Pu)O_2$ to which trace amounts of NaF, NaCl, C, and UN had been added. Complete dissolutions of 1-g samples of $(U,Pu)O_2$ were

accomplished by refluxing in either 5 ml of concentrated H_3PO_4 for 4 to 6 h, or 5 ml of concentrated H_3PO_4 containing 3 drops of 48% HF for 2 h.

Two sets of samples were dissolved in H_3PO_4-HF and one set in H_3PO_4. Devarda's alloy was added to each solution, NaOH was added to make the solution strongly alkaline, and the N_2 was distilled as NH_3 into a boric acid trap. A colored N_2 complex was formed with Nessler's reagent in the distillate and measured spectrophotometrically at 410 mμ. The concentration of N_2 was determined from a calibration curve. The results (Table 501-IV) showed that satisfactory results were obtained

Table 501-IV

Determination of N_2 in $(U,Pu)O_2$

Determinations	Solvent	N Present, ppm	N Found, ppm
4	H_3PO_4	54	47 ± 4^a
6	H_3PO_4-HF	49	45 ± 10^a
4	H_3PO_4-HF	47	39 ± 3^a

[a]Standard deviation (1 σ)

with either solvent. The recovery of N_2 was 85 to 90%, and the standard deviation (1 σ) was no greater than 10 ppm. The HF, while not necessary for complete dissolution of the sample, reduced the digestion time and apparently was not deleterious.

The results for N_2 following the sealed-tube dissolution were unbiased, and the standard deviation (1 σ) was 1 to 2 ppm in measuring 35 ppm of added N_2.

Separation of the N_2 by heating the solid sample in a flow of Ar eliminates the need for dissolving the oxides. This is done in a LECO Nitrox-6 analyzer in which the sample is heated inductively in a C crucible to a temperature between 1900 and 2100°C to free the N_2 which is measured in a simple gas chromatographic system. Unfortunately, O_2 in the sample reacts with the C crucible to form CO which interferes with the measurement of N_2 in the gas chromatographic system. A LECO Nitrox-6 analyzer was modified by adding a heated tube filled with CuO to oxidize the CO, and absorbants for the CO_2 formed. Calibration of the apparatus using LECO standards (KSCN) and NBS No. 10 g steel samples, and repeated determinations of the apparatus blank, showed that the standard deviation (1 σ) was 1 μg of N. The lower limit of reliable determination, therefore, was 3 μg of N_2. Continuing work was directed toward reduction of the apparatus blank to a level that would permit reliable measurement of N_2 at low ppm levels in small (< 0.5 g) samples.

E. Determination of Burnup

(R. G. Hurley, E. A. Hakkila, and J. W. Dahlby)

Measuring the concentrations of fission product Nd by x-ray fluorescence offers promise as a method of determining burnup. A proposed method was tested by analyzing solutions prepared from normal U, Ru, Th, Mo, Zr, Nb, and Nd at relative concentrations expected in a U fuel having undergone 10% burnup. The Nd, with Y carrier and Tb internal standard, was separated by fluoride precipitation and purified further by adsorption from HCl-butanol onto cation exchange resin filter paper. The intensities of the $L\beta_1$ x ray for Nd and the $L\alpha_1$ x ray for Tb on the paper were compared to x-ray intensities measured from discs having known concentration of each rare earth. The relative standard deviation (1 σ) was 0.7% in measuring 20 to 50 μg of Nd in 200 mg of U and increased to 5 and 16%, respectively, in measuring 5 and 1 μg of Nd. Expected quantities of other rare earth elements and stainless steel did not interfere.

Equations were derived for calculating percent burnup for ^{235}U and mixed ^{235}U ^{239}Pu fuels from the total Nd found. It was assumed that fission of ^{238}U was negligible compared to fission of ^{235}U, and a correction was included for the amount of Nd formed by decay of ^{144}Ce. Six samples of irradiated U fission alloy, reported to have undergone an average of 0.90% burnup, were analyzed by the x-ray fluorescence method. The average burnup measured was 0.69%, and the standard deviation was 0.05%. The reason for the difference in burnup values was not known. Dissolution of a $(U,Pu)O_2$ sample, having undergone about 5.7% burnup, was started to provide additional test solutions.

F. Spectrochemical Analysis of PuO_2, UO_2, and $(U,Pu)O_2$ (W. M. Myers, J. V. Pena, C. B. Collier, C. J. Martell, R. T. Phelps)

Control of impurity elements in sintered $(U,Pu)O_2$ depends on the purity of the starting PuO_2 and UO_2, and

requires reliable spectrochemical analyses of these raw materials. Carrier-distillation excitation spectrographic methods were satisfactory for the measurement of impurities in PuO_2 provided three sets of conditions were used to obtain adequate sensitivities for various elements. These conditions included use of 4% Ga_2O_3, 50% AgCl, and 15% AgCl as carriers. Standards prepared to contain the elements whose maximum concentrations in the product were specified were used in the studies to establish the proper conditions. Using the first set of conditions, 12 elements (Al, Ca, Cd, Cr, Fe, Mg, Mn, Ni, Pb, Si, Sn, and Zn) in the nominal concentration range of 5 to 500 ppm and 6 elements (Ag, B, Be, Cu, Li, and Na) at the 1 to 500 ppm concentration range were measured (Table 501-V). This set of conditions included an electrode charge that contained 4% Ga_2O_3 to serve as carrier and 500 ppm of Co as an internal standard. By photometering the spectrogram, in conjunction with the use of the internal standard, the relative precision (1 σ) of the method was 25%. Evaluation of concentration by the faster visual comparison of spectrograms was less precise (50% relative standard deviation).

For the determination of Mo, Ti, V, W, and Co, the conditions included addition of 50% AgCl to the electrode charge to serve as the carrier, and use of $PdCl_2$ as an internal standard. A 50-mg electrode charge was arced in an O_2 atmosphere, and the characteristic spectra obtained using a high-dispersion spectrograph were photographed. The relative precision (1 σ) was 20% in determining the 5 elements in the nominal concentration range of 10 to 500 ppm. The detection limits were Co-2 ppm, Mo-3, Ti-5, V-1 and W-5 (Table 501-V).

Table 501-V

Lower Limits of Measurement of Impurities in UO_2 and PuO_2 by Carrier Distillation Methods

Sample	Carrier	Internal Std.	Impurity	Lower Limit, ppm
PuO_2	4% Ga_2O_3	500 ppm Co	Al, Ca, Cd, Cr, Fe, Mg, Mn, Ni, Pd, Si, Sn, and Zr	5 (each)
			Ag, B, Be, Cu, Li, and Na	1 (each)
PuO_2	50% AgCl	$PdCl_2$	Mo	3
			Co	2
			V	1
			Ti and W	5 (each)
PuO_2	15% AgCl	-	Ta	50
			Zr	25
UO_2 as U_3O_8	4% Ga_2O_3 + 2.5% C	500 ppm Co	Li and Be	0.1 (each)
			B	0.2
			Na, Mg, Al, Si, Cr, Mn, Fe, Cu, Cd, Sn, and Pb	1 (each)
			Ca and Ni	2 (each)
			Co	5
			V	20
			Mo	25
			P	50
(U,Pu)O_2	6% Ga_2O_3		K	0.25

The third set of conditions were used for the determination of Ta and Zr with adequate detection sensitivity (Ta, 50 ppm; Zr, 25 ppm --see Table 501-V). An electrode charge of 120 mg containing 15% AgCl as carrier was arced in a deep (8 mm) graphite electrode cup. Low background SA-1 type emulsion was used in place of the faster 103-O type in order to improve the signal-to-noise ratio of the spectral lines. Both elements were measured in the concentration range of 50 to 1000 ppm with a relative precision (1 σ) of 20%.

Analyses of UO_2 also are performed using carrier-distillation methods following ignition of the sample to U_3O_8 at 800°C. The method described above for measuring Ta and Zr in PuO_2 was used for the determination of Mo, Nb, V, W, Ta, and Ti for which the usual Ga_2O_3 carrier distillation method lacked adequate sensitivity. The relative precision (1 σ) of the measurements was 20% for concentrations ranging from 30 to 1000 ppm. The detection sensitivities were adequate, being 3 ppm for V; 5 for Mo, W and Nb; 10 for Zr; and 30 for Ta (Table 501-V).

The other specified elements, such as Ag, B, Be, Ca, Fe, Li, Mn, Ni, Pb, and Si, were determined in the UO_2 starting material by a method used for several years to analyze U, U_3O_8 and UO_2. This carrier-distillation method used 4% Ga_2O_3 2.5% graphite as the carrier and 500 ppm of Co as an internal standard (Table 501-V).

The recent inclusion of K as a specification element in the (U, Pu)O_2 fuel pellet initiated an investigation of a method suitable for determining this element. Because the principal spectral lines, at 7665 Å and 7699 Å, were outside the spectral range that included the other specified elements, the determination of K required additional analysis. By modifying a method that used 6% Ga_2O_3 as a carrier for determining most common impurities in

sintered $(U, Pu)O_2$, satisfactory measurement of K at 25 to 200 ppm concentrations was accomplished. The modification consisted of decreasing the arcing current from 18 to 9 amp. This minor modification also reduced the lower limit of detection for Li to 0.25 ppm (Table 501-V).

Batches of high-purity PuO_2 and U_3O_8 have been prepared for use as matrix material to make the PuO_2, U_3O_8 or UO_2-PuO_2 standards that may be needed in this program.

IV. REFERENCES

1. W. L. Lyon, GEAP-4271 (1963).
2. T. D. Chikalla, "Quarterly Progress Report, October-December 1966," F. W. Albaugh et al, pp 4.1, BNW-L-CC-957 (1967).
3. C. F. Metz and G. R. Waterbury, LA Report 3559, Los Alamos Scientific Laboratory (1966).

V. TALKS AND PUBLICATIONS

1. J. W. Dahlby, G. R. Waterbury, and C. F. Metz, "The Determination of Oxygen to Metal Atom Ratios in Sintered Oxides," 13th Conference on Analytical Chemistry in Nuclear Technology, Gatlinburg, Tenn., September 30 to October 2, 1969.
2. D. E. Vance, M. E. Smith, and G. R. Waterbury, "Determination of Oxygen in Refractory Oxides: Gas Chromatographic Method," LA-4439 (1970).
3. J. E. Rein, R. K. Zeigler, and C. F. Metz, "LMFBR/FFTF Fuel Development Analytical Chemistry Program," LA-4407 (1970).

SPECIAL DISTRIBUTION

Atomic Energy Commission, Washington

Division of Research

D. K. Stevens

Division of Naval Reactors

R. H. Steele

Division of Reactor Development and Technology

G. W. Cunningham
D. E. Erb
Nicholas Grossman
W. H. Hannum (2)
K. E. Horton
J. R. Humphreys
R. E. Pahler
J. M. Simmons (2)
E. E. Sinclair
Bernard Singer
C. E. Weber
G. W. Wensch
M. J. Whitman

Division of Space Nuclear Systems

G. K. Dicker
F. C. Schwenk

Safeguards & Materials Management

J. M. Williams

Idaho Operations Office

DeWitt Moss

Ames Laboratory, ISU

O. N. Carlson
W. L. Larsen
M. Smutz

Argonne National Laboratory

A. Amorosi
R. Avery
F. G. Foote
Sherman Greenberg
J. H. Kittel
W. B. Loewenstein
P. G. Shewmon

Idaho Falls, Idaho

D. W. Cissel
Milton Levenson
R. C. Robertson

Atomics International

R. W. Dickinson, Director (2)
Liquid Metals Information Center

J. L. Ballif

Babcock & Wilcox

C. Baroch
J. H. MacMillan

Donald W. Douglas Laboratories

R. W. Andelin

General Electric Co., Cincinnati, Ohio

V. P. Calkins

General Electric Co., Sunnyvale, California

R. E. Skavdahl

Gulf General Atomic, Inc.

E. C. Creutz

Idaho Nuclear Corporation

W. C. Francis

IIT Research Institute

R. Van Tyne

Lawrence Radiation Laboratory

Leo Brewer
J. S. Kane
A. J. Rothman

LMFBR Program Office

D. K. Butler (Physics)
P. F. Gast
L. R. Kelman (Fuel & Materials)
J. M. McKee (Sodium Technology)

Mound Laboratory

R. G. Grove

NASA, Lewis Research Center

J. J. Lombardo

Naval Research Laboratory

L. E. Steele

Oak Ridge National Laboratory

G. M. Adamson
J. E. Cunningham
J. H. Frye, Jr.
C. J. McHargue
P. Patriarca
O. Sisman
M. S. Wechsler
J. R. Weir

Pacific Northwest Laboratory

F. W. Albaugh
E. A. Evans
V. J. Ruykauskas
W. R. Wykoff

FFTF Project

E. R. Astley
B. M. Johnson
D. W. Shannon (2)

Battelle Memorial Institute

D. L. Keller
S. J. Paprocki

Brookhaven National Laboratory

D. H. Gurinsky
C. Klamut

Combustion Engineering, Inc.

S. Christopher

U. S. Department of Interior

Bureau of Mines, Albany, Oregon

H. Kato

United Nuclear Corporation

A. Strasser

Westinghouse, Advanced Research Division

E. C. Bishop

Australian Atomic Energy Commission

J. L. Symonds